

Wayne State University Dissertations

January 2020

Effective Field Theory And Machine Learning Approaches To Controlling Nonperturbative Uncertainties In Flavor Physics

Ayesh Gunawardana
Wayne State University

Follow this and additional works at: https://digitalcommons.wayne.edu/oa_dissertations

 Part of the [Elementary Particles and Fields and String Theory Commons](#), and the [Other Physics Commons](#)

Recommended Citation

Gunawardana, Ayesh, "Effective Field Theory And Machine Learning Approaches To Controlling Nonperturbative Uncertainties In Flavor Physics" (2020). *Wayne State University Dissertations*. 2438. https://digitalcommons.wayne.edu/oa_dissertations/2438

This Open Access Dissertation is brought to you for free and open access by DigitalCommons@WayneState. It has been accepted for inclusion in Wayne State University Dissertations by an authorized administrator of DigitalCommons@WayneState.

**EFFECTIVE FIELD THEORY AND MACHINE LEARNING APPROACHES
TO CONTROLLING NONPERTURBATIVE UNCERTAINTIES IN FLAVOR
PHYSICS**

by

AYESH GUNAWARDANA

DISSERTATION

Submitted to the Graduate School

of Wayne State University,

Detroit, Michigan

in partial fulfillment of the requirements

for the degree of

DOCTOR OF PHILOSOPHY

2020

MAJOR: PHYSICS

Approved By:

Advisor

Date

ACKNOWLEDGEMENTS

First and foremost, I would like to thank my advisor Gil Paz for all the support and guidance during the last six years. His advice was instrumental in advancing my career as a physicist, and I am eternally indebted to that. I want to thank my collaborators Alexey Petrov and Cody Grant, for their contribution to this work. Also, I would like to thank the members of my committee Alexey Petrov, Sean Gavin, Abhijit Majumder and Mark Baskaran, for reviewing my work and providing constructive feedback. I want to convey my gratitude to Ratna Naik and David Cinabro for their roles as Chair of the Department. Without their excellent leadership, this work would not be possible.

I want to thank my parents Kanishka Gunawardana and Pushpa Herath, for their unconditional support and encouragement to achieve my goals. I would also like to thank my in-laws for their constant support and guidance. Special thank goes to my sister Malsrini Malarachchi without her help I would not be here.

I acknowledge all my friends at Wayne State University and the University of Kelaniya for making my life more enjoyable. I specially thank Navoda Thushari for being such a great mentor and friend. Her enthusiastic teaching was pivotal to my scientific career.

Last but not least, I thank my wife, Nirasha Perera, who has always been there with me during all the ups and downs in my life. My journey would not have been possible without her sacrifices and endurance.

TABLE OF CONTENTS

Acknowledgments	ii
LIST OF FIGURES	v
LIST OF TABLES	vii
1 Background : Standard model	1
1.1 Elementary particle fields	1
1.2 Symmetries in particle physics	2
1.3 Constructing the SM Lagrangian	5
2 Background : Effective field theory approach	20
2.1 Operator product expansion (OPE)	20
2.2 Heavy quark effective theory (HQET)	24
2.3 Non-relativistic QCD	29
2.4 Applications	31
3 Background : The $\bar{B} \rightarrow X_s \gamma$ decay	34
3.1 The inclusive decay rate	34
3.2 The CP asymmetry	53
3.3 Reevaluating the resolved photon contributions	56
4 New results : On HQET and NRQCD operators of dimension 8 and above	57
4.1 General method	58
4.2 Spin-independent operators upto and including dimension 8	63
4.3 Spin dependent matrix elements upto and including dimension 8	66
4.4 HQET operators	70
4.5 NRQED and NRQCD operators	75
4.6 Applications	81

5	New results : Reevaluating the uncertainties in $\bar{B} \rightarrow X_s \gamma$	85
5.1	Moments of the sub-leading shape function g_{17}	85
5.2	Applications	89
5.3	Modeling of h_{17}	96
6	New results : Semileptonic decays of heavy mesons with artificial neural networks	103
6.1	Artificial Neural Networks	106
6.2	Neural network training	110
6.3	Form factor parameterization with neural networks	112
7	Conclusion and future work	114
7.1	Conclusion	114
7.2	Future work	117
	Appendix A	119
	Appendix B	121
	Bibliography	122
	Abstract	133
	Autobiographical Statement	135

LIST OF FIGURES

Figure 1.1	Summary of the SM elementary particles [4]	2
Figure 1.2	The electromagnetic penguin diagram [28].	17
Figure 2.1	Underlying quark process of β decay. (a) represent the SM description and (b) represent the effective representation [32]	21
Figure 2.2	Box diagram for two heavy quark exchanging gauge particles	29
Figure 3.1	Graphical illustration of the factorization for $\bar{B} \rightarrow X_s \gamma$ decay [78]	38
Figure 3.2	Figure (a) represent the diagram arised by matching the $Q_1^q - Q_{7\gamma}$ operator to SCET. Figure (b) represents the diagram obtained by matching same process to HQET [78].	42
Figure 3.3	Figure (a) and (c) represent the diagrams arised by matching the $Q_{7\gamma} - Q_{8g}$ operator to SCET. Figure (b) and (d) represents the diagrams obtained by matching same processes to HQET [78].. . . .	45
Figure 3.4	Figure (a) and (c) represent the diagrams arised by matching the $Q_{8\gamma} - Q_{8g}$ operator to SCET. Figure (b) and (d) represents the diagrams obtained by matching same processes to HQET [78].. . . .	47
Figure 5.1	A comparison of the extremal models for h_{17} as a sum of two lowest even Hermite polynomials times a Gaussian of width 0.5 GeV used in [78] (dashed blue) to the same models allowed by current (2019) data (solid black). Left hand side: The model with 2010 smallest possible second moment of -0.31 GeV^4 compared to 2019 smallest possible second moment of 0.03 GeV^4 . Right hand side: The model with 2010 largest possible second moment of 0.49 GeV^4 compared to 2019 largest possible second moment of 0.27 GeV^4	91
Figure 6.1	Structure of an artificial neural network with two hidden layers [117]. . .	107
Figure 6.2	The averaged ANN result for the differential decay rate plotted against the experimental measurement [117]. The purple data points are the experimental data from [137]. The black and cyan curves are the average value and one standard deviation, respectively, from the output of our averaged ANN	113

Figure 6.3 ANN fits for $|V_{cd}F_+(q^2)|$ plotted against the three models described in the text [117]. The black and cyan curves are the average value and one standard deviation, respectively, from the output of our neural network. The dotted red curve is the simple pole model. The dot-dashed green curve is the modified pole model. The dashed magenta curve is the BZ model. The purple data points are calculated from the experimental data in Ref [137]. 113

LIST OF TABLES

Table 1.1	Constituents of the SM	11
Table 4.1	Transformation of p, v, iD^μ and s^λ under P, T and PT symmetries	60

CHAPTER 1 BACKGROUND : STANDARD MODEL

1.1 Elementary particle fields

The *standard model* (SM) of particle physics describes three fundamental interactions in nature using quantum field theory. *Quantum electrodynamics* (QED) describes the electromagnetic interaction, which is responsible for attraction between electrons and nuclei in atoms and molecules. *Quantum chromodynamics* (QCD) describes the strong nuclear interactions between particles. QCD is responsible for the binding of quarks inside nucleons (protons and neutrons). The weak force is behind processes such as beta decay. This weak interaction can transmute protons into neutrons, and it played a vital role in synthesizing heavy elements in the early stages of universe [1]. The Glashow-Weinberg-Salam (GWS) theory [2,3] pointed out that electromagnetic interaction and weak interaction can be described by a single theory, which is known as *electro-weak theory*.

In the SM, there are matter fields and force mediating fields. The matter fields are associated with intrinsic spin $1/2$, and they are known as *fermions*. Whereas force-carrying fields are associated with integer spins. These force-carrying fields are also known as *gauge bosons*.

There are four force-carrying gauge fields in SM. The photon, which is obtained by the quantization of the electromagnetic field, mediates the electromagnetic interaction. The massive W^\pm and Z^0 gauge bosons mediate the weak interaction. The gluons mediate the strong nuclear interactions.

Finally, the Higgs boson is obtained by quantizing the Higgs field. Scalar Higgs field is involved with the mechanism that generates mass to the massive gauge bosons and matter fields except, perhaps, for neutrinos (see sec. 1.3.3).

The fermion fields are separated into two segments, which are known as *quarks* and *leptons*. The quarks have six flavors, which are up (u), down (d), charm (c), strange (s), top (t), and bottom (b). There are six leptons in the lepton family. They are electron (e), muon (μ), tau (τ), electron neutrino (ν_e), muon neutrino (ν_μ) and tau neutrino (ν_τ).

The SM elementary particle fields are summarized in figure 1.1.

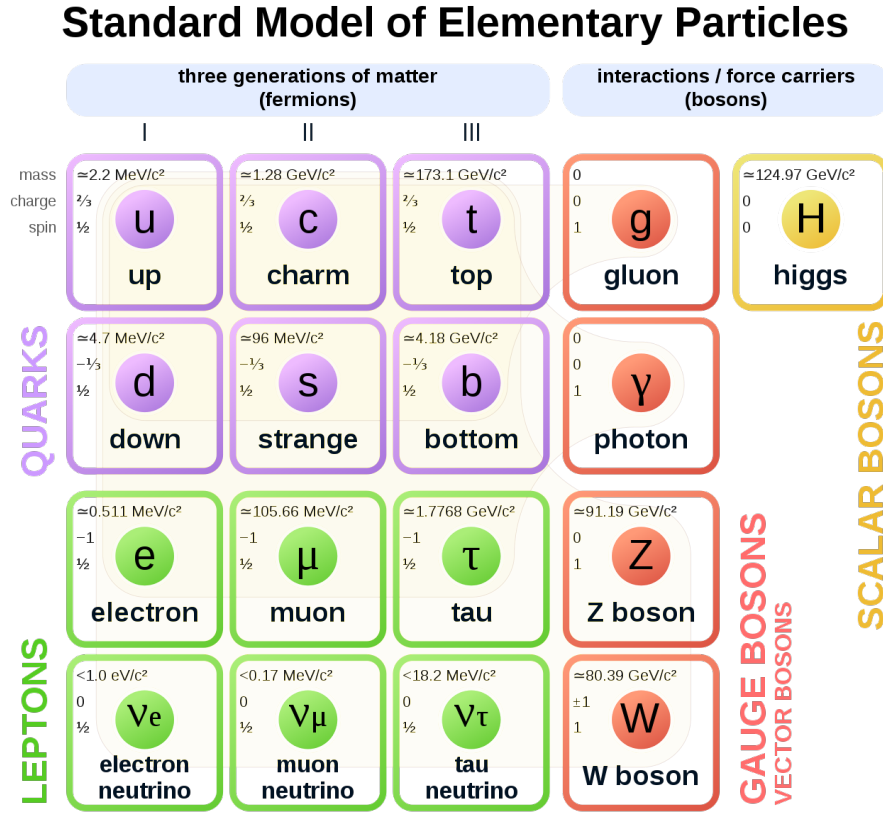


Figure 1.1: Summary of the SM elementary particles [4].

In figure 1.1, the particles that are denoted by purple and green colors represent the matter fields. The red color represents the spin-one gauge bosons. The color yellow represents the Higgs boson.

1.2 Symmetries in particle physics

Symmetry transformation is an operation that can be performed on a particular system, which leaves the system invariant. The symmetries are important because they provide the conservation laws that govern the dynamics of the system. In particular, Noether's theorem connects the symmetries with the corresponding conservation laws [5]. For example, Noether's theorem connects the space and time translation symmetries to energy and momentum conservation, respectively [6].

1.2.1 Discrete symmetries

Discrete symmetries are associated with the non-continuous change of the system. Under the discrete transformations, the system suddenly changes from one state to another. In particle physics, three important discrete symmetries govern the interactions, and they are known as *parity* (P), *charge conjugation* (C) and *time reversal* (T).

The parity symmetry implies that the physical processes are invariant under flipping of the sign of space coordinates. This can be used to test whether the fundamental interactions are invariant under parity. The experimental evidence implies that the electromagnetic and strong interaction are invariant under parity. However, the weak interaction does not preserve the parity invariance [7].

The charge conjugation transformation changes the sign of all the electromagnetic charges in the system. This implies an operator that changes the particle into an anti-particle. The strong and electromagnetic interaction both preserve charge conjugation, whereas the weak interaction does not remain invariant under C.

The time reversal symmetry implies that the invariance of the physical processes under the reversal of time. For example, under the T transformation a particle moving from point A to B along a certain path will reverse its direction from B to A on the same path [8]. The time reversal operator is an anti-unitary operator. This means the T operators act on quantum numbers as well as the operators [9], which provides

$$T(c - \text{number})\psi = (c - \text{number})^*T\psi \quad (1.1)$$

1.2.2 Continuous symmetries

Continuous transformations gradually change the system from its original state to another. These continuous transformations play an important role in understanding elementary particle interactions. The elementary particle fields are defined using the complex-valued mathematical spaces. Under the continuous symmetries, the physical process remains invari-

ant when the fields are rotated. For instance, electromagnetic interaction is invariant when the fields are rotated by a complex phase $e^{i\alpha}$, where α is a real number. This symmetry is known as $U(1)$ symmetry, and it is an abstract internal symmetry of the electromagnetic field. Similarly, the massless weak boson and fermion fields satisfy another abstract symmetry called $SU(2)_L$. These symmetries are based on the field rotations of two and three-dimensional spaces.

As the Yang-Mills theory [10] points out, the associated Lagrangian for these interacting fields should be invariant under local gauge transformations. This means the Lagrangian remains the same after an internal rotation. However, this theory seems to work well only for massless gauge fields such as photon field and gluon field. The heavy vector bosons, such as W and Z , require another mechanism to generate their masses. For this, a scalar field called *Higgs* field is employed.

Unlike the other fields, the lowest energy state of the Higgs field is a vacuum state (a state free of excitations) with non zero field value v , where v is known as the vacuum expectation value (vev). Thus, the system spontaneously chooses a new vacuum. This makes the ground state only possess a subset of the symmetries of Lagrangian. This process is known as *spontaneous symmetry breaking*. The broken Higgs field provides the source for the accumulation of mass for massless fermion and boson fields (see section 1.3.3) [11].

The standard model is specified by the special unitary group $SU(3)_c \times SU(2)_L \times U(1)_Y$. QCD has non-abelian gauge symmetry called $SU(3)_C$, the weak and electromagnetic interactions exhibit $SU(2)_L \times U(1)_Y$ symmetry. As stipulated by the Higgs mechanism, the $SU(2)_L \times U(1)_Y$ breaks to electromagnetic subgroup $U(1)_{EM}$. The coupling for strong, weak, and electromagnetic interactions are given by g_s for strong interaction, g' for weak hypercharge $U(1)_Y$, and g for weak isospin $SU(2)_L$. Y denotes the generator of weak hypercharge, and the three generators of weak isospin are given by τ^i where $i = 1, 2, 3$. For the $SU(3)_C$, there are eight generators, which are denoted by T^a , where $a = 1, \dots, 8$. Since the interactions between these fields have a complex structure, it is easier to divide the SM Lagrangian into

several sectors for the following analysis.

1.3 Constructing the SM Lagrangian

1.3.1 The gauge sector

The gauge field for strong interactions are given by G_μ^a , for the $SU(2)_L$ the gauge field is given by W_μ^i and the gauge field for the $U(1)_Y$ is given by B_μ . The corresponding abelian/non-abelian field strength tensors for these gauge fields are given as follows:

$$\begin{aligned} B_{\mu\nu} &= \partial_\mu B_\nu - \partial_\nu B_\mu \\ W_{\mu\nu}^i &= \partial_\mu W_\nu^i - \partial_\nu W_\mu^i - g\epsilon^{ijk}W_\mu^jW_\nu^k \\ G_{\mu\nu}^a &= \partial_\mu G_\nu^a - \partial_\nu G_\mu^a - g_s f^{abc}G_\mu^bG_\nu^c \end{aligned} \quad (1.2)$$

In the SM Lagrangian gauge sector is realized as follows:

$$\mathcal{L}_{\text{gauge}} = -\frac{1}{4}B_{\mu\nu}B^{\mu\nu} - \frac{1}{4}W_{\mu\nu}^iW^{i,\mu\nu} - \frac{1}{4}G_{\mu\nu}^aG^{a,\mu\nu} \quad (1.3)$$

1.3.2 The fermionic sector

The fermionic sector contains the matter fields. Also, it exhibits the $SU(2)_L \times U(1)_Y$ symmetry, which accounts the weak and electromagnetic interactions. There are three generations of fermions each consist of *neutrino* (v_i) with electromagnetic charge $Q_i = 0$, *lepton* (l_i) with $Q_i = -1$, up type *quark* with $Q_i = +2/3$ and down type quark with $Q_i = -1/3$. The $SU(2)_L$ determines the transformation properties of these fermion fields under weak charge. These fields are arrange as a 2×1 column vector. This is known as **2** representation. For an example, u_L and d_L together form **2** representation of $SU(2)_L$. Similarly, v_{eL} and e_L also transform together to form doublet. On the other hand, right handed fields transform as singlets under $SU(2)_L$.

The representation of $U(1)_Y$ is the *hypercharge* of the field. The hypercharge is assigned based on the final electromagnetic charge of the fermion. The representation of $SU(3)_C$ is determined by the color charge. The left and right handed quarks comes in three colors

as 3×1 column vector. This is the $\mathbf{3}$ representation in $SU(3)_C$. Leptons do not carry a color. They are in the singlet representation of $SU(3)_C$. Altogether, for an example, the transformation of up type quark under $SU(3)_c \times SU(2)_L \times U(1)_Y$ is

$$u_L \sim (3, 2, \frac{1}{3}) \quad (1.4)$$

The interaction between the matter and gauge fields is captured by the covariant derivative.

$$D_\mu = \partial_\mu + ig' B_\mu Y + ig W_\mu^i \tau^i + ig_s G_\mu^a T^a \quad (1.5)$$

Using this the fermionic part of the standard model Langrangian can be written as:

$$\mathcal{L}_{\text{fermionic}} = \sum_{i=1}^3 (\bar{E}_L^i i \not{D} E_L^i + \bar{Q}_L^i i \not{D} Q_L^i + \bar{e}_R^i i \not{D} e_R^i + \bar{u}_R^i i \not{D} u_R^i + \bar{d}_R^i i \not{D} d_R^i) \quad (1.6)$$

where

$$\begin{aligned} E_L^i &= P_L \begin{pmatrix} \nu_i \\ e_i \end{pmatrix} = \left(\begin{pmatrix} \nu_e \\ e \end{pmatrix}_L, \begin{pmatrix} \nu_\mu \\ \mu \end{pmatrix}_L, \begin{pmatrix} \nu_\tau \\ \tau \end{pmatrix}_L \right) \\ Q_L &= P_L \begin{pmatrix} u_i \\ d_i \end{pmatrix} = \left(\begin{pmatrix} u \\ d \end{pmatrix}_L, \begin{pmatrix} c \\ s \end{pmatrix}_L, \begin{pmatrix} t \\ b \end{pmatrix}_L \right), \end{aligned} \quad (1.7)$$

$$P_{L/R} = (1 \mp \gamma^5) / 2.$$

1.3.3 Higgs sector

As discussed in the section 1.2, the Higgs field is needed as a mass generating mechanism to heavy vector bosons. The Lagrangian is [11–13]:

$$\mathcal{L}_H = (D_\mu \phi)^\dagger (D^\mu \phi) + \frac{1}{2} \mu^2 \phi^\dagger \phi - \frac{1}{4} \lambda (\phi^\dagger \phi)^2 + \mathcal{L}_{\text{gauge}} \quad (1.8)$$

where

$$\langle \phi \rangle = \begin{pmatrix} \phi^+ \\ \phi^0 \end{pmatrix} = \frac{1}{\sqrt{2}} \begin{pmatrix} \phi_3 + i\phi_4 \\ \phi_1 + i\phi_2 \end{pmatrix} \quad (1.9)$$

Here μ and λ are both real parameters. However, the minimum of the Higgs potential is not at $\langle \phi \rangle = 0$. Thus, the potential term provides the spherical shell of minima at a radius $v = \left(\frac{\mu^2}{\lambda}\right)^{\frac{1}{2}}$. On the surface of this spherical shell there are infinitely many equivalent vacua. The Higgs field spontaneously pick one of these vacua and breaks the symmetry. For simplicity, consider the following vacuum field configuration:

$$(\phi_1^0)^2 = \frac{2\mu^2}{\lambda} = 2v^2, \quad \phi_2^0 = 0 \quad \phi_3^0 = 0 \quad \phi_4^0 = 0 \quad (1.10)$$

More concisely,

$$\langle \phi \rangle = \begin{pmatrix} 0 \\ v \end{pmatrix} \quad (1.11)$$

The symmetry breaking $SU(2)_L \times U(1)_Y \rightarrow U(1)_Q$ does not break all the symmetries. For instance, our choice of vacuum given in equation (1.11) is still invariant under $\hat{U} = e^{i(\frac{Y}{2} + I_3\tau^3)\alpha(x)}$ transformation. In fact $Q = \frac{Y}{2} + I_3$ where Q is the electromagnetic charge. Using this the above transformation can be written as $\hat{U} = e^{iQ\alpha(x)}$. According to the *Yang-Mills* theory this is equivalent to a $U(1)$ transformation. Therefore, the electromagnetic interaction emerges unbroken from this symmetry breaking.

The excitation above the vacuum state of the Higgs field is given below:

$$\phi(x) = \begin{pmatrix} 0 \\ v + \frac{h(x)}{\sqrt{2}} \end{pmatrix} \quad (1.12)$$

The first term in the Higgs Lagrangian becomes

$$(D_\mu^\dagger \phi)(D^\mu \phi) = \frac{1}{2}(\partial_\mu h(x))^2 + \frac{g^2 v^2}{4}(W_\mu^1)^2 + \frac{g^2 v^2}{4}(W_\mu^2)^2 + \frac{v^2}{4}(gW_\mu^3 - g'B_\mu)^2 \quad (1.13)$$

Note that the mass term of a spin-1 field has the form $\frac{1}{2}(\text{mass})^2 \times (\text{field})^2$. Following from this, the W_μ^1 and W_μ^2 fields obtain a mass $M_W^2 = \frac{g^2 v^2}{4}$. The linear combination of the fields $(gW_\mu^3 - g'B_\mu)$ also becomes massive. The Higgs field components ϕ_2, ϕ_3 and ϕ_4 disappeared from the interaction Lagrangian. The massive excitation of the scalar field is known as *Higgs* boson.

The linear combination $g'W_\mu^3 + gB_\mu$ does not appear in the above Lagrangian. Therefore, this combination is identified as the massless photon field. The *Weinberg angle* is defined as the ratio of coupling constants g and g' as $\tan \theta_W = \frac{g'}{g}$. Using this angle two new fields are defined as:

$$\begin{pmatrix} Z_\mu \\ A_\mu \end{pmatrix} = \begin{pmatrix} \cos \theta_W & -\sin \theta_W \\ \sin \theta_W & \cos \theta_W \end{pmatrix} \begin{pmatrix} W_\mu^3 \\ B_\mu \end{pmatrix} \quad (1.14)$$

where Z_μ is the Z boson field and A_μ is the photon field.

1.3.4 Yukawa sector

The Higgs couplings to the fermions in the SM is described by the *Yukawa* Lagrangian. The Lagrangian needs to be *Lorentz invariant* and have mass dimension 4. Its general form is

$$\mathcal{L}_{\text{Yukawa}} \ni -y_\psi \bar{\psi}_R \phi \psi_L + \text{c.c.}, \quad (1.15)$$

where ψ and ϕ are fermion field and scalar field respectively. y_ψ is the dimensionless coupling between the scalar and fermion fields, which is known as the *Yukawa coupling*.

1.3.4.1 Lepton sector

Using the above definition, the Yukawa term in the Lagrangian can be obtained for the $SU(2)_L$ doublet $E_L = (\nu_L, e_L)^T$ as follows:

$$\mathcal{L}_{\text{Yukawa}} \ni - [y_e \bar{e}_R \Phi^\dagger E_L + y_e^* \bar{E}_L \Phi e_R] \quad (1.16)$$

The coupling y_e is obtained using

$$\frac{y_e}{\sqrt{2}} = \frac{m_e}{v} \quad (1.17)$$

Also, this can be extended to all three generations in SM. This gives a generalized lepton sector as

$$\mathcal{L}_{\text{lepton}} \ni - [Y_{ij} \bar{e}_{Rj} \Phi^\dagger E_{Li} + Y_{ij}^* \bar{E}_{Li} \Phi e_{Rj}], \quad (1.18)$$

where Y_{ij} is the matrix element of the Yukawa matrix. Due to the absence of ν_{Ri} fields, in SM *neutrinos* do not couple to Higgs field. The neutrinos do not get their mass from the Higgs mechanism.

1.3.4.2 Quark sector

Similarly, the Yukawa interaction between $SU(2)_L$ quark doublet $Q_L = (u_L, d_L)^T$ and down type quark singlet d_R can be written as

$$\mathcal{L}_{\text{Yukawa}} \ni - [y_d \bar{d}_R \Phi^\dagger Q_L + y_d^* \bar{Q}_L \Phi d_R] \quad (1.19)$$

The mass generation of up type quarks is obtained by using the conjugate doublet transformation in $SU(2)$. The conjugate Higgs doublet is given by

$$\tilde{\phi} \equiv i\sigma^2\phi^* = i \begin{pmatrix} 0 & -i \\ i & 0 \end{pmatrix} \begin{pmatrix} \phi^- \\ \phi^{0*} \end{pmatrix} = \begin{pmatrix} \phi^{0*} \\ -\phi^- \end{pmatrix} \quad (1.20)$$

As an artifact of this, we obtain $Y = -\frac{1}{2}$. Using this, another gauge invariant term can be obtained,

$$\mathcal{L}_{\text{Yukawa}} \ni - \left[y_u \bar{u}_R \tilde{\phi}^\dagger Q_L + y_u^* \bar{Q}_L \tilde{\phi} u_R \right] \quad (1.21)$$

As shown before, the quark masses and the Higgs vev determine the Yukawa couplings. This can also be generalized to all 3 generations of quarks as well. The complete Yukawa term,

$$-\mathcal{L}_{\text{Yukawa}} = Y_{ij}^d \bar{Q}_{Li} \phi d_{Rj} + Y_{ij}^u \bar{Q}_{Li} \tilde{\phi} u_{Rj} + Y_{ij}^e \bar{E}_{Li} \phi e_{Rj} + \text{h.c.} \quad (1.22)$$

Also, this term is the source of all *flavor* interactions [14].

1.3.5 The Standard Model Lagrangian

Considering all the possible interactions between the gauge bosons, fermions and scalars the final Lagrangian that describes the SM can be written as follows:

$$\mathcal{L}_{\text{SM}} = \mathcal{L}_{\text{fermionic}} + \mathcal{L}_{\text{gauge}} + \mathcal{L}_{\text{Higgs}} + \mathcal{L}_{\text{Yukawa}} . \quad (1.23)$$

In the table 1.1 we summarize all the SM constituents and their corresponding gauge multiplets.

Table 1.1: Constituents of the SM

Type	spin	Field	Multiplet
Vector	1	B_μ	$(1,1,0)$
		W_μ	$(1,3,0)$
		G_μ	$(8,1,0)$
Spinor	$\frac{1}{2}$	E_{Li}	$(1,2,-\frac{1}{2})$
		Q_{Li}	$(3,2,\frac{1}{6})$
		e_{Ri}	$(1,1,-1)$
		u_{Ri}	$(3,1,\frac{2}{3})$
		d_{Ri}	$(3,1,-\frac{1}{3})$
Sacalar	0	ϕ	$(1,2,\frac{1}{2})$

1.3.6 Cabibbo-Kobayashi-Maskawa (CKM) matrix

Consider equations (1.19) and (1.21). They can be generalized to all three generations of quarks in the SM.

$$\mathcal{L}_{\text{Yukawa}}^{\text{quark}} = - \sum_{i=1}^3 \sum_{j=1}^3 \left[y_{ij}^u \bar{u}_{Ri} \tilde{\phi}^\dagger Q_{Lj} + y_{ij}^d \bar{d}_{Ri} \phi^\dagger Q_{Lj} \right] + \text{h.c.} \quad (1.24)$$

The dimensionless *Yukawa* couplings now become 3×3 matrices. These matrices contain 18 complex parameters. As shown in the section 1.3.3, replacing the Higgs by its vacuum configuration $\phi = (0, v/\sqrt{2})^T$ provides the mass term.

$$\mathcal{L}_{\text{Yukawa}}^q \supset - (\bar{u}_1, \bar{u}_2, \bar{u}_3)_R \mathcal{M}^u \begin{pmatrix} u_1 \\ u_2 \\ u_3 \end{pmatrix}_L - (\bar{d}_1, \bar{d}_2, \bar{d}_3)_R \mathcal{M}^d \begin{pmatrix} d_1 \\ d_2 \\ d_3 \end{pmatrix}_L + \text{h.c.}, \quad (1.25)$$

where

$$\mathcal{M}_{ij}^u = \frac{v}{\sqrt{2}} y_{ij}^u, \quad \mathcal{M}_{ij}^d = \frac{v}{\sqrt{2}} y_{ij}^d. \quad (1.26)$$

The \mathcal{M}_{ij}^u and \mathcal{M}_{ij}^d are known as the quark mass matrices in the *generation* space. The diagonalization of these mass matrices provide the quark mass eigenstates. This is done by multiplying the mass matrices by unitary matrices U_L, U_R, D_L and D_R . They are defined by

$$\begin{pmatrix} u_1 \\ u_2 \\ u_3 \end{pmatrix}_{L,R} = U_{L,R} \begin{pmatrix} u \\ c \\ t \end{pmatrix}_{L,R}, \quad \begin{pmatrix} d_1 \\ d_2 \\ d_3 \end{pmatrix}_{L,R} = D_{L,R} \begin{pmatrix} d \\ s \\ b \end{pmatrix}_{L,R}, \quad (1.27)$$

where u, c, t, d, s and b are quark mass eigenstates. This gives us the diagonalized mass matrices.

$$U_R^{-1} \mathcal{M}^u U_L = \begin{pmatrix} m_u & 0 & 0 \\ 0 & m_c & 0 \\ 0 & 0 & m_t \end{pmatrix}, \quad D_R^{-1} \mathcal{M}^d D_L = \begin{pmatrix} m_d & 0 & 0 \\ 0 & m_s & 0 \\ 0 & 0 & m_b \end{pmatrix}. \quad (1.28)$$

Also, \mathcal{M}^u and \mathcal{M}^d diagonalizes *Yukawa* matrices $y_{ij}^u = \frac{\sqrt{2}}{v} \mathcal{M}_{ij}^u$ and $y_{ij}^d = \frac{\sqrt{2}}{v} \mathcal{M}_{ij}^d$.

These mass eigenstates (physical states) of up and down type quarks can be coupled in charged current interactions.

$$J_L^{+\mu} = (\bar{u}_1, \bar{u}_2, \bar{u}_3)_L \gamma^\mu \begin{pmatrix} d_1 \\ d_2 \\ d_3 \end{pmatrix} = (\bar{u}, \bar{c}, \bar{t})_L U_L^\dagger \gamma^\mu D_L \begin{pmatrix} d \\ s \\ b \end{pmatrix}_L = (\bar{u}, \bar{c}, \bar{t})_L \gamma^\mu V \begin{pmatrix} d \\ s \\ b \end{pmatrix}_L. \quad (1.29)$$

Here $V = U_L^\dagger D_L$ is known as the *Cabibbo-Kobayashi-Maskawa* (CKM) matrix, and it is given

by

$$V_{\text{CKM}} = \begin{pmatrix} V_{ud} & V_{us} & V_{ub} \\ V_{cd} & V_{cs} & V_{cb} \\ V_{td} & V_{ts} & V_{tb} \end{pmatrix}. \quad (1.30)$$

The CKM is unitary

$$V^\dagger V = \left(U_L^\dagger D_L \right)^\dagger \left(U_L^\dagger D_L \right) = D_L^\dagger U_L U_L^\dagger D_L = 1 \quad (1.31)$$

Since the CKM matrix is a 3×3 matrix it is defined by nine complex parameters (18 real numbers). The constraint $V_{ab}^\dagger V_{bc} = \delta_{ac}$ reduce this to nine real parameters. The redefinition $q_L \rightarrow e^{i\alpha_{qL}} q_L$ can technically remove six phases because there are six different quark fields. However, the common phase redefinition of all the quarks does not affect the CKM matrix. This, in turn, reduces the number of nonphysical phases to five. Altogether, there are $9 - 5 = 4$ independent parameters to describe the CKM matrix. There is no unique parameterization for the CKM matrices. The most common ones are “Standard parameterization” [16] and “Wolfenstein parameterization” [17].

1.3.6.1 Standard Parameterization

The Standard parameterization is given by

$$V_{\text{CKM}} = \begin{pmatrix} c_{12}c_{13} & s_{12}c_{13} & s_{13}e^{-i\delta} \\ -s_{12}c_{23} - c_{12}s_{23}s_{13}e^{i\delta} & c_{12}c_{23} - s_{12}s_{23}s_{13}e^{i\delta} & s_{23}c_{13} \\ s_{12}s_{23} - c_{12}c_{23}s_{13}e^{i\delta} & -s_{23}c_{12} - s_{12}c_{23}s_{13}e^{i\delta} & c_{23}c_{13} \end{pmatrix}, \quad (1.32)$$

where $s_{ij} = \sin \theta_{ij}$ and $c_{ij} = \cos \theta_{ij}$ ($i = 1, 2, 3$). The phase δ is necessary for the CP violation, and its range $0 \leq \delta \leq 2\pi$. The measurements of CPV in K decays constrain this range to $0 \leq \delta \leq \pi$ [15].

The s_{13} and s_{23} are in the order of 10^{-3} , and $c_{13} = c_{23} = 1$ [18]. This leaves 4 independent

parameters

$$s_{12} = |V_{us}|, \quad s_{13} = |V_{ub}|, \quad s_{23} = |V_{cb}|, \quad \delta \quad (1.33)$$

1.3.6.2 Wolfenstein Parameterization

The Wolfenstein Parameterization can be obtained by expressing the independent parameters in standard parameterization by λ, A, ρ, η [19].

$$s_{12} = \lambda, \quad s_{23} = A\lambda^2, \quad s_{13}e^{-i\delta} = A\lambda^3(\rho - i\eta) \quad (1.34)$$

This is an approximate parameterization, in which each CKM elements is expanded in power series of small parameter $\lambda = |V_{us}| = 0.22$. This gives us

$$\hat{V} = \begin{pmatrix} 1 - \frac{\lambda^2}{2} & \lambda & A\lambda^3(\rho - i\eta) \\ -\lambda & 1 - \frac{\lambda^2}{2} & A\lambda^2 \\ A\lambda^3(1 - \rho - i\eta) & -A\lambda^2 & 1 \end{pmatrix} + \mathcal{O}(\lambda^4). \quad (1.35)$$

1.3.6.3 Unitarity triangles

Unitarity relationships can be expressed by triangle relations defined in a complex plane.

For example,

$$\begin{aligned} V_{ud}V_{ub}^* + V_{cd}V_{cb}^* + V_{td}V_{tb}^* &= 0 \\ V_{us}V_{ub}^* + V_{cs}V_{cb}^* + V_{ts}V_{tb}^* &= 0 \\ V_{ud}V_{us}^* + V_{cd}V_{cs}^* + V_{td}V_{ts}^* &= 0 \\ V_{ud}V_{td}^* + V_{us}V_{ts}^* + V_{ub}V_{tb}^* &= 0 \\ V_{cd}V_{td}^* + V_{cs}V_{ts}^* + V_{cb}V_{tb}^* &= 0 \\ V_{ud}V_{cd}^* + V_{us}V_{cs}^* + V_{ub}V_{cb}^* &= 0 \end{aligned} \quad (1.36)$$

The area of the unitarity triangles provide the measurement of CP violation. This measurement is obtained by [20]

$$|J_{CP}| = 2 \cdot A_{\Delta} \quad (1.37)$$

where $|J_{CP}|$ is the *Jarlskog invariant* and A_{Δ} is the area of the unitarity triangle. Therefore, precise measurements of the CKM parameters along with these unitarity relationships gives us important information on CP violation. Also, unitarity triangles are important for understanding the flavor changing neutral current processes (see sec. 1.3.7.2).

1.3.7 Flavor physics

In *flavor physics*, the interactions between different flavors are studied extensively. Massless gauge bosons such as *gluons* and *photons* do not distinguish between different flavors. However, the weak and the Yukawa interactions are directly affected by the flavor of the participants in the interaction. When it comes to beyond the standard model interactions, there may be some new degrees of freedom that are affected by the flavors.

During a *flavor changing* interaction, flavor quantum numbers change. There are two types of flavor changing interactions. If the interaction is between both up type and down type flavors or charged leptons and neutrinos, then it involves *flavor changing charged current* (FCCC). For the interactions between either up type or down type flavors but not both and/or either charged leptons and neutrinos but not both, then it involves the *flavor changing neutral currents* (FCNC). No term in the SM Lagrangian changes flavor in Z^0, g and γ interactions. Therefore, it makes FCNC are highly sensitive to the new physics.

1.3.7.1 Weak interactions

The weak interactions are summarized in the following form

$$\mathcal{L}_{\text{int}}^{\text{EW}} = \mathcal{L}_{CC} + \mathcal{L}_{NC} \quad (1.38)$$

where \mathcal{L}_{CC} and \mathcal{L}_{NC} describe the charged current and the neutral current interactions. In

particular, the CC is given by [15]

$$\mathcal{L}_{\text{CC}} = \frac{g}{2\sqrt{2}} (J_{\mu}^{+} W^{+\mu} + J_{\mu}^{-} W^{-\mu}), \quad (1.39)$$

where

$$J_{\mu}^{+} = J_{\mu}^1 + iJ_{\mu}^2 = \bar{U}_L \gamma_{\mu} D_L + \bar{l} \gamma_{\mu} \nu_L, \quad (1.40)$$

U_L is an up type quark, D is a down type quark, l is a lepton and ν is a neutrino. The NC is given by

$$\mathcal{L}_{\text{NC}} = -e J_{\mu}^{\text{em}} A^{\mu} + \frac{g}{2 \cos \theta_W} J_{\mu}^0 Z^{\mu}, \quad (1.41)$$

where e is the QED coupling. The neutral electromagnetic and weak currents are given by

$$\begin{aligned} J_{\mu}^{\text{em}} &= \sum_f Q_f \bar{f} \gamma_{\mu} f \\ J_{\mu}^0 &= \sum_f \bar{f} \gamma_{\mu} (v_f - a_f \gamma_5) f \end{aligned} \quad (1.42)$$

where

$$v_f = T_3^f - 2Q_f \sin^2 \theta_W, \quad a_f = T_3^f. \quad (1.43)$$

The Q_f and T_3^f denotes the charge and the third component of the weak isospin of the left-handed fermion. The photonic and gluonic vertices are vector-like (V), the W^{\pm} vertices involve only vector-axial minus vector-like ($V - A$) and the Z^0 vertices involve both $V - A$ and $V + A$ structures. Also, the vertices that involve Higgs play an important role. This relates the CP-violating decays and transitions.

1.3.7.2 FCNC

At one loop order the possible FCNC interactions are summarized by triple and quartic effective vertices. In the literature these vertices are known as *penguin* and *box* diagrams. The name “penguin” was coined by J.Ellis [24]. Penguin diagrams are defined by a single exchange of a W boson. Whereas, the box diagrams contain two W exchanges.

The importance of the penguin diagrams was pointed out in the work of Vainshtein, Zakharov, and Shifman [25]. For instance, penguin diagrams are responsible for the enhancement of the $\Delta I = 1/2$ amplitude compared to the $\Delta I = 3/2$ amplitude in weak $K \rightarrow \pi\pi$ decays. The importance of the penguins to CP violation was first pointed out by Bander, Silverman and Soni [26]. They showed that the interference between the tree level diagrams and the penguin diagrams can give a large CP asymmetry in B decays.

In b transitions to lighter quarks such as s and d , the penguin effects are rather pronounced. In these penguins the t quark is primarily contributing to the loop. This is because the amplitude of the penguin is proportional to the kinematic factor $(m_q/M_W)^2$ and $(m_t/M_W)^2 \gg (m_{c,u}/M_W)^2$ (see sec 1.3.8). Also, there is a large coupling between b and t because $|V_{tb}| \sim 1$. This feature of b penguins makes $b \rightarrow s$ and $b \rightarrow d$ transitions sensitive to $|V_{ts}|$ and $|V_{td}|$.

In particular, the decays such as $b \rightarrow s(d)$ are classified into a class of diagrams that are known as *electromagnetic penguins*. In these decays a hard photon is emitted from a charged particle. This hard photon is an excellent experimental signature. The Feynman diagram for $b \rightarrow s, d\gamma$ transition is given in figure 1.2.

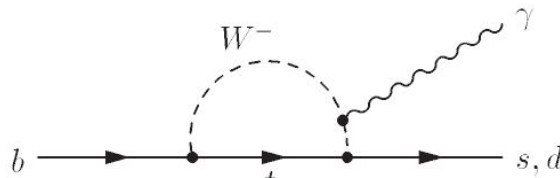


Figure 1.2: The electromagnetic penguin diagram [28].

The figure 1.2 shows that the $b \rightarrow s, d\gamma$ transition is a loop suppressed process. In the

SM there exist no tree level diagrams for these FCNC transitions.

1.3.8 GIM mechanism

The suppression of the $b \rightarrow s(d)$ was further explained by the Glashow-Illiopoulos-Maiani (GIM) mechanism. The amplitude of figure 1.2 is given by [29]

$$\mathcal{M} = eq_\mu \epsilon_\nu \bar{u}(p_s) \sigma^{\mu\nu} \left(\frac{1 + \gamma_5}{2} \right) u(p_b) \frac{m_b}{M_W^2} \frac{g^2}{16\pi^2} \cdot I, \quad (1.44)$$

where

$$I = \sum_{i=u,c,t} V_{ib} V_{is}^* F \left(\frac{m_i^2}{M_W^2} \right). \quad (1.45)$$

The term $\frac{g^2}{16\pi^2}$ is a loop factor, and it can be given as $\frac{g^2}{16\pi^2} \sim \frac{\alpha}{4\pi \cos^2 \theta_W}$. We insert the b quark mass m_b to flip the chirality of the b quark.

In equation (1.45), the function $F(x)$ arises by the explicit calculation of the diagram. Since $m_t \gg M_W$, we cannot safely Taylor expand the function $F(m_i/M_W)$. The function I is invariant under $F(x) \rightarrow F(x) + \text{constant}$ from the unitarity of the CKM matrix. Under this transformation $F(0) = 0$ without loss of generality. Besides, the unitarity of the CKM matrix elements provide $V_{tb} V_{ts}^* = -\sum_{i=u,c} V_{ib} V_{is}^*$. Following from this, we obtain

$$I = -V_{cb} V_{cs}^* \left(F \left(\frac{m_t^2}{M_W^2} \right) - F \left(\frac{m_c^2}{M_W^2} \right) \right) - V_{ub} V_{us}^* \left(F \left(\frac{m_t^2}{M_W^2} \right) - F \left(\frac{m_u^2}{M_W^2} \right) \right). \quad (1.46)$$

Since $m_u, m_c \ll M_W$, the term $F(m_{u,c}^2/M_W^2)$ can be expanded in Taylor series. This gives

$$\begin{aligned} I &= -V_{cb} V_{cs}^* \left(F \left(\frac{m_t^2}{M_W^2} \right) - F'(0) \frac{m_c^2}{M_W^2} \right) - V_{ub} V_{us}^* \left(F \left(\frac{m_t^2}{M_W^2} \right) - F'(0) \frac{m_u^2}{M_W^2} \right) + \dots \\ &= F \left(\frac{m_t^2}{M_W^2} \right) V_{tb} V_{ts}^* + F'(0) \sum_{i=u,c} V_{ib} V_{is}^* \frac{m_i^2}{M_W^2} + \dots \\ &\sim \epsilon^2 F \left(\frac{m_t^2}{M_W^2} \right), \end{aligned} \quad (1.47)$$

where $\epsilon^2 = A\lambda^2$ in the Wolfenstein parameterization. The combination of loop suppression, mass suppression and CKM suppression is provided by GIM mechanism. As a result, the FCNC are highly suppressed in the SM. Also, the contribution from $F(m_u^2/M_W^2)$ and $F(m_c^2/M_W^2)$ is negligible compared to the $F(m_t^2/M_W^2)$. Thus, the virtual top quark exchanges dominate the $b \rightarrow s(d)$ amplitude.

1.3.9 Effective weak interactions

In the SM, the coupling of the W^\pm bosons to the fermions are the only flavor changing interactions [30]. At low energies, i.e. $E \ll M_W$, we can ignore the effects of the heavy bosons. This is known as integrating out of the heavy degrees of freedom (see sec 2.2). As a result, a full SM interaction is converted into a local four fermion interaction. The effective Lagrangian can be expressed by a series of effective vertices and their effective coupling constants (see sec 2.1.1). These *effective coupling* constants provide the short distant (high energy) physics, and they are known as Wilson coefficients (C_i). The long distant (low energy) physics is given by effective operators $\langle Q_i \rangle$. Since the Wilson coefficients are associated with high energy scales, where $\frac{\alpha_s}{\pi} \sim 0.1$, they can be perturbatively expanded in α_s . This is because at high energy scales the C_i are obtained by matching the effective diagrams with the full theory diagrams at the weak scale ($\mu \sim M_W$). For example, the explicit form of the first two Wilson coefficients are [30]

$$\begin{aligned} C_1(\mu) &= 1 + \frac{3}{N_c} \frac{\alpha_s(\mu)}{4\pi} \left(\ln \frac{M_W^2}{\mu^2} - \frac{11}{6} \right) + O(\alpha_s^2) \\ C_2(\mu) &= -3 \frac{\alpha_s(\mu)}{4\pi} \left(\ln \frac{M_W^2}{\mu^2} - \frac{11}{6} \right) + O(\alpha_s^2) \end{aligned} \quad (1.48)$$

In equation (1.48) C_1 and C_2 are expanded in terms of $\frac{\alpha_s}{\pi} \ln \frac{M_W^2}{\mu^2}$ instead of $\frac{\alpha_s}{\pi}$. The $\frac{\alpha_s}{\pi} \ln \frac{M_W^2}{\mu^2} \sim 0.8$. These large logarithmic terms needs to resummed to all orders.

The solution to the problem of large logarithms is by using renormalization-group (RG) improved perturbation theory. It treats $\alpha_s \ln \frac{M}{\mu}$ as $\mathcal{O}(1)$ and $\alpha_s \ll 1$. In appendix A we provide the RG evaluation of the dominant Wilson coefficients of $\bar{B} \rightarrow X_s \gamma$.

CHAPTER 2 BACKGROUND : EFFECTIVE FIELD THEORY APPROACH

In explaining natural phenomena, the separation of scales plays an important role. For instance, to explain the dynamics of gasses, we use a set of macroscopic variables such as pressure, volume, and temperature, which do not provide insight about the molecular (microscopic) structure of the gas molecules. The molecular description of gas is not useful to explain the most day to day phenomena. The microscopic nature of the molecules is needed to understand the chemical structure of these atoms [31]. In the above example, the macroscopic view of gasses is the effective theory of the microscopic picture. This effective approach is prevalent in many branches of Physics. As another example, in the quantum mechanical (QM) description of a hydrogen atom does not involve in dynamics of quarks and gluons inside the proton. However, if we zoom in to the hydrogen nucleus, then the dynamics of the quarks and gluons inside the proton becomes essential. More rigorously, the term “zoom in” can be thought of as an increase in the energy scale that is being probed.

2.1 Operator product expansion (OPE)

The effective description of a decay process is given by the effective Hamiltonian. For instance, consider the effective Hamiltonian for β decay,

$$\mathcal{H}_{eff}^{(\beta)} = \frac{G_F}{\sqrt{2}} \cos \theta_c [\bar{u}\gamma_\mu (1 - \gamma_5) d \otimes \bar{e}\gamma^\mu (1 - \gamma_5) \nu_e] \quad (2.1)$$

where equation (2.1) describe the underlying quark process of the β decay and θ_c is the Cabibbo angle. This effective interaction is shown in figure 2.1.

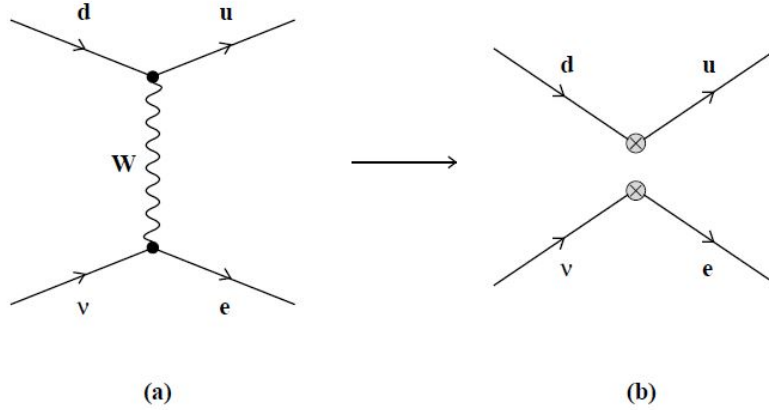


Figure 2.1: Underlying quark process of β decay. (a) represent the SM description and (b) represent the effective representation [32] .

In general, the phenomenology of any weak hadronic decay is given by the following effective Hamiltonian.

$$\mathcal{H}_{eff} = \frac{G_F}{\sqrt{2}} \sum_i V_{CKM}^i C_i(\mu) Q_i(\mu). \quad (2.2)$$

Here Q_i are relevant local operators that govern the particular decay, $C_i(\mu)$ are the Wilson coefficients, which describe the strength of a given operator that enters the Hamiltonian and V_{CKM}^i is the relevant CKM matrix element to the decay. Simply, the equation (2.2) can be thought of as a series of vertices multiplied by effective coupling constants C_i [32]. This effective series is known as an operator product expansion (OPE) [33–35]. The local operators (vertices) in the OPE involved with the strong and weak interactions, and they can be classified with respect to the Dirac structure, color structure and the type of quarks and leptons relevant for the decay.

2.1.1 OPE for B meson decays

The B meson is a bound state of a b quark and a parton (light quark). The decay of B is governed by the processes that involve W , Z and t quark, and they represent the physics

at short distance (high energy) scales $\mathcal{O}(M_{W,Z}, m_t)$. At the long distance (energy $\sim \Lambda_{\text{QCD}}$) scale, the hadronization process govern the decay since $\alpha_s(\Lambda_{\text{QCD}}) \sim \mathcal{O}(1)$, where at Λ_{QCD} the nonperturbative effects become prominent. The hadronic decay at $\mathcal{O}(m_b)$ is given by effective point like vertices, which are represented by local operators Q_i . The Wilson coefficients can be thought of as the coupling constants associated with these Q_i .

For instance, the non-leptonic B meson decays involve the following set of local operators.

Current-Current:

$$Q_1 = (\bar{c}_\alpha b_\beta)_{V-A} (\bar{s}_\beta c_\alpha)_{V-A} \quad Q_2 = (\bar{c}b)_{V-A} (\bar{s}c)_{V-A} \quad (2.3)$$

QCD-Penguins :

$$\begin{aligned} Q_3 &= (\bar{s}b)_{V-A} \sum_{q=u,d,s,c,b} (\bar{q}q)_{V-A} & Q_4 &= (\bar{s}_\alpha b_\beta)_{V-A} \sum_{q=u,d,s,c,b} (\bar{q}_\beta q_\alpha)_{V-A} \\ Q_5 &= (\bar{s}b)_{V-A} \sum_{q=u,d,s,c,b} (\bar{q}q)_{V+A} & Q_6 &= (\bar{s}_\alpha b_\beta)_{V-A} \sum_{q=u,d,s,c,b} (\bar{q}_\beta q_\alpha)_{V+A} \end{aligned} \quad (2.4)$$

Electroweak-Penguins :

$$\begin{aligned} Q_7 &= \frac{3}{2} (\bar{s}b)_{V-A} \sum_{q=u,d,s,c,b} e_q (\bar{q}q)_{V+A} & Q_8 &= \frac{3}{2} (\bar{s}_\alpha b_\beta)_{V-A} \sum_{q=u,d,s,c,b} e_q (\bar{q}_\beta q_\alpha)_{V+A} \\ Q_9 &= \frac{3}{2} (\bar{s}b)_{V-A} \sum_{q=u,d,s,c,b} e_q (\bar{q}q)_{V-A} & Q_{10} &= \frac{3}{2} (\bar{s}_\alpha b_\beta)_{V-A} \sum_{q=u,d,s,c,b} e_q (\bar{q}_\beta q_\alpha)_{V-A} \end{aligned} \quad (2.5)$$

where α and β are corresponding color indices, e_q is the electric charge of quarks. The operators Q_2, Q_{3-6} and Q_7, Q_9 are generated due to the tree level W^\pm exchange, gluon penguin and γ, Z^0 penguin diagrams respectively. The Wilson coefficients provide the contribution of the short distant (energy scale higher than μ) physics. Since QCD is asymptotically free, these Wilson coefficients can be perturbatively calculated. The C_i include the contributions from the t quark, W, Z , Higgs and SM extensions. In general, Wilson coefficients depend on m_t and the masses of new particles from SM extensions.

The scale μ separates the physics contribution to the decay amplitude to long distance and short distance. Short distance physics governs the interaction at energies that are higher

than the value of μ . Whereas, long distance physics governs the interaction at the energies lower than the value of μ . In practice μ is chosen at the order of m_b (mass of the decaying hadron). Since $\mu = \mathcal{O}(m_b) \gg \Lambda_{\text{QCD}}$, the C_i can be calculated perturbatively in B decays.

Long distance physics are contained in local matrix elements $\langle Q_i(\mu) \rangle$. Using the *renormalization group equation* (RGE) we evolve the scale from $\mu = \mathcal{O}(M_W)$ down to $\mathcal{O}(m_b)$. The full amplitude is independent of μ , and it implies the cancellation of the μ dependence in C_i with the μ dependence of $\langle Q_i(\mu) \rangle$.

2.1.1.1 Inclusive and exclusive B decays

Exclusive decays imply the measurement of energy and momenta of all the final state particles. Whereas, in *inclusive* decays the probability of particle decay into a sum of final states (X) with a given set of global quantum numbers such as energy and momentum is measured.

The amplitude for exclusive decays such as B decay in to final states $F = \pi\nu\bar{\nu}, \pi\pi, DK$ is given by

$$A(M \rightarrow F) = \langle F | \mathcal{H}_{eff} | B \rangle = \frac{G_F}{\sqrt{2}} \sum_i V_{CKM}^i C_i(\mu) \langle F | Q_i(\mu) | B \rangle \quad (2.6)$$

where $\langle F | Q_i(\mu) | B \rangle$ are the hadronic matrix elements of operators Q_i between the initial B meson state and the final state F . Evaluation of this matrix element is necessary for the calculation of the exclusive amplitude. The Wilson coefficients $C_i(\mu)$ in equation (2.6) depends on both the scale μ and the renormalization scheme that was used for local operators. This is calculated in the renormalization group improved perturbation theory. The hadronic matrix elements $\langle Q_i \rangle$ also depend on both μ and the renormalization scheme.

The evaluation of $\langle Q_i(\mu) \rangle$ requires nonperturbative methods such as lattice calculations, the $1/N_c$ expansion (N_c is the number of colors), QCD sum rules, hadronic sum rules, chiral perturbation theory and so on. Also, for some B meson decays these matrix elements can be analyzed using the *heavy quark effective theory* (HQET).

The amplitude for an inclusive B decay is given by

$$A(B \rightarrow X) = \frac{G_F}{\sqrt{2}} \sum_{f \in X} V_{\text{CKM}}^i C_i(\mu) \langle f | Q_i(\mu) | B \rangle \quad (2.7)$$

Unlike the exclusive decays, the scheme dependence in inclusive decay matrix elements can be effectively evaluated. Because of this, the cancellation of this scheme dependence with the scheme dependence in C_i can be systematically studied [36]. Therefore, studying the inclusive B meson decays become important from the practitioner's point of view.

Inclusive decays have two main advantages over exclusive decays.

- The bound state related effects such as Fermi motion [36] of heavy quark inside the hadron can be systematically described by heavy quark expansion
- The bound state effects related to the final state hadrons are removed due to the consideration of final state as a sum of hadronic channels.

The second feature is realized due to the application of *quark hadron duality* [37, 38]. This suggests that at high energy scales (μ) the cross section of hadronic decays, which are averaged over the energy range, can be approximately given by the cross sections that are evaluated by quark and gluon perturbation theory.

2.2 Heavy quark effective theory (HQET)

2.2.1 Heavy quark symmetry

Due to asymptotic freedom [40] at large momentum transfer (short distance scale), the effective coupling constants C_i become small. Whereas at low energy transfer (long-distance scale), the coupling becomes strong, and the process becomes nonperturbative. This property of QCD makes studying the processes that include decay of heavy quarks easier than the processes that include only the light quarks. These nonperturbative phenomena are dominated at the scale $R_{\text{had}} \sim 1/\Lambda_{\text{QCD}} \sim 1 \text{ fm}$ [41]. This scale also determines the size of the hadrons. When a mass of a quark (M_Q) is much larger than the Λ_{QCD} ($M_Q \gg \Lambda_{\text{QCD}}$), then we call it a heavy quark. In the SM c , b and t quarks are considered as heavy.

The system of heavy quark and light quarks is a bound state, which is complicated to analyze. The typical momentum exchange between these heavy and light constituents are of $\mathcal{O}(\Lambda_{\text{QCD}})$. This bound state of heavy quark and light quarks can be thought of as heavy quark sitting at the center of the strongly interacting cloud of *partons* (light quarks). The corresponding Compton wavelength (λ_Q) for a heavy quark is much less than the size of hadron $\lambda_Q \ll R_{\text{had}}$. This means the heavy quark's quantum numbers are resolved at very small distances compared to R_{had} . In contrast, the soft gluons exchanged between the heavy quark and the light quarks are resolved at much larger distances than the heavy quark. Due to this, the light degrees of freedom become blind to the flavor and spin orientation of the heavy quark. These light quarks will only feel the color field generated by the heavy quark, and it is extended over a larger area compared to the scale of the heavy quark. As shown above, this nature of the interactions between heavy quark and the partons provide a clear separation of scales, which makes this bound state a suitable candidate for an EFT analysis.

Since the heavy quark is irrelevant for the effective analysis, we use the limit $M_Q \rightarrow \infty$ in deriving the theory. Also, in this limit, the differences between various hadronic states that have different heavy flavors tend to have the same configuration. In fact, the configuration of these different hadronic states is determined by the configuration of the light quarks. This property provides the relation between the heavy meson states such as B, D, B^* and D^* or between the heavy baryon states such as Λ_b and Λ_c . This means if we change the heavy quark with velocity v in the system with another heavy quark with the same four-velocity and different flavor or spin, the configuration of the light quarks remains the same. Both heavy quarks will remain as static *color sources*. Therefore, we obtain a new symmetry in the effective theory, which includes N_h number of heavy quarks. This symmetry is known as *heavy quark symmetry*, and it is $SU(2N_h)$ internal continuous symmetry [41].

2.2.2 Constructing the HQET Lagrangian

Since the presence of the heavy quark is irrelevant for the configuration of light quarks, at low energies, we can construct a low energy theory in which the heavy degrees of freedom

does not appear. This is known as the “*integrating out*”. This integrating out procedure is similar to the above discussed *Fermi theory* of weak interactions.

The *heavy quark effective theory* (HQET) is constructed to simplify the complicated interaction between the heavy quark and the partons by the exchange of soft gluons [42–45]. The heavy quark masses M_Q is the high energy scale of the theory. Whereas, we construct the theory to study the interactions at the scale of Λ_{QCD} . As shown in the section 2.1.1, scale μ separates long distance and short distance physics contributions. The short distance physics are obtained at the energy scales larger than the heavy quark mass. By considering these two limits for the scale μ , we introduce the scale as in the range $\Lambda_{\text{QCD}} \ll \mu \ll M_Q$ [41].

Since we assume the heavy quark is static inside the heavy hadron’s rest frame, heavy quark’s velocity is equal to the hadron’s velocity v . Therefore, the momentum of the heavy quark inside the bound state is given by

$$p_Q^\mu = M_Q v^\mu + k^\mu, \quad (2.8)$$

where v is the four-velocity of the heavy meson, and it is given by $v = (1, 0, 0, 0)$. The $v \cdot v = 1$ and k is the residual momentum. The k determines the off-shellness of heavy quarks due to the interactions with light partons. This provides $k \sim \Lambda_{\text{QCD}} \ll M_Q v$. The changes to the heavy quark velocity v due to these soft interactions are small, and they vanish as $\Lambda_{\text{QCD}}/m_Q \rightarrow 0$.

As shown in [30,31] the near on shell Dirac spinor has two large and two small components, using this, the quantum field for the heavy quark can be defined as follows:

$$Q(x) = e^{-iM_Q v \cdot x} [h_v(x) + H_v(x)]. \quad (2.9)$$

Where $h_v(x) = e^{iM_Q v \cdot x} \frac{(1 + \psi)}{2} Q(x)$ represents the large “upper” component and $H_v(x) = e^{iM_Q v \cdot x} \frac{(1 - \psi)}{2} Q(x)$ represents the small “lower” components. These large and small com-

ponent fields satisfy $\psi h_v = h_v$ and $\psi H_v = -H_v$. Now the full QCD Lagrangian

$$\mathcal{L}_Q = \bar{Q} (i\not{D} - m_Q) Q \quad (2.10)$$

can be re written as follows:

$$\mathcal{L}_Q = \bar{h}_v i v \cdot D h_v - \bar{H}_v (i v \cdot D + 2m_Q) H_v + \bar{h}_v i \not{D}_\perp H_v + \bar{H}_v i \not{D}_\perp h_v, \quad (2.11)$$

where $D_\perp^\mu = D^\mu - v^\mu v \cdot D$ is the orthogonal component of the covariant derivative to the heavy quark velocity ($v \cdot D_\perp = 0$). In the rest frame of the heavy quark D_\perp only contains the spatial components of the covariant derivative ($D_\perp = (0, \vec{D})$). From equation (2.11), we find that h_v describes massless degree of freedom. Whereas, the H_v describes a heavy degree of freedom with mass $2M_Q$. The third and fourth terms in the equation (2.11) describe pair creation and annihilation of heavy quark and heavy anti-quark. These heavy degrees of freedom can be eliminated using the equation of motion. The HQET equation of motion provides

$$(i v \cdot D + 2M_Q) H_v = i \not{D}_\perp h_v \quad (2.12)$$

by solving the equation (2.12) for H_v

$$H_v = \frac{1}{2M_Q + i v \cdot D} i \not{D}_\perp h_v \quad (2.13)$$

This eliminate the small component of the heavy quark field in the equation (2.11).

$$\mathcal{L}_{\text{eff}} = \bar{h}_v i v \cdot D h_v + \bar{h}_v i \not{D}_\perp \frac{1}{2M_Q + i v \cdot D} i \not{D}_\perp h_v \quad (2.14)$$

In momentum space the derivatives that are acting on h_v produce powers of residual momentum k . Because of $k \ll M_Q v$, we expand the equation (2.13) in a *Taylor series*. Applying

this expansion in equation (2.14):

$$\mathcal{L}_{\text{eff}} = \bar{h}_v i v \cdot D h_v + \bar{h}_v \frac{i \not{D}_\perp}{2M_Q} \left(1 + \sum_{n=0}^{\infty} \left(-\frac{i v \cdot D}{2M_Q} \right)^n \right) i \not{D}_\perp h_v \quad (2.15)$$

For $n = 0$ the above expression can be further simplified using the following identity

$$\not{D}_\perp \not{D}_\perp = g_{\mu\nu} D_\perp^\mu D_\perp^\nu - i \sigma_{\mu\nu} D_\perp^\mu D_\perp^\nu \quad (2.16)$$

where $\sigma_{\mu\nu} = \frac{i}{2} [\gamma_\mu, \gamma_\nu]$. Following from this the resulting Lagrangian is obtained as an expansion in $1/M_Q^n$.

$$\mathcal{L}_{\text{eff}} = \bar{h}_v \left(i v \cdot D - \frac{D^2}{2M_Q} - \frac{g}{4M_Q} \sigma_{\mu\nu} G^{\mu\nu} \right) h_v + O\left(\frac{1}{M_Q^2}\right), \quad (2.17)$$

where, $G^{\mu\nu}$ is Chromo-electromagnetic field strength tensor.

In the limit $M_Q \rightarrow \infty$ only the first term in equation (2.17) remains

$$\mathcal{L}_\infty = \bar{h}_v i v \cdot D h_v. \quad (2.18)$$

2.2.2.1 Operators at order $\mathcal{O}(1/M_Q)$ in the HQET Lagrangian

Consider the second and the third terms in equation (2.17). The operator,

$$\mathcal{O}_{\text{kin}} = \frac{1}{2M_Q} \bar{h}_v (i D_\perp)^2 h_v \rightarrow -\frac{1}{2M_Q} \bar{h}_v (i \vec{D})^2 h_v, \quad (2.19)$$

is the kinematic energy of the heavy quark's residual motion. The operator, \mathcal{O}_{mag} defined in equation (2.20) is the color-magnetic coupling between heavy quark spin and gluon field.

$$\mathcal{O}_{\text{mag}} = \frac{g_s}{4M_Q} \bar{h}_v \sigma_{\mu\nu} G^{\mu\nu} h_v \rightarrow -\frac{g_s}{M_Q} \bar{h}_v \vec{S} \cdot \vec{B}_c h_v, \quad (2.20)$$

where \vec{S} are the Pauli spin matrix elements, and $B_c^i = -\frac{1}{2}\epsilon^{ijk}G^{jk}$, which are the components of color magnetic field. [46–48].

2.3 Non-relativistic QCD

HQET describes systems that include a single heavy quark and light partons. In HQET the heavy quark's kinetic energy is considered as a power correction. When considering multiple heavy quarks the strong interaction between them at short distances is determined by a single gluon exchange [12]. This gluon exchange is defined by a Coulomb potential, and for $\bar{Q}Q$ in a color single state this potential is an attractive potential. This attractive potential is then compensated by heavy quark kinetic energy. This makes the kinetic energy of the heavy quark field play an important role in stabilizing the heavy mesons. The heavy quark kinetic energy cannot be treated as a power correction. Thus, we use a different power counting scheme in NRQCD compared to HQET. This difference is further illustrated in the following example.

Consider the figure 2.2, which represents a box diagram with two heavy quarks exchange gauge particles (gluons or photons).

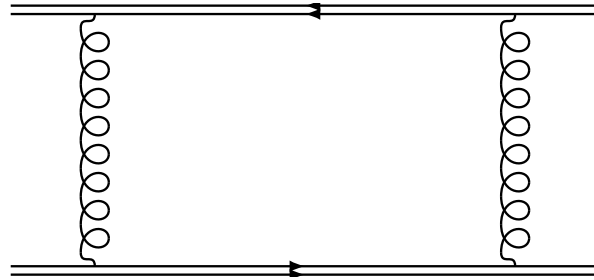


Figure 2.2: Box diagram for two heavy quark exchanging gauge particles

The integral I that corresponds to the figure 2.2 is given by [31]

$$I \sim \int \frac{d^d q}{(2\pi)^d} \frac{1}{q^0 + i\epsilon} \frac{1}{-q^0 + i\epsilon} \frac{1}{(q+k)^2 + i\epsilon} \frac{1}{(q-k)^2 + i\epsilon} \quad (2.21)$$

In the equation (2.21), we find two poles at $q^0 = \pm i\epsilon$. These poles are coming from

the heavy quark propagators, and they cause a “pinch singularity”. As a result, we cannot deform the contour of the integration without crossing one of these poles [31]. To overcome this singularity we need to introduce a new power counting scheme. In this new power counting scheme the importance of the heavy quark kinetic energy is pronounced.

In NRQCD the quarkonium is described by an effective Lagrangian, which is expanded as a power series in v/c , where c is the vacuum speed of light. The NRQCD Lagrangian can be obtained by using the $c \rightarrow \infty$ limit in the full QCD Lagrangian.

2.3.1 NRQCD Lagrangian

As shown above, the difference between the HQET and NRQCD is manifested in the first two terms of the effective Lagrangian.

$$\mathcal{L} = Q^\dagger (iD^0)Q + Q^\dagger \frac{\mathbf{D}^2}{2m}Q. \quad (2.22)$$

In HQET the first term is of $\mathcal{O}(\Lambda_{\text{QCD}})$ and second term is considered as a correction term of $\mathcal{O}(\Lambda_{\text{QCD}}^2/m)$. Whereas, in NRQCD both terms are of $\mathcal{O}(mv^2)$. Because of this, the heavy quark propagator in both effective theories have different forms. For instance, the heavy quark propagator in HQET is given by $i/(k^0 + i\epsilon)$. The NRQCD heavy quark propagator is given by

$$\frac{i}{(k^0 - \mathbf{k}^2/2m + i\epsilon)} \quad (2.23)$$

This full NRQCD propagator causes problems in matching calculations. As shown above, the HQET propagator is m_Q independent. Because of this we count the powers of $1/m_Q$ directly from the vertex factors. For instance, if $s < r$ the effective vertex of $\mathcal{O}(1/m_Q^r)$ does not provide any contribution to terms of $\mathcal{O}(1/m_Q^s)$. Then the matching in HQET is done by expanding Greens function to the desired order in $1/m_Q$. But the NRQCD propagator contains additional power suppressed factors. These factors can wreck the simple power counting of Greens function [31]. The solution for this problem is provided in [55].

In [55] the full NRQCD propagator is expanded, and the extra terms were treated as a perturbation. The expansion of full NRQCD propagator is given by

$$\frac{1}{k^0 - \mathbf{k}^2/2m + i\epsilon} = \frac{1}{k^0} + \frac{\mathbf{k}^2}{2m(k^0)^2} + \dots \quad (2.24)$$

The series expansion of propagator prevents the appearance of positive powers of the mass terms. Whereas, the full NRQCD propagator provides these positive powers. Thus, by expanding the NRQCD propagator the NRQCD and HQET matching conditions can be computed using the same procedure.

The NRQCD Lagrangian upto dimension seven ($\mathcal{O}(1/m^3)$) is provided in equation (4.43). This Lagrangian is computed to one loop, and it only considers the terms that are bilinear in fermions [55]. In equation (4.56) we provide the dimension eight Lagrangian. This is first obtained in our work [56].

2.4 Applications

2.4.1 Heavy quark spectroscopy

As shown in the section 2.2.1, the dynamics of hadronic bound state with one heavy quark does not depend on its heavy quark's flavor or spin. Because of this, states with different heavy quark flavors can be related to each other. The hadronic states, therefore, are classified by the quantum numbers of the light degrees of freedom [59]. From the spin symmetry we find that the total spin of these partons are doubly degenerated with total spin $J = j \pm \frac{1}{2}$ [60].

The mass of a hadron H_Q is related to it's heavy quark as follows:

$$M_{H_Q} = M_Q + \bar{\Lambda} + \frac{\Delta M^2}{2M_Q} + O(1/M_Q^2), \quad (2.25)$$

where $\bar{\Lambda} = M_{H_Q} - M_Q$ and ΔM^2 is originated from the order $1/M_Q$ terms in effective

Lagrangian. In particular, the mass splitting (ΔM^2) for heavy hadrons are defined as

$$\Delta M^2 = -\lambda_1 + 2 \left[J(J+1) - \frac{3}{2} \right] \lambda_2, \quad (2.26)$$

where λ_1 and λ_2 are nonperturbative parameters, which parametrize the kinetic energy and the chromo-magnetic interaction of heavy quark in heavy hadron. For instance, consider the B and B^* mesons. These hadronic states are the members of spin doublet $j = \frac{1}{2}$, and they are ground-state pseudo scalar ($J = 0$) and vector ($J = 1$) states respectively. Using the equations (2.25) and (2.26) we obtain

$$\begin{aligned} M_B &= M_b + \bar{\Lambda} - \frac{\lambda_1}{2M_b} - \frac{3\lambda_2}{2M_b} \\ M_{B^*} &= M_b + \bar{\Lambda} - \frac{\lambda_1}{2M_b} + \frac{\lambda_2}{2M_b} \end{aligned} \quad (2.27)$$

Therefore, the mass splitting between these states is given by

$$M_{B^*}^2 - M_B^2 = 4\lambda_2 + O(1/M_b) \quad (2.28)$$

PDG average for the B and B^* mass splitting is

$$M_{B^*}^2 - M_B^2 = 0.478 \pm 0.003 \text{ GeV}^2 \quad (2.29)$$

From this we obtain

$$\lambda_2 = 0.119 \pm 0.001 \text{ GeV}^2 \quad (2.30)$$

These results are obtained by assuming the $m_b \rightarrow \infty$ limit.

The nonperturbative parameter λ_1 contains the information about “smearing” in heavy

quark momentum [63]. This parameter is defined as

$$2\lambda_1 = -\langle H_Q | \bar{h}_v D_\perp^2 h_v | H_Q \rangle. \quad (2.31)$$

The λ_1 can be calculated using the QCD sum rule approach [63]. Theoretical estimate for the λ_1 is given in [64].

CHAPTER 3 BACKGROUND : THE $\bar{B} \rightarrow X_s \gamma$ DECAY

The inclusive radiative $\bar{B} \rightarrow X_s \gamma$ decay is an important new physics probe. Since this is a FCNC process, it does not occur at tree level in the SM. Therefore, it can be highly sensitive to new physics. In particular, these new physics sources can modify the Wilson coefficient $C_{7\gamma}$, and they may introduce new weak phases that can enhance the SM CP asymmetry.

The $b \rightarrow s \gamma$ is the underlying partonic decay of the inclusive $B \rightarrow X_s \gamma$ decay. This b to s transition is one of the most reliably calculable FCNC processes in SM [66]. The final states X_s represent a final state that contains a s quark

The current SM next to-next to leading (NNLO) prediction for the $\bar{B} \rightarrow X_s \gamma$ branching ration is $\mathcal{B}_{X_s \gamma}^{\text{SM}} = (3.36 \pm 0.23) \times 10^{-4}$ [27, 69]. The experimental world average is $\mathcal{B}_{X_s \gamma}^{\text{exp}} = (3.32 \pm 0.15) \times 10^{-4}$ [70–76]. The experimental uncertainty on the branching ratio is expected to reduce from $\pm 4.5\%$ to around $\pm 2.6\%$ in future thanks to Belle II measurements [79]. With these new precision measurements, SM prediction can strongly constrain the BSM. Therefore, improving the precision of the theoretical prediction is important.

The uncertainty of the SM prediction arise from several sources. These uncertainties were combined in quadrature to obtain the total uncertainty ($\pm 6.8\%$). The breakdown of these uncertainties is as follows: The nonperturbative contribution to the uncertainty is $\pm 5\%$ [78], parametric uncertainty is $\pm 2\%$, perturbative uncertainty is $\pm 3\%$, the uncertainty from interpolating the charm mass in two-loop is $\pm 3\%$ [69].

Since the nonperturbative uncertainty provides the largest contribution to the total uncertainty, we would like to explore the possibility of improving this estimate. The question that we are prompt to ask is “how do we reduce this uncertainty?”. In the following work, we address the issue of reducing the nonperturbative contribution of the theoretical prediction.

3.1 The inclusive decay rate

The inclusive decay rate for the $\bar{B} \rightarrow X_s \gamma$ is obtained by using the optical theorem. This theorem relates the decay rate to the imaginary part of the forward scattering amplitude.

The $\bar{B} \rightarrow X_s \gamma$ decay is can be written as

$$\Gamma(\bar{B} \rightarrow X_s \gamma) = \frac{1}{M_B} \text{Im} \langle \bar{B} | \mathbf{T} | \bar{B} \rangle, \quad (3.1)$$

where \mathbf{T} is related to the effective Lagrangian. However, instead of effective Lagrangian we use the effective Hamiltonian (\mathcal{H}_{eff})

$$\mathbf{T} = i \int d^4x T \{ \mathcal{H}_{\text{eff}}(x), \mathcal{H}_{\text{eff}}(0) \}, \quad (3.2)$$

where \mathcal{H}_{eff} is obtained after integrating out the W boson [78]. The effective Hamiltonian is given by

$$\mathcal{H}_{\text{eff}} = \frac{G_F}{\sqrt{2}} \sum_{q=u,c} \lambda_q \left(C_1 Q_1^q + C_2 Q_2^q + \sum_{i=3,\dots,6} C_i Q_i + C_{7\gamma} Q_{7\gamma} + C_{8g} Q_{8g} \right), \quad (3.3)$$

where $\lambda_q = V_{qb}V_{qs}^*$, C_i are the Wilson coefficients and Q_i are the effective operators. This Hamiltonian describes the underlying are weak interaction in the decay process.

The decay rate and the photon spectrum related to the restricted discontinuity of forward scattering matrix element [78].

$$d\Gamma(\bar{B} \rightarrow X_s \gamma) \propto \text{Disc}_{\text{restr}} \left[i \int d^4x \langle \bar{B} | \mathcal{H}_{\text{eff}}^\dagger(x) \mathcal{H}_{\text{eff}}(0) | \bar{B} \rangle \right], \quad (3.4)$$

where the restricted discontinuity implies that the discontinuity is restricted by the requirement that the cut must be applied on photon and strange quark propagators.

3.1.1 Kinematics of the decay

In its rest frame, the B meson is decaying into a hadronic jet, which carries a momentum P_X , and to a photon, which carries a momentum q . The momentum of the heavy hadron is $M_B v = P_X + q$, where v is the four velocity of the B meson. In the B meson rest frame $v = (1, 0, 0, 0)$. We can align \vec{q} in the negative z direction and define two light-like vectors $n^\mu = (1, 0, 0, 1)$ and $\bar{n}^\mu = (1, 0, 0, -1)$. These n and \bar{n} vectors satisfy $\bar{n} + n = 2v$, $\bar{n} \cdot n = 2$

and $n \cdot v = \bar{n} \cdot n = 1$ [80]. In general, any four vector can be decomposed as

$$a^\mu = \bar{n} \cdot a \frac{n^\mu}{2} + n \cdot a \frac{\bar{n}^\mu}{2} + a_\perp^\mu. \quad (3.5)$$

For the choice of v, n, \bar{n} the transverse component (\perp) is spanned by $(0, 1, 0, 0)$ and $(0, 0, 1, 0)$. These transverse indices can be contracted using

$$g_\perp^{\mu\nu} = g^{\mu\nu} - \frac{n^\mu \bar{n}^\nu + n^\nu \bar{n}^\mu}{2}, \quad \epsilon_\perp^{\mu\nu} = \frac{1}{2} \epsilon^{\mu\nu\alpha\beta} \bar{n}_\alpha n_\beta \quad (3.6)$$

where we use the following convention for the levi-civita tensor $\epsilon_{0123} = 1$.

The conservation of four momentum provides that there is only one independent kinematical variable in $\bar{B} \rightarrow X_s \gamma$ decay that is the photon energy E_γ .

3.1.2 Factorization

At the leading order the $\bar{B} \rightarrow X_s \gamma$ decay can be thought of as a decay of constituent b quark decaying into an s quark and a photon. This constituent quark decay is expressed by the electromagnetic dipole operator $Q_{7\gamma}$

$$Q_{7\gamma} = \frac{-em_b}{8\pi^2} \bar{s} \sigma_{\mu\nu} (1 + \gamma_5) F^{\mu\nu} b. \quad (3.7)$$

However, this is not the only way to produce a photon. For instance, a gluon or a quark pair that was produced at the weak vertex can be converted to a photon, and these processes are described by the operators $Q_{8g} = (-g/8\pi^2) m_b \bar{s} \sigma_{\mu\nu} G^{\mu\nu} (1 + \gamma_5) b$ and $Q_1^c = (\bar{c}b)_{V-A} (\bar{s}c)_{V-A}$ respectively. The effective Hamiltonian for $\bar{B} \rightarrow X_s \gamma$ needs to account for all of these operators to accurately describe the decay process.

The major contribution to the effective Hamiltonian arises from the operators $Q_1^q, Q_{7\gamma}$ and Q_{8g} [78]. This is because the Wilson coefficients of these operators are relatively larger than the rest.

At the leading order the only the operator pair $Q_{7\gamma} - Q_{7\gamma}$ contributes to the decay rate.

The contributions from operators such as Q_1^q and Q_{8g} give higher order contributions, and they either “cost” a factor of α_s or $1/m_b$ in the decay rate calculation.

The shape of the $\bar{B} \rightarrow X_s \gamma$ photon spectrum probes the nonperturbative hadronic physics in the decay. At the leading order this photon spectrum is related to a universal shape function that parametrizes the b quark momentum in the B meson bound state. This shape function also parameterizes the leading order bound state effects of semileptonic decay $\bar{B} \rightarrow X_u l \nu$. However, the contributions of operators other than $Q_{\tau\gamma} - Q_{\gamma\tau}$ to $\bar{B} \rightarrow X_s \gamma$ make the analysis of the photon spectrum more involved than the semileptonic $\bar{B} \rightarrow X_u l \nu$ decays. This is manifested in their corresponding factorization theorems. For instance, the factorization theorem for the $\bar{B} \rightarrow X_u l \nu$ decay in the end point region can be schematically expressed as follows [81–83]:

$$d\Gamma(\bar{B} \rightarrow X_u l \bar{\nu}) = \sum_{n=0}^{\infty} \frac{1}{m_b^n} \sum_i H_i^{(n)} J_i^{(n)} \otimes S_i^{(n)}, \quad (3.8)$$

where the hard functions $H_i^{(n)}$ paramterize the physics at the scale of m_b , the jet functions $J_i^{(n)}$ provides the physics of hadronic final state X_u , which has the invariant mass $M_X \sim \sqrt{m_b \Lambda_{\text{QCD}}}$, and the soft function $S_i^{(n)}$ describes the hadronic physics at the scale Λ_{QCD} . These soft functions are defined as forward scattering non-local HQET matrix elements. The symbol \otimes represents convolution [78].

The higher order processes that were discussed above are known as *resolved photon contributions* [78]. These processes describe the photon coupling to light partons instead of directly connecting to the effective weak vertex. The presence of the resolved photon contributions complicates the decay rate calculation compared to the processes that contain only the direct photon coupling processes. By considering all these effects the factorization

theorem for the $\bar{B} \rightarrow X_s \gamma$ decay can be schematically represented as [78]:

$$d\Gamma(\bar{B} \rightarrow X_s \gamma) = \sum_{n=0}^{\infty} \frac{1}{m_b^n} \sum_i H_i^{(n)} J_i^{(n)} \otimes S_i^{(n)} + \sum_{n=1}^{\infty} \frac{1}{m_b^n} \left[\sum_i H_i^{(n)} J_i^{(n)} \otimes S_i^{(n)} \otimes \bar{J}_i^{(n)} + \sum_i H_i^{(n)} J_i^{(n)} \otimes S_i^{(n)} \otimes \bar{J}_i^{(n)} \otimes \bar{J}_i^{(n)} \right]. \quad (3.9)$$

Note that equation (3.9) contains both direct contributions, which are similar to the contributions present in equation (3.8), and resolved photon contributions. The resolved photon contributions probe the hadronic substructure of the photon at the scale $\sqrt{2E_\gamma \Lambda_{\text{QCD}}}$. The effect of these new sub-processes requires new jet functions $\bar{J}_i^{(n)}$. In equation (3.9), we find two types of resolved photon contributions. The term $\sum_i H_i^{(n)} J_i^{(n)} \otimes S_i^{(n)} \otimes \bar{J}_i^{(n)}$ refers to single resolved photon contribution. Whereas, the term $\sum_i H_i^{(n)} J_i^{(n)} \otimes S_i^{(n)} \otimes \bar{J}_i^{(n)} \otimes \bar{J}_i^{(n)}$ refers to double resolved photon contributions. The graphical illustration of $\bar{B} \rightarrow X_s \gamma$ factorization is provided in the figure 3.1

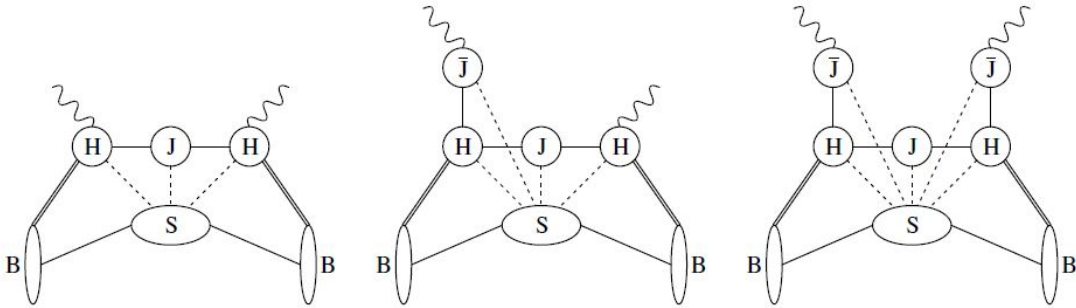


Figure 3.1: Graphical illustration of the factorization for $\bar{B} \rightarrow X_s \gamma$ decay [78]

Note that this notation is symbolic. Because of this different quantities in different terms can be represented by the same symbol.

3.1.3 Review of the known results

The factorization formula for the CP-averaged $\bar{B} \rightarrow X_s \gamma$ photon spectrum at the end point region is

$$\frac{d\Gamma}{dE_\gamma} = \frac{G_F^2 \alpha |V_{tb} V_{ts}^*|^2}{2\pi^4} \bar{m}_b^2(\mu) E_\gamma^3 \left[|H_\gamma(\mu)|^2 \int_{-p_+}^{\bar{\Lambda}} d\omega m_b J(m_b(\omega + p_+), \mu) S(\omega, \mu) + \frac{1}{m_b} \sum_{i \leq j} \text{Re}[C_i^*(\mu) C_j(\mu)] F_{ij}(E_\gamma, \mu) + \dots \right], \quad (3.10)$$

where $p_+ \equiv m_b - 2E_\gamma = \mathcal{O}(\Lambda_{\text{QCD}})$, $\bar{\Lambda}$ is defined as $\bar{\Lambda} = M_B - m_b$ and the ellipses denotes the order $1/m_b^2$ terms. The b quark mass is defined in the $\overline{\text{MS}}$ scheme (see appendix 7.2).

The first line in the equation represents the leading power contribution, and an extensive discussion regarding this contribution can be found in [80, 85]. The hard function $H_\gamma(\mu)$ is the matching coefficient, and it is $H_\gamma(\mu) = C_{7\gamma}(\mu) + \mathcal{O}(\alpha)$. In particular, this was obtained by matching the leading current operator to the soft collinear effective field theory (SCET). Also, this current receives contributions from all the operators in the effective Hamiltonian. The dominant contribution is received from $Q_{7\gamma}$, and this is known to $\mathcal{O}(\alpha_s^2)$ [86]. The contributions from the operators other than $Q_{7\gamma}$ are known for $\mathcal{O}(\alpha_s)$ [78]. The $H_\gamma(\mu)$ receives virtual corrections of the scale $\mu_h \sim m_b$.

By matching the current operator further onto HQET the single jet function $J(p^2, \mu) = \delta(p^2) + \mathcal{O}(\alpha_s)$ arises. The jet functions describe the cut dependent effects. Specifically, $J(p^2, \mu)$ is obtained by the discontinuity of the quark propagator in the axial gauge [87]. In particular, the jet function describe the properties of the final state hadronic jet. In the end point region the mass of jet scales as $\mu_{hc} \sim \sqrt{m_b \Lambda_{\text{QCD}}}$.

The shape function $S(\omega, \mu)$ is a soft function defined by the HQET matrix element [88]:

$$S(\omega, \mu) = \int \frac{dt}{2\pi} e^{-i\omega t} \frac{\langle \bar{B}(v) | \bar{h}(tn) S_n(tn) S_n^\dagger(0) h(0) | \bar{B}(v) \rangle}{2M_B}, \quad (3.11)$$

where the soft Wilson line is defined by

$$S_n(x) = \mathbf{P} \exp \left(ig \int_{-\infty}^0 du n \cdot A_s(x + un) \right). \quad (3.12)$$

The path ordering \mathbf{P} in equation (3.12) means that the fields with larger u value are placed to the left of those fields with smaller u values. The conjugate Wilson line S_n^\dagger has the opposite path ordering relative to S_n . The combination $S_n(tn)S_n^\dagger(0) = [tn, 0]$ is a straight line segment, which connects the points tn and 0 . The soft function S encodes the nonperturbative hadronic physics associated with the soft scale $\mu_s \sim p_+ \sim \Lambda_{\text{QCD}}$.

The power suppressed terms in the equation (3.10) are given by [78]

$$\begin{aligned} F_{77}(E_\gamma, \mu) &= \frac{C_F \alpha_s(\mu)}{4\pi} \int_{-p_+}^{\bar{\Lambda}} d\omega \left(16 \ln \frac{m_b(\omega + p_+)}{\mu^2} + 9 \right) S(\omega, \mu) + F_{77}^{\text{SSF}}(E_\gamma, \mu) \\ F_{88}(E_\gamma, \mu) &= \frac{C_F \alpha_s(\mu)}{4\pi} \int_{-p_+}^{\bar{\Lambda}} d\omega \left(\frac{2}{9} \ln \frac{m_b(\omega + p_+)}{\mu^2} - \frac{1}{3} \right) S(\omega, \mu) + 4\pi \alpha_s(\mu) f_{88}(-p_+, \mu) \\ F_{78}(E_\gamma, \mu) &= \frac{C_F \alpha_s(\mu)}{4\pi} \frac{10}{3} \int_{-p_+}^{\bar{\Lambda}} d\omega S(\omega, \mu) + 4\pi \alpha_s(\mu) \text{Re} \left[f_{78}^{(\text{I})}(-p_+, \mu) + f_{78}^{(\text{II})}(-p_+, \mu) \right] \\ F_{17}(E_\gamma, \mu) &= \frac{C_F \alpha_s(\mu)}{4\pi} \left(-\frac{2}{3} \right) \int_{-p_+}^{\bar{\Lambda}} d\omega S(\omega, \mu) + \sum_{q=c,u} \delta_q \text{Re} f_{17,q}(-p_+, \mu) \\ F_{11}(E_\gamma, \mu) &= F_{18}(E_\gamma, \mu) = \frac{C_F \alpha_s(\mu)}{4\pi} \frac{2}{9} \int_{-p_+}^{\bar{\Lambda}} d\omega S(\omega, \mu), \end{aligned} \quad (3.13)$$

where

$$\begin{aligned} F_{77}^{\text{SSF}}(E_\gamma, \mu) &= p_+ S(-p_+, \mu) + s(-p_+, \mu) - t(-p_+, \mu) + u(-p_+, \mu) - v(-p_+, \mu) \\ &\quad - \pi \alpha_s(\mu) \left[f_u^{(s)}(-p_+, \mu) + f_v^{(s)}(-p_+, \mu) \right] + \mathcal{O} \left(\frac{\alpha_s(\mu)}{4\pi} \right). \end{aligned} \quad (3.14)$$

The soft functions in F_{77}^{SSF} are called subleading shape function, and they describe the direct photon contributions from the operator pair $Q_{7\gamma} - Q_{\bar{7}\gamma}$ [89]. The definitions of the soft

functions S, s, t, u, v, f_u and $f_v^{(s)}$ are given as [80, 89]:

$$\begin{aligned}
\langle (\bar{h}S)_0 (S^\dagger h)_{x_-} \rangle &= \int d\omega e^{-\frac{i}{2}\omega\bar{n}\cdot x} S(\omega) \\
\langle i \int d^4z T \left\{ (\bar{h}S)_0 (S^\dagger h)_{x_-} \mathcal{L}_h^{(2)}(z) \right\} \rangle &= \frac{1}{m_b} \int d\omega e^{-\frac{i}{2}\omega\bar{n}\cdot x} s(\omega) \\
\langle \bar{h}(0) \not{h} [0, x_-] (i \not{D}_\perp h) (x_-) \rangle &= \int d\omega e^{-\frac{i}{2}\omega\bar{n}\cdot x} t(\omega) \\
-i \int_0^{\bar{n}\cdot x/2} dt \langle \bar{h}(0) [0, tn] (iD_\perp)^2 (tn) [tn, x_-] h(x_-) \rangle &= \int d\omega e^{-\frac{i}{2}\omega\bar{n}\cdot x} u(\omega) \\
-i \int_0^{\bar{n}\cdot x/2} dt \langle \bar{h}(0) \frac{\not{h}}{2} [0, tn] \sigma_{\mu\nu}^\perp g G_\perp^{\mu\nu} (tn) [tn, x_-] h(x_-) \rangle &= \int d\omega e^{-\frac{i}{2}\omega\bar{n}\cdot x} v(\omega),
\end{aligned} \tag{3.15}$$

and

$$\begin{aligned}
2(-i)^2 \int_0^{\bar{n}\cdot x/2} \int_{t_1}^{\bar{n}\cdot x/2} dt_2 \langle [(\bar{h}S)_0 t_a]_k [t_a (S^\dagger h)_{x_-}]_l [(\bar{q}S)_{t_2 n}]_l \mu [(S^\dagger q)_{t_1 n}]_k \rangle \\
= \int d\omega e^{-\frac{i}{2}\omega\bar{n}\cdot x} f_u(\omega) \\
\bar{n}\cdot x / 2 \bar{n}\cdot x / 2 \\
2(-i)^2 \int_0^0 dt_1 \int_{t_1}^{\bar{n}\cdot x/2} dt_2 \langle [(\bar{h}S)_0 t_a]_k \not{\mu} \gamma_5 [t_a (S^\dagger h)_{x_-}]_l [(\bar{q}S)_{t_2 n}]_l \mu \gamma_5 [(S^\dagger q)_{t_1 n}]_k \rangle \\
= \int d\omega e^{-\frac{i}{2}\omega\bar{n}\cdot x} f_v(\omega),
\end{aligned} \tag{3.16}$$

where k, l are color indices and

$$\langle \bar{h} \dots h \rangle \equiv \frac{\langle \bar{B}(v) | \bar{h} \dots h | \bar{B}(v) \rangle}{2m_B}. \tag{3.17}$$

The term \mathcal{L}_h in equation (3.15) is the next-to-leading term in the HQET Lagrangian, which was defined in equation (2.17). Following from this, we find

$$\mathcal{L}_h^{(2)} = \frac{1}{2m_b} \left[\bar{h} (iD_s)^2 h + \frac{C_{\text{mag}}}{2} \bar{h} \sigma_{\mu\nu} g G_s^{\mu\nu} h \right]. \tag{3.18}$$

Only the operators $Q_1^q - Q_{7\gamma}, Q_{7\gamma} - Q_{8g}$ are $Q_{8g} - Q_{8g}$ arise at order $1/m_b$ in equation (3.10).

The resolved photon contribution provide the largest uncertainty on the decay rate. Because of this, it is important to understand the nature of these operators. In the next section we describe them.

3.1.3.1 Contribution from $Q_1^q - Q_{7\gamma}$

In the equation (3.13) the direct photon contributions from F_{17} are given by

$$F_{17}(E_\gamma, \mu) = \frac{C_F \alpha_s(\mu)}{4\pi} \left(-\frac{2}{3} \right) \int_{-p_+}^{\bar{\Lambda}} d\omega S(\omega, \mu) \quad (3.19)$$

The resolved photon contribution of the operator pair $Q_1^q - Q_{7\gamma}$ is suppressed by a factor Λ_{QCD}/m_b . By matching this operator pair to the SCET we obtain the diagram in the figure 3.2 (a). Also, by integrating out the (anti)-hard collinear fields we obtain the diagram in the figure 3.2 (b) [78].

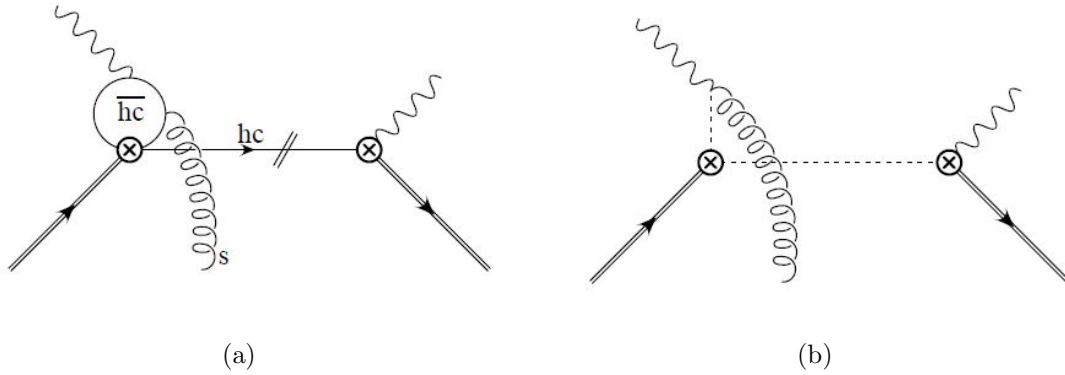


Figure 3.2: Figure (a) represent the diagram arised by matching the $Q_1^q - Q_{7\gamma}$ operator to SCET. Figure (b) represents the diagram obtained by matching same process to HQET [78].

The single resolved photon contribution of the operator $Q_1^q - Q_{7\gamma}$ is given by a non local soft function [78]

$$f_{17,q}(\omega, \mu) = \frac{2}{3} \int_{-\infty}^{\infty} \frac{d\omega_1}{\omega_1 + i\varepsilon} \left[1 - F \left(\frac{m_q^2 - i\varepsilon}{(m_b + \omega) \omega_1} \right) \right] g_{17}(\omega, \omega_1, \mu), \quad (3.20)$$

where the penguin function F is defined as

$$F(x) = 4x \arctan^2 \left(\frac{1}{\sqrt{4x-1}} \right). \quad (3.21)$$

The expansion of $F(x)$ around $x = 0$ is

$$1 - F(x) = -\frac{1}{12x} - \frac{1}{90x^2} - \frac{1}{560x^3} - \dots \quad (3.22)$$

The soft function $g_{17}(\omega, \omega_1, \mu)$ is defined as

$$g_{17}(\omega, \omega_1, \mu) = \int \frac{dr}{2\pi} e^{-i\omega_1 r} \int \frac{dt}{2\pi} e^{-i\omega t} \times \frac{\langle \bar{B} | (\bar{h} S_n)(tn) \bar{\eta} (1 + \gamma_5) (S_n^\dagger S_{\bar{n}})(0) i\gamma_\alpha^\perp \bar{n}_\beta (S_{\bar{n}}^\dagger g_s^{\alpha\beta} S_{\bar{n}})(r\bar{n}) (S_{\bar{n}}^\dagger h)(0) | \bar{B} \rangle}{2M_B}, \quad (3.23)$$

where r and t are defined utilizing the topology of the HQET diagrams. For example, the weak vertex in the figure 3.2 (b) is at $x = tn + x_+ + x_\perp$ and the vertex of the soft gluon is defined at $y = r\bar{n} + y_- + y_\perp$.

The variables ω and ω_1 in equation (3.23) are defined using the light cone projections of parton momenta in B meson. Since the total parton momenta including b quark is equal to $M_B v$, the momentum of the partons in the B meson can be given as

$$\sum_{i \neq b} n \cdot p_i + n \cdot k = \bar{\Lambda}, \quad \sum_{i \neq b} \bar{n} \cdot p_i + \bar{n} \cdot k = \bar{\Lambda}, \quad (3.24)$$

where k is the residual momentum and $\bar{\Lambda} = M_B - m_b$. Also, note that these light cone projections of parton momenta $n \cdot p_i$ and $\bar{n} \cdot p_i$ are non negative. This provides $(n \cdot k, \bar{n} \cdot k) > -m_b$ for $i \neq b$. Besides, it implies $-\infty < n \cdot k \leq \bar{\Lambda}$ and $0 \leq \bar{n} \cdot p_i < \infty$ in the heavy quark

limit. These conditions are extended to $\bar{n} \cdot k$ and $\bar{n} \cdot p_i$ as well. Intuitively, the ω in soft function g_{17} can be thought of as the residual momentum component $n \cdot k$ of the initial state heavy quark. The ω_1 corresponds to either the momentum component $n \cdot p_g$ in final state B meson or the component $-n \cdot p_g$ in initial state B meson. Furthermore, this implies that $-\infty < \omega \leq \bar{\Lambda}$, and $-\infty < \omega_1 < \infty$.

The direct photon contributions and resolved photon contributions are combined into the final expression for F_{17} in equation (3.13) as

$$F_{17}(E_\gamma, \mu) = \frac{C_F \alpha_s(\mu)}{4\pi} \left(-\frac{2}{3} \right) \int_{-p_+}^{\bar{\Lambda}} d\omega S(\omega, \mu) + \sum_{q=c,u} \delta_q \text{Re} f_{17,q}(-p_+, \mu), \quad (3.25)$$

where

$$\delta_q = \frac{\text{Re} [\lambda_q C_1(\mu) (-\lambda_t^*) C_{7\gamma}^*(\mu)]}{|\lambda_t|^2 \text{Re} [C_1(\mu) C_{7\gamma}^*(\mu)]}, \quad \lambda_q = V_{qb} V_{qs}^*. \quad (3.26)$$

3.1.3.2 $Q_{7\gamma} - Q_{8g}$ contribution

The direct photon contribution from the operator pair $Q_{7\gamma} - Q_{8g}$ is given by

$$F_{78}^{(a)}(E_\gamma, \mu) = \frac{C_F \alpha_s(\mu)}{4\pi} \frac{m_b}{2E_\gamma} \frac{10}{3} \int_{-p_+}^{\bar{\Lambda}} d\omega S(\omega, \mu) \quad (3.27)$$

The operator Q_{8g} provides two SCET operators, and these operators are combined with the tree level SCET operator arising in $Q_{7\gamma}$. These two operators provide the $Q_{7\gamma} - Q_{8g}$ contribution. Figure 3.3 was obtained by matching the SCET operators onto HQET operators [78].

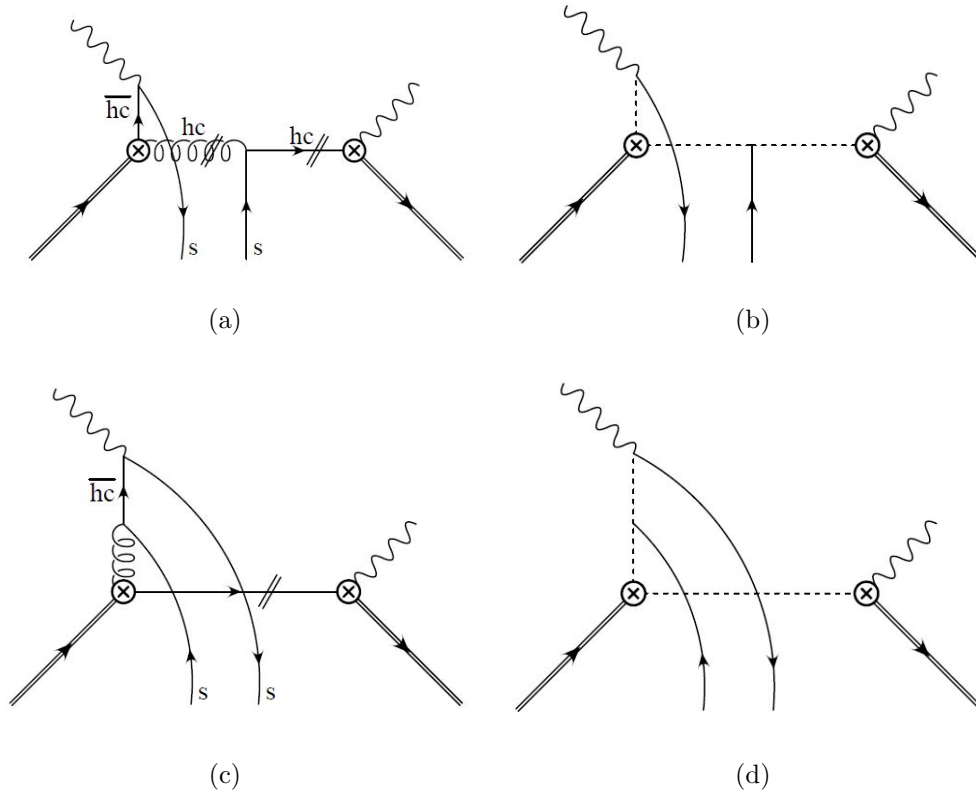


Figure 3.3: Figure (a) and (c) represent the diagrams arised by matching the $Q_{7\gamma} - Q_{8g}$ operator to SCET. Figure (b) and (d) represents the diagrams obtained by matching same processes to HQET [78].

The contribution from the operator pair $Q_{7\gamma} - Q_{8g}$ to the photon spectrum is provided as [78]

$$\begin{aligned}
 F_{78}(E_\gamma, \mu) = & \frac{C_F \alpha_s(\mu)}{4\pi} \frac{m_b}{2E_\gamma} \frac{10}{3} \int_{-p_+}^{\bar{\Lambda}} d\omega S(\omega, \mu) \\
 & + 4\pi \alpha_s(\mu) \frac{m_b}{2E_\gamma} \text{Re} \left[f_{78}^{(I)}(-p_+, \mu) + f_{78}^{(II)}(-p_+, \mu) \right],
 \end{aligned} \tag{3.28}$$

where $f^{(I)}$ and $f^{(II)}$ are soft functions that encode the long distance physics. Unfortunately there is little information on these functions. The effect of these soft functions can be roughly approximated using *vacuum insertion approximation* (VIA). In VIA, the matrix elements are evaluated by inserting vacuum states between light quark fields. Since the $Q_{7\gamma} - Q_{8g}$ operators involve light quark fields, the vacuum insertion model provides an estimate to the

matrix element. Using the VIA model $f^{(I)}$ and $f^{(II)}$ as obtained as [78]

$$\begin{aligned} \int_{-\infty}^{\bar{\Lambda}} d\omega f_{78}^{(II)}(\omega, \mu) \Big|_{\text{VIA}} &= -e_{\text{spec}} \frac{F^2(\mu)}{8} \left(1 - \frac{1}{N_c^2}\right) \left\{ \frac{1}{\lambda_B^2(\mu)} + 2\pi i \int_0^\infty d\omega \frac{[\phi_+^B(\omega, \mu)]^2}{\omega} \right\} \\ \int_{-\infty}^{\bar{\Lambda}} d\omega \text{Re} f_{78}^{(II)}(\omega, \mu) \Big|_{\text{VIA}} &= -e_{\text{spec}} \frac{F^2(\mu)}{8} \left(1 - \frac{1}{N_c^2}\right) \frac{1}{\lambda_B^2(\mu)}, \end{aligned} \quad (3.29)$$

where $\lambda_B = \int_0^\infty d\omega \phi_+^B(\omega, \mu)/\omega$ and ϕ_+^B is the leading light cone distribution amplitude [96]. The nonperturbative quantity $F(\mu)$ is the HQET matrix element that relates to the asymptotic value of $f_B \sqrt{M_B}|_{M_b \rightarrow \infty}$ and f_B is the B meson decay constant.

3.1.3.3 $Q_{8g} - Q_{8g}$ contribution

The direct photon contribution of $Q_{8g} - Q_{8g}$ is given by [78]

$$F_{88}^{(a)}(E_\gamma, \mu) = \frac{C_F \alpha_s(\mu)}{4\pi} \left(\frac{m_b}{2E_\gamma}\right)^2 \int_{-p_+}^{\bar{\Lambda}} d\omega \left(\frac{2}{9} \ln \frac{m_b(\omega + p_+)}{\mu^2} + \frac{1}{9} - \frac{4}{9} c_{\text{RS}} \right) S(\omega, \mu), \quad (3.30)$$

where c_{RS} is a scheme dependent coefficient. For instance, in $\overline{\text{MS}}$ scheme $c_{\overline{\text{MS}}} = 0$. In the dimensional reduction scheme, which set $d = 4$ instead of $d = 4 - 2\epsilon$ for Dirac algebra, the $c_{\text{DR}} = 1$. The equation (3.30) is further simplified as

$$F_{88}^{(a)}(E_\gamma, \mu) = \frac{C_F \alpha_s(\mu)}{4\pi} \left(\frac{m_b}{2E_\gamma}\right)^2 \int_{-p_+}^{\bar{\Lambda}} d\omega \left(\frac{2}{9} \ln \frac{m_b(\omega + p_+)}{\mu^2} - \frac{1}{3} \right) S(\omega, \mu), \quad (3.31)$$

The $Q_{8g} - Q_{8g}$ receives double resolved photon contributions. This is shown in the figure 3.4

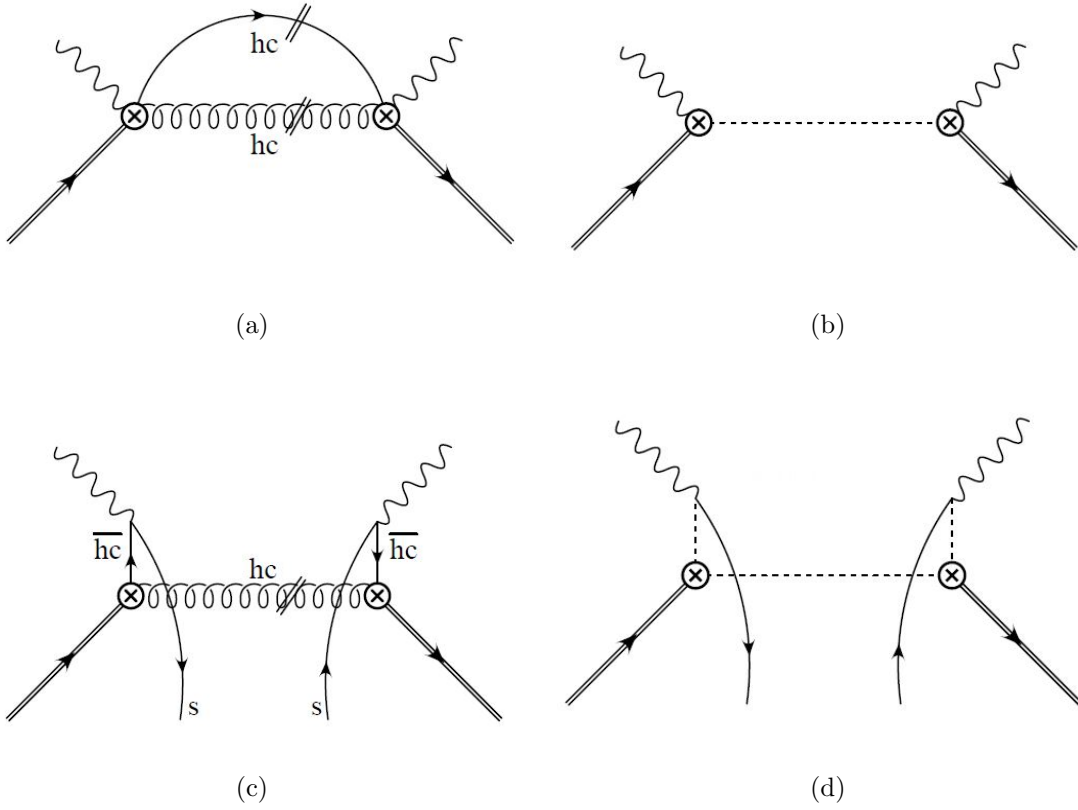


Figure 3.4: Figure (a) and (c) represent the diagrams arised by matching the $Q_{8\gamma} - Q_{8g}$ operator to SCET. Figure (b) and (d) represents the diagrams obtained by matching same processes to HQET [78].

The double resolved contribution to the photon spectrum is given by [78]

$$F_{88}^{(b)}(E_\gamma, \mu) = 4\pi\alpha_s(\mu) \left(\frac{m_b}{2E_\gamma}\right)^2 f_{88}(-p_+, \mu), \quad (3.32)$$

where f_{88} encodes the long distance physics. This function is defined as

$$f_{88}(\omega, \mu) = \frac{2}{9} \int_{-\infty}^{\infty} \frac{d\omega_1}{\omega_1 + i\varepsilon} \int_{-\infty}^{\infty} \frac{d\omega_2}{\omega_2 - i\varepsilon} g_{88}^{\text{cut}}(\omega, \omega_1, \omega_2, \mu), \quad (3.33)$$

where non-local matrix element g_{88}^{cut} is given by

$$\begin{aligned}
& g_{88}^{\text{cut}}(\omega, \omega_1, \omega_2, \mu) \\
&= \int \frac{dr}{2\pi} e^{-i\omega_1 r} \int \frac{du}{2\pi} e^{i\omega_2 u} \int \frac{dt}{2\pi} e^{-i\omega t} \\
& \times \frac{\langle \bar{B} | (\bar{h}S_n) (tn)T^A (S_n^\dagger S_{\bar{n}}) (\text{tn})\bar{\Gamma}_{\bar{n}} (S_{\bar{n}}^\dagger s) (tn + u\bar{n}) (\bar{s}S_{\bar{n}}) (r\bar{n})\Gamma_{\bar{n}} (S_{\bar{n}}^\dagger S_n) (0)T^A (S_n^\dagger h) (0) | \bar{B} \rangle}{2M_B}
\end{aligned} \tag{3.34}$$

The matrix element in equation (3.34) is obtained by summing over soft intermediate states with strangeness $S = -1$ (\mathcal{X}_s).

3.1.4 Resolved photon contributions to the total rate

If the photon spectrum is integrated over a much larger interval in the phase space than the end point region (integrated rate), then the direct photon contributions can be further simplified. Typically, the direct photon contributions are given by a series of hard coefficients that are multiplied by a set of forward B meson matrix elements of local operators. The correction terms of order $\frac{\Lambda_{\text{QCD}}}{m_b}$ are integrated to zero. This is due to the absence of local gauge operators that can account such terms at the order $\frac{\Lambda_{\text{QCD}}}{m_b}$. However, the resolved photon contributions do not reduced to such matrix elements of local operators [78]. The effects of these operators on total rate should be addressed by using non-local operators [84]

As shown in [78], single resolved photon contributions arise from the operator pairs $Q_{8g} - Q_{7\gamma}$ and $Q_1^c - Q_{7\gamma}$. In addition, double resolved photon contributions arise from the operator pairs $Q_{8g} - Q_{8g}$, $Q_1^c - Q_1^c$ and $Q_1^c - Q_{8g}$. Direct photon contributions arise from all the operator pairs.

The breakdown of the operators in leading order, next-to-leading order, and next-to-next-to-leading order in HQET power counting is as follows:

- The contribution of the operators $Q_{7\gamma} - Q_{7\gamma}$ is the leading power correction.
- The operators $Q_1^q - Q_{7\gamma}$, $Q_{8g} - Q_{8g}$ and $Q_{8g} - Q_{7\gamma}$, are order $1/m_b$ in the power

corrections.

- The operators $Q_1^c - Q_1^e$ and $Q_1^c - Q_{8g}$ contribute at order $1/m_b^2$. Since our primary focus is on improving the order $1/m_b$ corrections, we do not consider these order $1/m_b^2$ operators in our analysis.

In the following, we discuss these order $1/m_b$ corrections.

3.1.5 Contribution from nonperturbative correction

The function \mathcal{F}_E quantifies the effects of resolved photon contributions to the total rate [78]

$$\mathcal{F}_E(\Delta) = \frac{\Gamma(E_0) - \Gamma(E_0)|_{\text{OPE}}}{\Gamma(E_0)|_{\text{OPE}}}, \quad (3.35)$$

where $\Delta = m_b - 2E_0$. The $\Gamma(E_0)|_{\text{OPE}}$ [90] is obtained by a local operator product expansion, which does not consider the nonlocal power corrections from resolved photon contributions.

The contribution from $1/m_b$ operators is

$$\begin{aligned} \mathcal{F}_E(\Delta) = & \frac{C_1(\mu)}{C_{7\gamma}(\mu)} \frac{\Lambda_{17}(m_c^2/m_b, \mu)}{m_b} + \frac{C_{8g}(\mu)}{C_{7\gamma}(\mu)} 4\pi\alpha_s(\mu) \frac{\Lambda_{78}^{\text{spec}}(\mu)}{m_b} \\ & + \left(\frac{C_{8g}(\mu)}{C_{7\gamma}(\mu)} \right)^2 \left[4\pi\alpha_s(\mu) \frac{\Lambda_{88}(\Delta, \mu)}{m_b} - \frac{C_F\alpha_s(\mu)}{9\pi} \ln \frac{\Delta}{m_b} \right] + \dots, \end{aligned} \quad (3.36)$$

where

$$\begin{aligned} \Lambda_{17}\left(\frac{m_c^2}{m_b}, \mu\right) &= e_c \text{Re} \int_{-\infty}^{\infty} \frac{d\omega_1}{\omega_1} \left[1 - F\left(\frac{m_c^2 - i\varepsilon}{m_b\omega_1}\right) + \frac{m_b\omega_1}{12m_c^2} \right] h_{17}(\omega_1, \mu) \\ \Lambda_{78}^{\text{spec}}(\mu) &= \text{Re} \int_{-\infty}^{\infty} \frac{d\omega_1}{\omega_1 + i\varepsilon} \int_{-\infty}^{\infty} \frac{d\omega_2}{\omega_2 - i\varepsilon} h_{78}^{(5)}(\omega_1, \omega_2, \mu) \\ \Lambda_{88}(\Delta, \mu) &= e_s^2 \left[\int_{-\infty}^{\Lambda_{\text{UV}}} \frac{d\omega_1}{\omega_1 + i\varepsilon} \int_{-\infty}^{\Lambda_{\text{UV}}} \frac{d\omega_2}{\omega_2 - i\varepsilon} 2h_{88}^{\text{cut}}(\Delta, \omega_1, \omega_2, \mu) - \frac{C_F}{8\pi^2} \Delta \left(\ln \frac{\Lambda_{\text{UV}}}{\Delta} - 1 \right) \right]. \end{aligned} \quad (3.37)$$

The functions h_{17} , h_{88} and h_{78} are non-local HQET matrix elements that encode the long-

distance nonperturbative effects [78]. These soft functions cannot be determined from the first principles, and the evaluation of their contribution to the total rate requires modeling. In the following, we provide a concise review regarding past evaluations their contribution.

3.1.5.1 Estimating $\mathcal{F}_E|_{17}$

In equation (3.37) the soft function h_{17} is defined as

$$\begin{aligned} h_{17}(\omega_1, \mu) &= \int_{-\Delta}^{\bar{\Lambda}} d\omega g_{17}(\omega, \omega_1, \mu) \approx \int_{-\infty}^{\bar{\Lambda}} d\omega g_{17}(\omega, \omega_1, \mu) \\ &= \int \frac{dr}{2\pi} e^{-i\omega_1 r} \frac{\langle \bar{B} | (\bar{h} S_{\bar{n}})(0) \not{n} i \gamma_{\alpha}^{\perp} \bar{n}_{\beta} (S_n^{\dagger} g G_s^{\alpha\beta} S_{\bar{n}})(r\bar{n}) (S_n^{\dagger} h)(0) | \bar{B} \rangle}{2M_B} \end{aligned} \quad (3.38)$$

The moments of the function h_{17} in equation (3.38) are related to the nonperturbative HQET parameters. Based on this feature, we can construct phenomenological models to describe this non-local function. For instance, in [78] there were several phenomenological models for function h_{17} that are related to the zeroth moment of h_{17} over ω_1 ($\langle \omega_1^0 h_{17}(\omega_1) \rangle$). Consider the following model

$$h_{17}(\omega_1, \mu) = \frac{2\lambda_2}{\sqrt{2\pi}\sigma} \frac{\omega_1^2 - \Lambda^2}{\sigma^2 - \Lambda^2} e^{-\frac{\omega_1^2}{2\sigma^2}}, \quad (3.39)$$

where σ is the width of the Gaussian function and Λ is a ad-hoc parameter. Scanning through different values for σ and Λ in h_{17} the maximum and minimum values for Λ_{17} obtained as [78]

$$-60\text{MeV} < \Lambda_{17} < 25\text{MeV}. \quad (3.40)$$

Based on this estimate of Λ_{17} the $\mathcal{F}_E|_{17}$ from equation (3.36)

$$\mathcal{F}_E|_{17} = \frac{C_1(\mu)}{C_{7\gamma}(\mu)} \frac{\Lambda_{17}(m_c^2/m_b, \mu)}{m_b} \quad (3.41)$$

3.1.5.2 Estimating $\mathcal{F}_E|_{78}$

The contribution of the operator pair $Q_{7\gamma} - Q_{8g}$ is obtained by using the flavor symmetry of the strong interaction. The flavor averaged estimate of the $\mathcal{F}_E|_{78}$ is given by [78]

$$\mathcal{F}_E^{\text{avg}}(\Delta)|_{78} = -(1 \pm 0.3) \frac{\Delta_{0-}}{3}, \quad (3.42)$$

where Δ_{0-} is the isospin asymmetry, which is given by

$$\Delta_{0-} = \frac{\Gamma(\bar{B}^0 \rightarrow X_s \gamma) - \Gamma(B^- \rightarrow X_s \gamma)}{\Gamma(\bar{B}^0 \rightarrow X_s \gamma) + \Gamma(B^- \rightarrow X_s \gamma)} \quad (3.43)$$

Also, $\mathcal{F}_E|_{78}$ can be evaluated by using the vacuum insertion approximation (VIA). From equation (3.36)

$$\mathcal{F}_E|_{78} = \frac{C_{8g}(\mu)}{C_{7\gamma}(\mu)} 4\pi\alpha_s(\mu) \frac{\Lambda_{78}^{\text{spec}}(\mu)}{m_b}, \quad (3.44)$$

In the unbroken $SU(3)$ flavor symmetry limit, the nonperturbative parameter $\Lambda_{78}^{\text{spec}}$ is

$$\Lambda_{78}^{\text{spec}}|_{SU(3)} = e_{\text{spec}} \Lambda_{I=1}^{(8)}, \quad (3.45)$$

where e_{spec} is the electric charge of the spectator quark (i.e. $e_{\text{spec}} = 2/3$ for B^\pm and $e_{\text{spec}} = -1/3$ for $B^0(\bar{B}^0)$). The soft function that encodes the long distance physics from $Q_{7\gamma} - Q_{8g}$ operator pair can be written as a $SU(3)$ octet matrix element. The Wigner-Ekchart theorem is used to decompose the matrix element into isospin zero and isospin one components. The $\Lambda_{I=1}^{(8)}$ is the isospin 1 component of the $SU(3)$ octet. Using the VIA the estimate for $\Lambda_{I=1}^{(8)}$ is obtained as $\Lambda_{I=1}^{(8)}|_{\text{VIA}} \in [-386, -35] \text{ MeV}$ [78]. This estimate is used in equation (3.45) to

obtain $\mathcal{F}_E|_{78}$.

3.1.5.3 Estimating $\mathcal{F}_E|_{88}$

In equation (3.36) the contribution from operator pair $Q_{8g} - Q_{8g}$ is

$$\mathcal{F}_E|_{78} = \left(\frac{C_{8g}(\mu)}{C_{7\gamma}(\mu)} \right)^2 \left[4\pi\alpha_s(\mu) \frac{\Lambda_{88}(\Delta, \mu)}{m_b} - \frac{C_F\alpha_s(\mu)}{9\pi} \ln \frac{\Delta}{m_b} \right]. \quad (3.46)$$

Compared to the first term, the second term in the equation (3.46) provides a very small contribution to the $\mathcal{F}_E|_{78}$ [78]. The first term in $\mathcal{F}_E|_{78}$ is defined using the nonperturbative function Λ_{88} , which was defined in equation (3.37). Currently there is not much information on the soft function that describes Λ_{88} , and it is, however, estimated by [78]

$$\Lambda_{88}(\Delta, \mu) \approx e_s^2 \Lambda(\mu), \quad \Lambda(\mu) > 0, \quad (3.47)$$

where $\Lambda(\mu)$ is a parameter of order Λ_{QCD} . The electromagnetic charge of the s quark gives $e_s^2 = \frac{1}{9}$. The range of the $\Lambda(\mu)$ is defined as $0 < \Lambda(\mu) < 1$ GeV [78]. Based on this range the phenomenological estimate for the $\mathcal{F}_E|_{88}$ was obtained.

3.1.5.4 Phenomenological estimates of theoretical error

At order $1/m_b$, \mathcal{F}_E depends on $Q_1 - Q_{7\gamma}$, $Q_{8g} - Q_{8g}$ and $Q_{8g} - Q_{7\gamma}$; The contribution from each of these operators were obtained by Benzke *et al.* (2010) [78]:

$$\begin{aligned} \mathcal{F}_E|_{17} &\in [-1.7, +4.0]\% \\ \mathcal{F}_E|_{88} &\in [-0.3, +1.9]\% \end{aligned} \quad (3.48)$$

and

$$\begin{aligned} \mathcal{F}_E|_{78}^{\text{VIA}} &\in [-2.8, -0.3]\% \\ \mathcal{F}_E|_{78}^{\text{exp}} &\in [-4.4, +5.6]\% \quad (95\% \text{CL}) \end{aligned} \quad (3.49)$$

In total, the estimate for \mathcal{F}_E is obtained by using both experimental and theoretical estimates of $\Lambda_{78}^{\text{spec}}$. For instance, the 2010 theoretical estimate of uncertainty using VIA is [78].

$$-4.8\% < \mathcal{F}_E(\Delta) < +5.6\% \quad (\text{VIA for } \Lambda_{78}^{\text{spec}}). \quad (3.50)$$

Here the estimate for $\mathcal{F}_E|_{78}^{\text{VIA}}$ is obtained by plugging the value of $\Lambda_{I=1}^{(8)}|_{\text{VIA}}$.

The 2010 estimate of $\Lambda_{78}^{\text{spec}}$, which is obtained using isospin asymmetry Δ_{0-} , is given by

$$-6.4\% < \mathcal{F}_E(\Delta) < +11.5\% \quad (\Lambda_{78}^{\text{spec}} \text{ from } \Delta_{0-}), \quad (3.51)$$

where $\Delta_{0-} = (-1.3 \pm 5.9)\%$, which was measured by BaBar collaboration [71,91], and the uncertainty of Δ_{0-} is 95% confidence level (CL) [78].

3.2 The CP asymmetry

The CP violation (CPV) due to direct photon in $\bar{B} \rightarrow X_s \gamma$ arises by the interference of a weak phases in the CKM matrix elements and the possible BSM corrections to Wilson coefficients with the strong phases arising in the process [94]. These strong phases can be obtained by calculating the imaginary parts of the local operators in the effective Hamiltonian given in equation (3.3). For instance, the imaginary parts first arise at $\mathcal{O}(\alpha_s)$ in loop diagrams that contains c quarks or light partons [94]. The CP asymmetry is given by [95],

$$\mathcal{A}_{X_s \gamma} = \frac{\Gamma(\bar{B} \rightarrow X_s \gamma) - \Gamma(B \rightarrow X_{\bar{s}} \gamma)}{\Gamma(\bar{B} \rightarrow X_s \gamma) + \Gamma(B \rightarrow X_{\bar{s}} \gamma)}. \quad (3.52)$$

In [95] the SM estimate for CP asymmetry is provided as

$$-0.6\% < \mathcal{A}_{X_s \gamma}^{\text{SM}} < 2.8\% \quad (3.53)$$

This estimate is compared to the PDG average of the experimental measurement $1.5\% \pm 1.1\%$ [18]. These were first considered in [95]. The resolved photon contributions that arise in the photon spectrum is important to the analysis of the direct CP asymmetry.

The experimental measurement of the CP asymmetry ($\mathcal{A}_{X_s\gamma}(E_0)$) depend on the photon cut $E_\gamma \geq E_0$. Where E_0 is in the range $1.9 \text{ GeV} < E_0 < 2.2 \text{ GeV}$, and $\Delta = m_b - 2E_0 = \text{few} \times \Lambda_{\text{QCD}}$ [95]. This cut related CP asymmetry is known as *partially inclusive* asymmetry [95]. The direct photon contributions to the CP asymmetry can be expressed by using a power series in Δ/m_b and $\Lambda_{\text{QCD}}/\Delta$. At the $\mathcal{O}(\alpha_s)$, the direct photon contribution to $\mathcal{A}_{X_s\gamma}$ is

$$\mathcal{A}_{X_s\gamma}^{\text{dir}} = \alpha_s \left\{ \frac{40}{81} \text{Im} \frac{C_1}{C_{7\gamma}} - \frac{4}{9} \text{Im} \frac{C_{8g}}{C_{7\gamma}} - \frac{40\Lambda_c}{9m_b} \text{Im} \left[(1 + \epsilon_s) \frac{C_1}{C_{7\gamma}} \right] + \mathcal{O} \left(\frac{\Lambda_{\text{QCD}}^2}{m_b^2} \right) \right\}, \quad (3.54)$$

where the $C_1, C_{7\gamma}$ and C_{8g} are the Wilson coefficients (effective couplings) of current-current four quark operator (Q_1^q), electromagnetic dipole operator ($Q_{7\gamma}$) and gluon dipole operator (Q_{8g}) respectively. Also, the parameter Λ_c is defined as

$$\Lambda_c \equiv \frac{m_c^2}{m_b} \left(1 - \frac{2}{5} \ln \frac{m_b}{m_c} + \frac{4}{5} \ln^2 \frac{m_b}{m_c} - \frac{\pi^2}{15} \right), \quad (3.55)$$

The $\Lambda_c \sim \Lambda_{\text{QCD}}$ is obtained by plugging $m_b = 4.65 \text{ GeV}$ and $m_c = 1.13 \text{ GeV}$ in equation (3.55). Following from this we obtain $\Lambda_c \sim 0.38 \text{ GeV}$. The parameter ϵ_s is the ratio of CKM matrix elements, and it is defined as [94]

$$\epsilon_s = \frac{v_u}{v_t} = \frac{V_{us}^* V_{ub}}{V_{ts}^* V_{tb}} \approx \lambda^2 (i\eta - \rho) = \mathcal{O}(10^{-2}), \quad (3.56)$$

where the parameters λ, ρ and η are Wolfenstein parameters defined as $\lambda = \sin \theta_C \approx 0.22$ and $\rho, \eta = \mathcal{O}(1)$. Only the third term in the equation (3.54) is non-zero in the SM. This term is triply suppressed by the $\alpha_s, \text{Im}(\epsilon_s)$ and $(m_c/m_b)^2 \sim \Lambda_{\text{QCD}}/m_b$.

3.2.1 Resolved photon contributions to the CP asymmetry

Using the factorization formula provided in equation (3.9) the effects of resolved photon operators to the partially inclusive CP asymmetry can be evaluated. For instance, these nonlocal effects arise from the interference of $Q_{7\gamma} - Q_{7\gamma}$ amplitude with $Q_1^{(u,c)} - Q_{7\gamma}$ and

$Q_{7\gamma} - Q_{8g}$ amplitudes. Following from this, the resolved photon contribution to the CP asymmetry is obtained as

$$\mathcal{A}_{X_s\gamma}^{\text{res}} = \frac{\pi}{m_b} \left\{ \text{Im} \left[(1 + \epsilon_s) \frac{C_1}{C_{7\gamma}} \right] \tilde{\Lambda}_{17}^c - \text{Im} \left[\epsilon_s \frac{C_1}{C_{7\gamma}} \right] \tilde{\Lambda}_{17}^u + \text{Im} \frac{C_{8g}}{C_{7\gamma}} 4\pi\alpha_s \tilde{\Lambda}_{78}^{\bar{B}} \right\}, \quad (3.57)$$

where

$$\begin{aligned} \tilde{\Lambda}_{17}^u &= \frac{2}{3} h_{17}(0) \\ \tilde{\Lambda}_{17}^c &= \frac{2}{3} \int_{4m_c^2/m_b}^{\infty} \frac{d\omega}{\omega} f\left(\frac{m_c^2}{m_b\omega}\right) h_{17}(\omega) \\ \tilde{\Lambda}_{78}^{\bar{B}} &= 2 \int_{-\infty}^{\infty} \frac{d\omega}{\omega} \left[h_{78}^{(1)}(\omega, \omega) - h_{78}^{(1)}(\omega, 0) \right] \end{aligned} \quad (3.58)$$

and

$$f(x) = 2x \ln \frac{1 + \sqrt{1 - 4x}}{1 - \sqrt{1 - 4x}}. \quad (3.59)$$

In the unbroken $SU(3)$ limit, the $\tilde{\Lambda}_{78}$ is defined as

$$\tilde{\Lambda}_{78}^{\bar{B}} \approx e_{\text{spec}} \tilde{\Lambda}_{78} \approx e_{\text{spec}} \frac{2f_B^2 M_B}{9} \int_0^{\infty} d\omega \frac{[\phi_+^B(\omega)]^2}{\omega}, \quad (3.60)$$

where the f_B is the B meson decay constant and it is evaluated as $f_B \approx 193$ MeV [95].

The ϕ_+^B is the leading light cone distribution amplitude [96]. Using the models provided in sections 3.1.5.1 and 3.1.5.3 the parameters $\tilde{\Lambda}_{ij}$ can be obtained [95]

$$\begin{aligned} -330\text{MeV} &< \tilde{\Lambda}_{17}^u < +525\text{MeV}, \\ -9\text{MeV} &< \tilde{\Lambda}_{17}^c < +11\text{MeV}, \\ 17\text{MeV} &< \tilde{\Lambda}_{78} < 190\text{MeV}. \end{aligned} \quad (3.61)$$

The complete theoretical estimate of the CP asymmetry is obtained by combining the direct and the resolved photon contributions. Therefore, the SM estimate of the CP asymmetry is

obtained by using the expressions in equations (3.54) and (3.57), and they provide

$$\begin{aligned} \mathcal{A}_{X_s\gamma}^{\text{SM}} &\approx \pi \left| \frac{C_1}{C_{7\gamma}} \right| \text{Im} \epsilon_s \left(\frac{\tilde{\Lambda}_{17}^u - \tilde{\Lambda}_{17}^c}{m_b} + \frac{40\alpha_s \Lambda_c}{9\pi m_b} \right) \\ &= \left(1.15 \times \frac{\tilde{\Lambda}_{17}^u - \tilde{\Lambda}_{17}^c}{300\text{MeV}} + 0.71 \right) \%, \end{aligned} \quad (3.62)$$

where the following estimates for the Wolfenstein parameters are used: $\lambda = 0.2254$, $\rho = 0.144$, $\eta = 0.342$. The Wilson coefficients are evaluated at $\mu = 2 \text{ GeV}$, they are provided as: $C_1 = 1.204$, $C_{7\gamma} = -0.381$ and $C_{8g} = -0.175$ [95].

3.3 Reevaluating the resolved photon contributions

3.3.1 Updates on the $\mathcal{F}_E|_{78}$

A recent update on Δ_{0-} from Belle [93] provide $\Delta_{0-} = [-0.48 \pm 1.49(\text{stat}) \pm 0.97(\text{sys}) \pm 1.15(f_{+-}/f_{00})]\%$, where the last uncertainty is coming from the uncertainties attached to the production ratio of B^+B^- to $B^0\bar{B}^0$ in $\Upsilon(4S)$ decays [92]. The PDG average is $\Delta_{0-} = (-0.6 \pm 2.0)\%$ [71, 91, 93]. As shown in the equation (3.51), the uncertainty of the Δ_{0-} is calculated in 95% CL. Using this in equation (3.42) we find

$$\mathcal{F}_E|_{78}^{\text{exp}} \in [-1.4, +2]\%. \quad (3.63)$$

Comparing the estimates found in equation (3.48) and (3.63), we find that the currently the largest contribution to the \mathcal{F}_E comes from the operator pair $Q_1^q - Q_{7\gamma}$. Therefore, reducing the theoretical error generated by this operator pair is essential for the precise calculation of the branching ratio.

CHAPTER 4 NEW RESULTS : ON HQET AND NRQCD OPERATORS OF DIMENSION 8 AND ABOVE

As shown in section 3.1.5.1, the moments of the soft function h_{17} are related to the HQET parameters. The contribution from the operator pair $Q_1^q - Q_{7\gamma}$ is obtained using the information on these moments. To reevaluate the $Q_1^q - Q_{7\gamma}$ contribution, we develop a new model for h_{17} based on higher moments of h_{17} . These higher moments are related to the HQET matrix elements of mass dimension seven and above. The HQET matrix operators contain two heavy quark fields and covariant derivatives. The HQET and NRQCD Lagrangian operators are defined up to and including dimension seven in [55]. In section 2.3, we showed that these Lagrangians differ in power counting, but they can be related to each other using the field redefinition. The HQET/NRQCD operators up to and including the dimension seven are provided in [55]. There are six spin-independent operators and five spin-dependent operators at dimension seven. The comparison between the dimension seven HQET matrix elements and dimension seven HQET and NRQCD operators provides the following: for the spin-dependent operators the number is the same as the numbers of the spin-dependent matrix elements considered in [62], while the spin independent number of operators is different. Why is there a difference and what is the relation between these two bases? [56]

More recently, the NRQED Lagrangian up to and including power $1/M^4$ was calculated in [99]. It includes NRQED operators of dimension eight and below. The Lagrangian was constructed by considering all the possible rotationally invariant, P and T even, Hermitian combinations of iD_t , $i\mathbf{D}$, \mathbf{E} , \mathbf{B} , and $\boldsymbol{\sigma}$. The analogous construction of the NRQED Lagrangian up to $1/M^2$ was explicitly demonstrated in [100]. For higher power of $1/M$, corresponding to higher dimensional operators, this construction becomes tedious. There can be different choices for the form of the operators. It is not immediately clear if a pair of operators is linearly independent and what is the total number of linearly independent operators. It would be useful to find a simpler way to construct these operators. Furthermore,

the $1/M^4$ NRQED Lagrangian contains four spin-independent and eight spin-dependent operators. This is less than the number of matrix elements considered in [62]. Presumably the rest correspond to NRQCD operators that do not exist for NRQED. What are they?

In the following work we address these questions by considering a general decomposition of a matrix elements into linearly independent tensors. These matrix elements have the following form $\langle H | \bar{h} iD^{\mu_1} \dots iD^{\mu_n} (s^\lambda) h | H \rangle$, where H represent a pseudo scalar heavy meson state, h represent the heavy quark field, and s^λ is the four dimension generalization of Pauli matrices.

4.1 General method

4.1.1 Definitions

The chromo-electric and magnetic fields are defined as

$$\begin{aligned} [D_t, \mathbf{D}] &\equiv ig\mathbf{E} \\ [\mathbf{D}_i, \mathbf{D}_j] &\equiv -ig\epsilon_{ijk}\mathbf{B}^k, \end{aligned} \quad (4.1)$$

where $\mathbf{E} = \mathbf{E}_a T^a$, $\mathbf{B} = \mathbf{B}_a T^a$, and T^a are $SU(3)$ generators. The commutator and anti-commutators are defined as $[X, Y] \equiv XY - YX$ and $\{X, Y\} \equiv XY + YX$ respectively. Finally, we define the matrix $g^{\mu\nu}$ as $g^{\mu\nu} = \text{diag}(1, -1, -1, -1)$ and heavy quark four velocity (v) as $v = (1, 0, 0, 0)$.

The form of a generic operator in dimension $n + 3$ is [61]

$$\mathcal{O}_{\mu_1, \mu_2 \dots \mu_n}^{(r)} = \bar{h} (iD^{\mu_1}) (iD^{\mu_2}) \dots (iD^{\mu_n}) \Gamma h, \quad (4.2)$$

where n is a positive integer. The Dirac matrix Γ in equation (4.2) is expanded in the basis $\{1, \gamma_5, \gamma_\mu \gamma_5 \gamma_\mu, \sigma_{\mu\nu}\}$. The Γ is sandwiched between projection operator P_+ , which is defined by

$$P_+ = \frac{1}{2}(1 + \not{v}), \quad (4.3)$$

where $\psi = \gamma^\alpha v_\alpha$. Using the projection operators we transform the Dirac basis as follows [61]:

$$\begin{aligned} 1 &\rightarrow P_+ = \frac{1}{2}(1 + \psi) \\ \gamma_\mu &\rightarrow P_+ \gamma_\mu P_+ = v_\mu P_+ \end{aligned} \quad (4.4)$$

$$\begin{aligned} \gamma_\mu \gamma_5 &\rightarrow P_+ \gamma_\mu \gamma_5 P_+ = s_\mu \\ \gamma_5 &\rightarrow P_+ \gamma_5 P_+ = 0 \end{aligned} \quad (4.5)$$

$$(-i)\sigma_{\mu\nu} \rightarrow P_+ (-i)\sigma_{\mu\nu} P_+ = i v^\alpha \epsilon_{\alpha\mu\nu\beta} s^\beta, \quad (4.6)$$

where the sign of the Levi-Civita tensor is $\epsilon^{0123} = -1$ and $\epsilon_{0123} = 1$. Since $v \cdot s = 0$, there are only three independent s^μ . The Dirac matrix Γ then expanded into the four matrices 1 and s_μ as [61]:

$$P_+ \Gamma P_+ = \frac{1}{2} P_+ \text{Tr} \{P_+ \Gamma\} - \frac{1}{2} s_\mu \text{Tr} \{s^\mu \Gamma\}. \quad (4.7)$$

Following from the equation (4.7), the generic operator can be reduced to following two forms:

$$\begin{aligned} \text{Spin independent operators} &= \bar{h} (iD^{\mu_1}) (iD^{\mu_2}) \dots (iD^{\mu_n}) h \\ \text{Spin dependent operators} &= \bar{h} (iD^{\mu_1}) (iD^{\mu_2}) \dots (iD^{\mu_n}) s^\lambda h \end{aligned} \quad (4.8)$$

4.1.2 Constraints on matrix elements

The basis for the HQET matrix elements is constructed using the constraints obtained from the discrete symmetries, Hermiticity of the matrix elements, HQET equation of motion, and color structure.

4.1.2.1 Constraints from discrete symmetries and Hermiticity

HQET and NRQCD are invariant under P and T discrete symmetries. Therefore, the HQET matrix elements and HQET and NRQCD operators also satisfy these symmetries. In the table 4.1 we provide the P and T and PT transformation of momentum (p), four velocity

(v), covariant derivative (iD^μ), and generalized Pauli matrix (s^λ) [56]

Table 4.1: Transformation of p, v, iD^μ and s^λ under P, T and PT symmetries

Operator	Transformation under P	Transformation under T	transformation under PT
p	$(p^0, -\vec{p})$	$(p^0, -\vec{p})$	(p^0, \vec{p})
v	$(v^0, -\vec{v})$	$(v^0, -\vec{v})$	(v^0, \vec{v})
iD^μ	$(-1)^\mu(iD^\mu)$	$(-1)^\mu(iD^\mu)$	iD^μ
s^λ	$-(-1)^\lambda s^\lambda$	$(-1)^\lambda s^\lambda$	$-s^\lambda$

These transformations allow us to show that

$$\langle H | \bar{h} iD^{\mu_1} \dots iD^{\mu_n} h | H \rangle \stackrel{PT}{=} \langle H | \bar{h} iD^{\mu_1} \dots iD^{\mu_n} h | H \rangle^* \quad (4.9)$$

$$\langle H | \bar{h} iD^{\mu_1} \dots iD^{\mu_n} s^\lambda h | H \rangle \stackrel{PT}{=} - \langle H | \bar{h} iD^{\mu_1} \dots iD^{\mu_n} s^\lambda h | H \rangle^*, \quad (4.10)$$

where the complex conjugation arises due to the anti-linear T . It is important to note that there is a relative minus sign between PT transformation of spin-independent operators and spin-dependent operators. This implies that the spin-independent matrix elements are real, whereas spin-dependent matrix elements are imaginary.

Since $\bar{h}h, \bar{h}s^\lambda h$, and iD^μ are Hermitian, we use Hermitian conjugation to put further constraints on the matrix elements

$$\begin{aligned} \langle H | \bar{h} iD^{\mu_1} \dots iD^{\mu_n} (s^\lambda) h | H \rangle &= \left\langle H \left| \left(\bar{h} iD^{\mu_1} \dots iD^{\mu_n} (s^\lambda) h \right)^\dagger \right| H \right\rangle^* = \\ &= \langle H | \bar{h} iD^{\mu_n} \dots iD^{\mu_1} (s^\lambda) h | H \rangle^* \end{aligned} \quad (4.11)$$

Combining the constraints from PT symmetry and Hermitian conjugation we obtain a new symmetry, which we call “inversion symmetry”. The spin-independent (dependent) matrix

elements are symmetric (anti-symmetric) under inversion symmetry.

The state H is a pseudo scalar. The matrix element of $\langle H | \bar{h} iD^{\mu_1} \dots iD^{\mu_n} (s^\lambda) h | H \rangle$ can only depend on v_{μ_i} and $g^{\mu_i \mu_j}$ and $\epsilon^{\alpha\beta\rho\sigma}$. Following the notation in [62] we define $\Pi^{\mu\nu} = g^{\mu\nu} - v^\mu v^\nu$. In general, we have $v_\mu \Pi^{\mu\nu} = 0$ and $v_\nu \Pi^{\mu\nu} = 0$. For $v = (1, 0, 0, 0)$ we obtain Π^{00} and $\Pi^{ij} = -\delta^{ij}$. Also, note that all four indices in $\epsilon^{\alpha\beta\rho\sigma}$ cannot be orthogonal to v in a four dimensional space-time. As a result, we can replace $\epsilon^{\alpha\beta\rho\sigma} \rightarrow \epsilon^{\alpha\beta\rho\sigma} v_\alpha$ [56].

In four dimension, a given tensor can have four independent directions only. Following from this, we found certain tensors with more than four indices become not independent although they have different combination of indices. For instance, three indices must be the same in the tensor $\Pi^{\mu\nu} \epsilon^{\alpha\beta\rho\sigma} v_\alpha$. Because of this, not all the tensors obtained by the permutations of $\Pi^{\mu\nu}$ and $\epsilon^{\alpha\beta\rho\sigma} v_\alpha$ can be linearly independent.

The decomposition gives a correspondence between the operators $\bar{h} iD^{\mu_1} \dots iD^{\mu_n} (s^\lambda) h$ and non-perturbative parameters. Questions such as the linear independence of a given set of operators, and the number of linearly independent operators of a given dimension are answered by considering the vector space of non-perturbative parameters of a given dimension¹ [56].

4.1.2.2 Constraints from HQET equation of motion

As shown in section 2.2.2, the equation of motion obtained from the HQET Lagrangian provides

$$iv \cdot Dh = 0. \quad (4.12)$$

This equation provides that the multiplication of matrix element by v_{μ_1} or v_{μ_n} yields zero, and it implies that the v_{μ_1} and v_{μ_n} are orthogonal to v [61]. This relation holds in the NRQED and NRQCD as well [56]. As a consequence, the operators of the form $\dots iv \cdot D\psi$

¹A potential caveat to this argument is that one can imagine an operator that has a zero matrix element. The only such example is the operator $\bar{h} iv \cdot Dh$, which is the first term in the HQET and NRQCD (NRQED) Lagrangians. This term is unique in the sense that it is the only one that includes $iv \cdot D$ in the HQET Lagrangian or iD_t (not in a commutator) in the NRQCD (NRQED) Lagrangian.

or $\psi^\dagger i v \cdot D \dots$ can be removed by field redefinition.

4.1.2.3 Constraints on possible color structures

The covariant derivative $D^\mu = \partial^\mu + igA^{\mu a}T^a$ combines the unit matrix in color space (color singlet) and a product of an octet vector field $A^{\mu a}$ with octet of $SU(3)$ color matrices. Gauge invariance stipulates that both $A^{\mu a}$ and ∂_μ must appear together. Because of this, the covariant derivatives does not have an independent color singlet and octet parts .On the other hand, the product of two covariant derivatives can be decomposed into a commutator and an anti-commutator matrices. These commutators only contain a color octet part. Whereas, the anti-commutators possess both singlet and octet parts, which cannot be separated. The product of three covariant derivatives has an analogous structure to the two covariant derivatives [56].

For the product of four covariant derivatives we obtain products of commutators and anti-commutators for the first time. For instance, consider the NRQCD operator $\psi^\dagger E_a^i T^a E_b^i T^b \psi$ [101]. This operator contains a product of $SU(3)$ color matrices, which is given by

$$\{T^a, T^b\} = \frac{1}{3}\delta^{ab} + d^{abc}T^c. \quad (4.13)$$

In equation (4.13) the singlet and octet parts are not connected by gauge invariance and they give rise to two operators with different color structure. Instead of a singlet and an octet we can choose the basis of $\{T^a, T^b\}$ and δ^{ab} . Thus we have two different operators with two chromo-electric fields: $\psi^\dagger E_a^i E_b^i \{T^a, T^b\} \psi$ and $\psi^\dagger E_a^i E_b^i \delta^{ab} \psi$. Only the first one is generated by commutator and anti-commutators of covariant derivatives. The second operator is generated when we consider the one-loop self-energy corrections to the first operators. Thus a one gluon exchange between ψ^\dagger and ψ in $\psi^\dagger E_a^i E_b^i \{T^a, T^b\} \psi$ gives the color structures [56]:

$$T_{ij}^c \{T^a, T^b\}_{jk} T_{kl}^c = \{T^a, T^b\}_{jk} \left(\frac{1}{2}\delta_{il}\delta_{kj} - \frac{1}{6}\delta_{ij}\delta_{kl} \right) = \frac{1}{2}\delta^{ab}\delta_{il} - \frac{1}{6}\{T^a, T^b\}_{il}, \quad (4.14)$$

where $i, j, k, l = 1, 2, 3$ and $a, b, c = 1, \dots, 8$. Here we used a color identity for $T_{ij}^c T_{kl}^c$. In other words, when calculating observables at tree level only $\psi^\dagger E_a^i E_b^i \{T^a, T^b\} \psi$ appears [55]. At one loop we need to consider also $\psi^\dagger E_a^i E_b^i \delta^{ab} \psi$. The case of five covariant derivatives is discussed in sections 4.2.6 and 4.3.6. The appearance of color singlet structures at one loop-level was first pointed out in [101]. This was incorporated into our general decomposition of matrix elements.

4.2 Spin-independent operators upto and including dimension 8

Consider the generic HQET matrix element in the form of $\langle H | \bar{h} i D^{\mu_1} \dots i D^{\mu_n} (s^\lambda) h | H \rangle$. We then decompose this matrix element in terms of nonperturbative parameters multiplies by tensors ($\Pi^{\mu_i \nu_j}$) [56].

4.2.1 Dimension three

The dimension 3 operator does not contain any covariant derivatives.

$$\frac{1}{2M_H} \langle H | \bar{h} h | H \rangle = 1 \quad (4.15)$$

4.2.2 Dimension four operators

At dimension four we have one covariant derivative. This matrix element needed to be decomposed into tensor structure with one Lorentz index. The only possible choice is v_{μ_1} . Using the HQET equation of motion ($i v \cdot D h = 0$) we obtain

$$\frac{1}{2M_H} \langle H | \bar{h} i D^{\mu_1} h | H \rangle = 0. \quad (4.16)$$

4.2.3 Dimension five operators

Dimension five spin independent operator contains two covariant derivatives. Thus the matrix element can be decomposed into tensor with two Lorentz indices. The natural choice is $\Pi^{\mu_i \mu_j}$. Hence we have

$$\frac{1}{2M_H} \langle H | \bar{h} i D^{\mu_1} i D^{\mu_2} h | H \rangle = a^{(5)} \Pi^{\mu_1 \mu_2}, \quad (4.17)$$

where coefficient $a^{(5)}$ related to nonperturbative HQET parameter.

4.2.4 Dimension six operators

We need to consider $\langle H | \bar{h} i D^{\mu_1} i D^{\mu_2} i D^{\mu_3} h | H \rangle$. The tensor $\epsilon^{\rho\mu_1\mu_2\mu_3} v_\rho$ is ruled out by parity. This is most easily seen by taking $v = (1, 0, 0, 0)$ which requires μ_1, μ_2, μ_3 to be space-like. Hence the matrix element has a an odd number of space-like covariant derivatives and is zero by parity. The only possible tensor combination is a product of a v and Π . We must use $\Pi^{\mu_1\mu_3}$ and we find only one possible non-perturbative parameter [56]:

$$\frac{1}{2M_H} \langle H | \bar{h} i D^{\mu_1} i D^{\mu_2} i D^{\mu_3} h | H \rangle = a^{(6)} \Pi^{\mu_1\mu_3} v^{\mu_2}, \quad (4.18)$$

where the coefficient $a^{(6)}$ is a nonperturbative parameter. Under inversion $\Pi^{\mu_1\mu_3} v^{\mu_2} \rightarrow \Pi^{\mu_3\mu_1} v^{\mu_2} = \Pi^{\mu_1\mu_3} v^{\mu_2}$.

4.2.5 Dimension seven operators

Here we need more than one tensor structure. We can have a product of two Π 's or a product of Π and two v 's. For products of two Π 's we can contract μ_1 with μ_2, μ_3 , or μ_4 using Π . The other two indices are also contracted by Π . In total we have three such combinations of two Π 's. Using two v 's, they can only be contracted with μ_2 and μ_3 giving us a fourth tensor. In total we have

$$\begin{aligned} \frac{1}{2M_H} \langle H | \bar{h} i D^{\mu_1} i D^{\mu_2} i D^{\mu_3} i D^{\mu_4} h | H \rangle &= a_{12}^{(7)} \Pi^{\mu_1\mu_2} \Pi^{\mu_3\mu_4} + a_{13}^{(7)} \Pi^{\mu_1\mu_3} \Pi^{\mu_2\mu_4} + \\ &+ a_{14}^{(7)} \Pi^{\mu_1\mu_4} \Pi^{\mu_2\mu_3} + b^{(7)} \Pi^{\mu_1\mu_4} v^{\mu_2} v^{\mu_3}. \end{aligned} \quad (4.19)$$

It is easy to check that each tensor separately is invariant under inversion. Our notation

for the parameters is such that the subscript denotes the first two indices that are contracted via Π 's in numerical order, and the dimension of the operators appears in the superscript. We also use a different letters for tensors with a different number of v 's.

As was mentioned in the introduction, the NRQED Lagrangian has four spin-independent operators. We will show in section 4.4 that these can be related to the four operators above. It should be clear already though that it is easier to tabulate the operators as was done here than to construct them from \mathbf{E} , \mathbf{D} , and \mathbf{B} .

As was pointed out in [101] and discussed in section 4.1.2.3, there can be more than one color structure for operators constructed from four covariant derivatives. This is most easily seen when one constructs NRQCD operators and then consider the possible color structure, as we do in section 4.4. But we can anticipate the result by considering structures of the form $\bar{h} \{[iD^{\mu_i}, iD^{\mu_j}], [iD^{\mu_k}, iD^{\mu_l}]\} h$. It is a symmetric product of two $SU(3)$ color matrices that give rise to two possible color structures: a singlet and an octet. There can be three different structures $\bar{h} \{[iD^{\mu_1}, iD^{\mu_2}], [iD^{\mu_3}, iD^{\mu_4}]\} h$, $\bar{h} \{[iD^{\mu_1}, iD^{\mu_3}], [iD^{\mu_2}, iD^{\mu_4}]\} h$, and $\bar{h} \{[iD^{\mu_1}, iD^{\mu_4}], [iD^{\mu_2}, iD^{\mu_3}]\} h$, corresponding to the possible partitions of four indices into two pairs. In order to form scalar operators, we need to multiply these structures by one of the four possible tensors on the right hand side of equation (4.19): $\Pi^{\mu_1\mu_2}\Pi^{\mu_3\mu_4}$, $\Pi^{\mu_1\mu_3}\Pi^{\mu_2\mu_4}$, $\Pi^{\mu_1\mu_4}\Pi^{\mu_2\mu_3}$, and $\Pi^{\mu_1\mu_4}v^{\mu_2}v^{\mu_3}$. We find only two linearly independent combinations from all of the contractions, namely, $a_{13}^{(7)} - a_{14}^{(7)}$, and $b^{(7)}$. We confirm this result in section 4.4.1.3. We conclude that we can form only two such operators with two possible color structures each. Including the possible color structures, there are in total six possible NRQCD (HQET) operators.

4.2.6 Dimension eight operators

We have five covariant derivatives, so we must have an odd number of v 's. We cannot have five v 's and there is only one tensor with 3 v 's: $\Pi^{\mu_1\mu_5}v^{\mu_2}v^{\mu_3}v^{\mu_4}$. As a result of the inversion symmetry, tensors with one v must be of the form $v^{\mu_2}\Pi\Pi + v^{\mu_4}\Pi\Pi$ or $v^{\mu_3}\Pi\Pi$. All together we find seven possible tensors:

$$\begin{aligned}
\frac{1}{2M_H} \langle H | \bar{h} iD^{\mu_1} iD^{\mu_2} iD^{\mu_3} iD^{\mu_4} iD^{\mu_5} h | H \rangle &= a_{12}^{(8)} (\Pi^{\mu_1\mu_2} \Pi^{\mu_3\mu_5} v^{\mu_4} + \Pi^{\mu_1\mu_3} \Pi^{\mu_4\mu_5} v^{\mu_2}) + \\
a_{13}^{(8)} (\Pi^{\mu_1\mu_3} \Pi^{\mu_2\mu_5} v^{\mu_4} + \Pi^{\mu_3\mu_5} \Pi^{\mu_1\mu_4} v^{\mu_2}) &+ a_{15}^{(8)} (\Pi^{\mu_1\mu_5} \Pi^{\mu_3\mu_4} v^{\mu_2} + \Pi^{\mu_1\mu_5} \Pi^{\mu_2\mu_3} v^{\mu_4}) + \\
b_{12}^{(8)} \Pi^{\mu_1\mu_2} \Pi^{\mu_4\mu_5} v^{\mu_3} &+ b_{14}^{(8)} \Pi^{\mu_1\mu_4} \Pi^{\mu_2\mu_5} v^{\mu_3} + b_{15}^{(8)} \Pi^{\mu_1\mu_5} \Pi^{\mu_2\mu_4} v^{\mu_3} + \\
c^{(8)} \Pi^{\mu_1\mu_5} v^{\mu_2} v^{\mu_3} v^{\mu_4}. &
\end{aligned} \tag{4.20}$$

Our notion is same as in section 4.2.5, but we used different letters for the coefficients of these tensor structures.

We also need to consider the issue of possible color structures. Multiple colors structures for a given operator arise from the anti-commutator of two color octets. For five covariant derivatives there are two possibilities of color octets: $[iD^{\mu_i}, iD^{\mu_j}]$ and $[iD^{\mu_k}, [iD^{\mu_l}, iD^{\mu_m}]]$. If we combine them together we get two structures² $\bar{h} \{[iD^{\mu_i}, iD^{\mu_j}], [iD^{\mu_k}, [iD^{\mu_l}, iD^{\mu_m}]]\} h$ and $\bar{h} \{[iD^{\mu_i}, iD^{\mu_j}], [iD^{\mu_m}, [iD^{\mu_k}, iD^{\mu_l}]]\} h$. There are $\binom{5}{2} \times 2 = 20$ such structures. We can also combine $\{[iD^{\mu_i}, iD^{\mu_j}], [iD^{\mu_k}, iD^{\mu_l}]\}$ with an anti-commutator of a fifth covariant derivative³: $\bar{h} \{iD^{\mu_m}, \{[iD^{\mu_i}, iD^{\mu_j}], [iD^{\mu_k}, iD^{\mu_l}]\}\} h$. There are $\binom{5}{1} \times 3 = 15$ such structures. Contracting each of the possible structure with the tensors on the left hand side of (4.20), we find only one non-zero linear combination: $a_{12}^{(8)} - a_{15}^{(8)} - b_{14}^{(8)} + b_{15}^{(8)}$ from $\bar{h} \{iD^{\mu_m}, \{[iD^{\mu_i}, iD^{\mu_j}], [iD^{\mu_k}, iD^{\mu_l}]\}\} h$. We will obtain the same result in section 4.4.1.4. Including the two possible color structures there are eight operators in total.

4.3 Spin dependent matrix elements upto and including dimension 8

The spin dependent matrix elements are given by $\langle H | \bar{h} iD^{\mu_1} \dots iD^{\mu_n} s^\lambda h | H \rangle$, where $n =$ operator dimension-3. As we did in section 4.2, the matrix elements are decomposed into nonperturbative constants multiplied by tensor structures that are allowed by symmetries.

²A third possible structure $\bar{h} \{[iD^{\mu_i}, iD^{\mu_j}], [iD^{\mu_l}, [iD^{\mu_m}, iD^{\mu_k}]]\} h$ is related to the first two by the Jacobi identity.

³using a commutators does not give a new structures since $[iD^{\mu_m}, \{[iD^{\mu_i}, iD^{\mu_j}], [iD^{\mu_k}, iD^{\mu_l}]\}] = \{[iD^{\mu_i}, iD^{\mu_j}], [iD^{\mu_m}, [iD^{\mu_k}, iD^{\mu_l}]]\} + \{[iD^{\mu_k}, iD^{\mu_l}], [iD^{\mu_m}, [iD^{\mu_i}, iD^{\mu_j}]]\}$.

4.3.1 Dimension three operators

At dimension three the matrix element contains only one covariant derivative. The matrix element is decomposed into tensor structure with one Lorentz index, which is $v^{\mu\lambda}$. Contracting the matrix element by four velocity we obtain $v \cdot s = 0$ in the left hand side. Therefore, at dimension three there are no spin dependent matrix elements.

$$\frac{1}{2M_H} \langle H | \bar{h} s^\lambda h | H \rangle = 0 \quad (4.21)$$

4.3.2 Dimension four operators

The dimension four matrix element contains one covariant derivative. This provides two Lorentz indices. The matrix is then decomposed into $\Pi^{\mu_1\lambda}$. This is because the contracting by v_{μ_1} and v_λ yields zero. For the choice $v = (1, 0, 0, 0)$, the D^{μ_1} is a space-like, which is due to $\bar{h}v \cdot D = 0$. The matrix element with odd number of space-like derivatives gives zero due to the parity. Hence at the dimension four the spin dependent matrix element vanishes.

$$\frac{1}{2M_H} \langle H | \bar{h} i D^{\mu_1} s^\lambda h | H \rangle = 0 \quad (4.22)$$

4.3.3 Dimension five operators

The operator $\bar{h} i D^{\mu_1} i D^{\mu_2} s^\lambda h$ has three indices, all of which are orthogonal to v . As a result, we cannot use three v 's or a product of one Π and one v . There is only one possible structure:

$$\frac{1}{2M_H} \langle H | \bar{h} i D^{\mu_1} i D^{\mu_2} s^\lambda h | H \rangle = i \tilde{a}^{(5)} \epsilon^{\rho\mu_1\mu_2\lambda} v_\rho \quad (4.23)$$

The tensor $\epsilon^{\rho\mu_1\mu_2\lambda} v_\rho$ is antisymmetric under inversion as required.

4.3.4 Dimension six operators

There is only one possible tensor, a product of v and ϵ . Thus

$$\frac{1}{2M_H} \langle H | \bar{h} i D^{\mu_1} i D^{\mu_2} i D^{\mu_3} s^\lambda h | H \rangle = i \tilde{a}^{(6)} v^{\mu_2} \epsilon^{\rho \mu_1 \mu_3 \lambda} v_\rho \quad (4.24)$$

Again the inversion symmetry is manifest.

4.3.5 Dimension seven operators

For the matrix elements of dimension seven spin-dependent operators there are five independent tensors. One has 2 v 's and ϵ and four that have Π and ϵ . Thus

$$\begin{aligned} & \frac{1}{2M_H} \langle H | \bar{h} i D^{\mu_1} i D^{\mu_2} i D^{\mu_3} i D^{\mu_4} s^\lambda h | H \rangle = \\ & i \tilde{a}_{12}^{(7)} (\Pi^{\mu_1 \mu_2} \epsilon^{\rho \mu_3 \mu_4 \lambda} v_\rho - \Pi^{\mu_4 \mu_3} \epsilon^{\rho \mu_2 \mu_1 \lambda} v_\rho) + i \tilde{a}_{13}^{(7)} (\Pi^{\mu_1 \mu_3} \epsilon^{\rho \mu_2 \mu_4 \lambda} v_\rho - \Pi^{\mu_4 \mu_2} \epsilon^{\rho \mu_3 \mu_1 \lambda} v_\rho) + \\ & + i \tilde{a}_{14}^{(7)} \Pi^{\mu_1 \mu_4} \epsilon^{\rho \mu_2 \mu_3 \lambda} v_\rho + i \tilde{a}_{23}^{(7)} \Pi^{\mu_2 \mu_3} \epsilon^{\rho \mu_1 \mu_4 \lambda} v_\rho + i \tilde{b}^{(7)} v^{\mu_2} v^{\mu_3} \epsilon^{\rho \mu_1 \mu_4 \lambda} v_\rho, \end{aligned} \quad (4.25)$$

where we have imposed the inversion symmetry by combining tensors in the second line of equation (4.25) with the same non-perturbative parameters.

Naively it might seem that there are two other possible independent tensors that involve $\Pi^{\lambda \mu_i}$, namely $\Pi^{\mu_1 \lambda} \epsilon^{\rho \mu_2 \mu_3 \mu_4} v_\rho - \Pi^{\mu_4 \lambda} \epsilon^{\rho \mu_3 \mu_2 \mu_1} v_\rho$ and $\Pi^{\mu_2 \lambda} \epsilon^{\rho \mu_1 \mu_3 \mu_4} v_\rho - \Pi^{\mu_3 \lambda} \epsilon^{\rho \mu_4 \mu_2 \mu_1} v_\rho$. But this would be an over-counting. The tensor $\Pi^{\mu \nu} \epsilon^{\sigma \alpha \beta \rho} v_\sigma$ has five indices orthogonal to v , but in four space-time dimensions there can be only three different indices orthogonal to v . Since $\alpha \neq \beta \neq \rho$ and $\mu = \nu$, it follows that three of the indices in the set $\{\alpha, \beta, \rho, \mu, \nu\}$ are equal. Therefore, if λ is equal to any μ_i it is also equal to some μ_j and hence $\mu_i = \mu_j$ and already included in the tensors of equation (4.25).

For the dimension seven spin-independent case one can construct operators with the same Lorentz structure but different color structure. We can check whether this is possible for the spin-dependent operators by contracting $\bar{h} \{[i D^{\mu_i}, i D^{\mu_j}], [i D^{\mu_k}, i D^{\mu_l}]\} h$ with the tensors on

the right hand side of equation (4.25). We find that all of these vanish, so there are no such operators. We will find the same result in section 4.4.2.3.

4.3.6 Dimension eight operators

For the matrix elements of the dimension eight spin-dependent operators we can have one tensor with 3 v 's, $v^{\mu_2}v^{\mu_3}v^{\mu_4}\epsilon^{\rho\mu_1\mu_5\lambda}v_\rho$, and tensors which are of the form $v\Pi\epsilon$. Following the discussion above, the Π 's should depend only on μ_i . Once we fix v^{μ_i} to be v^{μ_2} , v^{μ_3} , or v^{μ_4} , there are four indices left, which gives six pairs $\{\mu_j, \mu_k\}$ for Π . Including the constraints from inversion symmetry, we find

$$\begin{aligned}
& \frac{1}{2M_B} \langle B | \bar{h} iD^{\mu_1} iD^{\mu_2} iD^{\mu_3} iD^{\mu_4} iD^{\mu_5} s^\lambda h | B \rangle = \\
& i\tilde{a}_{12}^{(8)} (v^{\mu_3} \Pi^{\mu_1\mu_2} \epsilon^{\rho\mu_4\mu_5\lambda} v_\rho - v^{\mu_3} \Pi^{\mu_4\mu_5} \epsilon^{\rho\mu_2\mu_1\lambda} v_\rho) + i\tilde{a}_{14}^{(8)} (v^{\mu_3} \Pi^{\mu_1\mu_4} \epsilon^{\rho\mu_2\mu_5\lambda} v_\rho - v^{\mu_3} \Pi^{\mu_5\mu_2} \epsilon^{\rho\mu_4\mu_1\lambda} v_\rho) + \\
& + i\tilde{a}_{15}^{(8)} v^{\mu_3} \Pi^{\mu_1\mu_5} \epsilon^{\rho\mu_2\mu_4\lambda} v_\rho + i\tilde{a}_{24}^{(8)} v^{\mu_3} \Pi^{\mu_2\mu_4} \epsilon^{\rho\mu_1\mu_5\lambda} v_\rho + \\
& + i\tilde{b}_{13}^{(8)} (v^{\mu_2} \Pi^{\mu_1\mu_3} \epsilon^{\rho\mu_4\mu_5\lambda} v_\rho - v^{\mu_4} \Pi^{\mu_5\mu_3} \epsilon^{\rho\mu_2\mu_1\lambda} v_\rho) + i\tilde{b}_{14}^{(8)} (v^{\mu_2} \Pi^{\mu_1\mu_4} \epsilon^{\rho\mu_3\mu_5\lambda} v_\rho - v^{\mu_4} \Pi^{\mu_5\mu_2} \epsilon^{\rho\mu_3\mu_1\lambda} v_\rho) + \\
& + i\tilde{b}_{15}^{(8)} (v^{\mu_2} \Pi^{\mu_1\mu_5} \epsilon^{\rho\mu_3\mu_4\lambda} v_\rho - v^{\mu_4} \Pi^{\mu_1\mu_5} \epsilon^{\rho\mu_3\mu_2\lambda} v_\rho) + i\tilde{b}_{34}^{(8)} (v^{\mu_2} \Pi^{\mu_3\mu_4} \epsilon^{\rho\mu_1\mu_5\lambda} v_\rho - v^{\mu_4} \Pi^{\mu_3\mu_2} \epsilon^{\rho\mu_5\mu_1\lambda} v_\rho) + \\
& + i\tilde{b}_{35}^{(8)} (v^{\mu_2} \Pi^{\mu_3\mu_5} \epsilon^{\rho\mu_1\mu_4\lambda} v_\rho - v^{\mu_4} \Pi^{\mu_3\mu_1} \epsilon^{\rho\mu_5\mu_2\lambda} v_\rho) + i\tilde{b}_{45}^{(8)} (v^{\mu_2} \Pi^{\mu_4\mu_5} \epsilon^{\rho\mu_1\mu_3\lambda} v_\rho - v^{\mu_4} \Pi^{\mu_2\mu_1} \epsilon^{\rho\mu_5\mu_3\lambda} v_\rho) + \\
& + i\tilde{c}^{(8)} v^{\mu_2} v^{\mu_3} v^{\mu_4} \epsilon^{\rho\mu_1\mu_5\lambda} v_\rho.
\end{aligned} \tag{4.26}$$

The possible multiple color structures are obtained by contracting the As for the spin-independent case we can check if there are operators with the same Lorentz structure but different color structure by contracting $\bar{h} \{[iD^{\mu_i}, iD^{\mu_j}], [iD^{\mu_k}, [iD^{\mu_l}, iD^{\mu_m}]]\} h$, $\bar{h} \{[iD^{\mu_i}, iD^{\mu_j}], [iD^{\mu_m}, [iD^{\mu_k}, iD^{\mu_l}]]\} h$, and $\bar{h} \{iD^{\mu_m}, \{[iD^{\mu_i}, iD^{\mu_j}], [iD^{\mu_k}, iD^{\mu_l}]\}\} h$ with the tensors of the right hand side of equation (4.26). We find six linearly-independent combinations, indicating that there will be six operators with two possible color structures. We will find the same result in section 4.6.2. Including these possible color structures, there seventeen NRQCD (HQET) operators in total.

4.4 HQET operators

Using the tensor decomposition of the spin independent and spin dependent matrix elements provided in the sections 4.2 and 4.3, we now relate the matrix elements to HQET parameters. This list of HQET parameters are found in [62]. As discussed in the section 4.1.2.3, the tree level matching of power corrections to inclusive B decays are relevant to octet color structures. The list of HQET parameters provided in [62] are relevant to these tree level operators. We list the color singlet operators along with the color octet operators in the section 4.6.2.

4.4.1 Spin independent operators

4.4.1.1 Dimension five

The dimension five spin independent operator is defined by [61]

$$\frac{1}{2M_H} \langle H(v) | \bar{Q}_v iD^{\mu_1} iD^{\mu_2} Q_v | H(v) \rangle = \frac{1}{3} \lambda_1 \Pi^{\mu_1 \mu_2}. \quad (4.27)$$

In [62] the matrix elements is defined as

$$\frac{1}{2M_B} \langle B | \bar{b}_v iD^{\mu_1} iD^{\mu_2} b_v | B \rangle \Pi_{\mu_1 \mu_2} = -\mu_\pi^2. \quad (4.28)$$

Using the $\Pi^{\mu_1 \mu_2} \Pi_{\mu_1 \mu_2} = 3$ and tensor decomposition of dimension five matrix element we obtain $-\mu_\pi^2 = \lambda_1 = 3a^{(5)}$. It is important to note that the μ_π^2 is not defined in the heavy quark limit. The parameter μ_π^2 is defined using the full QCD b fields [62]. Following from this we obtain a relation between μ_π^2 and λ_1 , which contains $1/m_b$ corrections.

4.4.1.2 Dimension six

The dimension six spin independent matrix element is defined as [61]

$$\frac{1}{2M_H} \langle H(v) | \bar{Q}_v iD^{\mu_1} iD^{\mu_2} iD^{\mu_3} Q_v | H(v) \rangle = \frac{1}{3} \rho_1 \Pi^{\mu_1 \mu_3} v^{\mu_2}. \quad (4.29)$$

while in [62] the same matrix element is defined as

$$\frac{1}{2M_B} \langle B | \bar{h} \left[iD^{\mu_1}, [iD^{\mu_2}, iD^{\mu_3}] \right] h | B \rangle \frac{1}{2} \Pi_{\mu_1 \mu_3} v_{\mu_2} = \rho_D^3. \quad (4.30)$$

Comparing this to equation (4.18), we find that $\rho_D^3 = \rho_1 = 3a^{(6)}$.

4.4.1.3 Dimension seven

In the dimension seven there are four matrix elements [62]

$$\begin{aligned} 2M_B m_1 &= \langle B | \bar{b}_v iD_\rho iD_\sigma iD_\lambda iD_\delta b_v | B \rangle \frac{1}{3} (\Pi^{\rho\sigma} \Pi^{\lambda\delta} + \Pi^{\rho\lambda} \Pi^{\sigma\delta} + \Pi^{\rho\delta} \Pi^{\sigma\lambda}) \\ 2M_B m_2 &= \langle B | \bar{b}_v [iD_\rho, iD_\sigma] [iD_\lambda, iD_\delta] b_v | B \rangle \Pi^{\rho\delta} v^\sigma v^\lambda \\ 2M_B m_3 &= \langle B | \bar{b}_v [iD_\rho, iD_\sigma] [iD_\lambda, iD_\delta] b_v | B \rangle \Pi^{\rho\lambda} \Pi^{\sigma\delta} \\ 2M_B m_4 &= \langle B | \bar{b}_v \left\{ iD_\rho, [iD_\sigma, [iD_\lambda, iD_\delta]] \right\} b_v | B \rangle \Pi^{\sigma\lambda} \Pi^{\rho\delta} \end{aligned} \quad (4.31)$$

Using the tensor decomposition in equation (4.19) we find

$$m_1 = 5 \left[a_{12}^{(7)} + a_{13}^{(7)} + a_{14}^{(7)} \right], \quad m_2 = 3b^{(7)}, \quad m_3 = 12 \left[a_{13}^{(7)} - a_{14}^{(7)} \right], \quad m_4 = 12 \left[a_{12}^{(7)} - 2a_{13}^{(7)} + a_{14}^{(7)} \right]. \quad (4.32)$$

4.4.1.4 Dimension eight

In [62] seven spin-independent matrix elements are listed⁴ as:

$$\begin{aligned} 2M_B r_1 &= \langle B | \bar{b} iD_\rho (iv \cdot D)^3 iD^\rho b | B \rangle \\ 2M_B r_2 &= \langle B | \bar{b} iD_\rho (iv \cdot D) iD^\rho iD_\sigma iD^\sigma b | B \rangle \\ 2M_B r_3 &= \langle B | \bar{b} iD_\rho (iv \cdot D) iD_\sigma iD^\rho iD^\sigma b | B \rangle \end{aligned}$$

⁴The change $b_v \rightarrow b$ is presumably a typo in [62].

$$\begin{aligned}
2M_B r_4 &= \langle B | \bar{b} i D_\rho (i v \cdot D) i D_\sigma i D^\sigma i D^\rho b | B \rangle \\
2M_B r_5 &= \langle B | \bar{b} i D_\rho i D^\rho (i v \cdot D) i D_\sigma i D^\sigma b | B \rangle \\
2M_B r_6 &= \langle B | \bar{b} i D_\rho i D_\sigma (i v \cdot D) i D^\sigma i D^\rho b | B \rangle \\
2M_B r_7 &= \langle B | \bar{b} i D_\rho i D_\sigma (i v \cdot D) i D^\rho i D^\sigma b | B \rangle
\end{aligned} \tag{4.33}$$

Comparison between these operators with our tensor decomposition in equation (4.20) yields

$$\begin{aligned}
r_1 &= 3c^{(8)} \\
r_2 &= 3 \left[3a_{12}^{(8)} + a_{13}^{(8)} + a_{15}^{(8)} \right], \quad r_3 = 3 \left[a_{12}^{(8)} + 3a_{13}^{(8)} + a_{15}^{(8)} \right], \quad r_4 = 3 \left[a_{12}^{(8)} + a_{13}^{(8)} + 3a_{15}^{(8)} \right] \\
r_5 &= 3 \left[3b_{12}^{(8)} + b_{14}^{(8)} + b_{15}^{(8)} \right], \quad r_6 = 3 \left[b_{12}^{(8)} + b_{14}^{(8)} + 3b_{15}^{(8)} \right], \quad r_7 = 3 \left[b_{12}^{(8)} + 3b_{14}^{(8)} + b_{15}^{(8)} \right]
\end{aligned} \tag{4.34}$$

4.4.2 Spin dependent operators

The dimension three and four matrix elements are zero. We find the first non zero matrix element at dimension five.

4.4.2.1 Dimension five

The dimension five spin dependent matrix element is defined as [61]

$$\frac{1}{2M_H} \langle H(v) | \bar{Q}_v i D^{\mu_1} i D^{\mu_2} s^\lambda Q_v | H(v) \rangle = \frac{1}{2} \lambda_2 i \epsilon^{\rho \mu_1 \mu_2 \lambda} v_\rho, \tag{4.35}$$

The same matrix element is defined as [62]

$$\frac{1}{2M_B} \langle B | \bar{b}_v [i D^{\mu_1}, i D^{\mu_2}] (-i \sigma^{\mu_1 \mu_2}) b_v | B \rangle \Pi_{\mu_1 \mu_2} = \mu_G^2. \tag{4.36}$$

Using the relationship between $\sigma^{\mu\nu}$ and s^λ defined in equation (4.6), we found $\mu_G^2 = 3\lambda_2 = -6\tilde{a}^{(5)}$. Similar to μ_π^2 in section 4.4.1.1, the relationship between μ_G^2 and λ_2 receives corrections at order $1/m_b$.

4.4.2.2 Dimension six

The dimension six spin dependent matrix element is defined by [61]

$$\frac{1}{2M_H} \langle H(v) | \bar{Q}_v iD^{\mu_1} iD^{\mu_2} iD^{\mu_3} s^\lambda Q_v | H(v) \rangle = \frac{1}{2} \rho_2 i v_\nu \epsilon^{\nu\mu_1\mu_3\lambda} v^{\mu_2}, \quad (4.37)$$

The same matrix element is defined in [62] as

$$\frac{1}{2M_B} \langle B | \bar{b}_v \frac{1}{2} \{ iD^{\mu_1}, [iD^{\mu_2}, iD^{\mu_3}] \} (-i\sigma^{\alpha\beta}) b_v | B \rangle \Pi_{\mu_1\alpha} \Pi_{\mu_3\beta} v_{\mu_2} = \rho_{LS}^3. \quad (4.38)$$

Comparing these expressions with the tensor decomposition obtained in equation (4.24), we found $\rho_{LS}^3 = 3\rho_2 = -6\tilde{a}^{(6)}$.

4.4.2.3 Dimension seven

In the dimension seven there are five matrix elements. They are defined as [62]

$$\begin{aligned} 2M_B m_5 &= \langle B | \bar{b}_v [iD_\rho, iD_\sigma] [iD_\lambda, iD_\delta] (-i\sigma_{\alpha\beta}) b_v | B \rangle \Pi^{\alpha\rho} \Pi^{\beta\delta} v^\sigma v^\lambda \\ 2M_B m_6 &= \langle B | \bar{b}_v [iD_\rho, iD_\sigma] [iD_\lambda, iD_\delta] (-i\sigma_{\alpha\beta}) b_v | B \rangle \Pi^{\alpha\sigma} \Pi^{\beta\lambda} \Pi^{\rho\delta} \\ 2M_B m_7 &= \langle B | \bar{b}_v \left\{ \{ iD_\rho, iD_\sigma \}, [iD_\lambda, iD_\delta] \right\} (-i\sigma_{\alpha\beta}) b_v | B \rangle \Pi^{\sigma\lambda} \Pi^{\alpha\rho} \Pi^{\beta\delta} \\ 2M_B m_8 &= \langle B | \bar{b}_v \left\{ \{ iD_\rho, iD_\sigma \}, [iD_\lambda, iD_\delta] \right\} (-i\sigma_{\alpha\beta}) b_v | B \rangle \Pi^{\rho\sigma} \Pi^{\alpha\lambda} \Pi^{\beta\delta} \\ 2M_B m_9 &= \langle B | \bar{b}_v \left[iD_\rho, [iD_\sigma, [iD_\lambda, iD_\delta]] \right] (-i\sigma_{\alpha\beta}) b_v | B \rangle \Pi^{\rho\beta} \Pi^{\lambda\alpha} \Pi^{\sigma\delta}. \end{aligned} \quad (4.39)$$

Comparing this result with the tensor decomposition in equation (4.25) we found

$$\begin{aligned} m_5 &= 6\tilde{b}^{(7)}, \quad m_6 = 6 \left[-2\tilde{a}_{13}^{(7)} + \tilde{a}_{14}^{(7)} + \tilde{a}_{23}^{(7)} \right], \quad m_7 = -12 \left[4\tilde{a}_{12}^{(7)} - 3\tilde{a}_{14}^{(7)} + 3\tilde{a}_{23}^{(7)} \right] \\ m_8 &= 48 \left[3\tilde{a}_{12}^{(7)} - \tilde{a}_{14}^{(7)} + \tilde{a}_{23}^{(7)} \right], \quad m_9 = 12 \left[5\tilde{a}_{12}^{(7)} - 4\tilde{a}_{14}^{(7)} - 3\tilde{a}_{14}^{(7)} + 2\tilde{a}_{23}^{(7)} \right] \end{aligned} \quad (4.40)$$

4.4.2.4 Dimension eight

The dimension eight matrix elements are defined as [62]

$$\begin{aligned}
2M_{Br_8} &= \langle B|\bar{b}iD_\mu(iv \cdot D)^3iD_\nu(-i\sigma^{\mu\nu})b|B\rangle \\
2M_{Br_9} &= \langle B|\bar{b}iD_\mu(iv \cdot D)iD_\nu iD_\rho iD^\rho(-i\sigma^{\mu\nu})b|B\rangle \\
2M_{Br_{10}} &= \langle B|\bar{b}iD_\rho(iv \cdot D)iD^\rho iD_\mu iD_\nu(-i\sigma^{\mu\nu})b|B\rangle \\
2M_{Br_{11}} &= \langle B|\bar{b}iD_\rho(iv \cdot D)iD_\mu iD^\rho iD_\nu(-i\sigma^{\mu\nu})b|B\rangle \\
2M_{Br_{12}} &= \langle B|\bar{b}iD_\mu(iv \cdot D)iD_\rho iD_\nu iD^\rho(-i\sigma^{\mu\nu})b|B\rangle \\
2M_{Br_{13}} &= \langle B|\bar{b}iD_\rho(iv \cdot D)iD_\mu iD_\nu iD^\rho(-i\sigma^{\mu\nu})b|B\rangle \\
2M_{Br_{14}} &= \langle B|\bar{b}iD_\mu(iv \cdot D)iD_\rho iD^\rho iD_\nu(-i\sigma^{\mu\nu})b|B\rangle \\
2M_{Br_{15}} &= \langle B|\bar{b}iD_\mu iD_\nu(iv \cdot D)iD_\rho iD^\rho(-i\sigma^{\mu\nu})b|B\rangle \\
2M_{Br_{16}} &= \langle B|\bar{b}iD_\rho iD_\mu(iv \cdot D)iD_\nu iD^\rho(-i\sigma^{\mu\nu})b|B\rangle \\
2M_{Br_{17}} &= \langle B|\bar{b}iD_\mu iD_\rho(iv \cdot D)iD^\rho iD_\nu(-i\sigma^{\mu\nu})b|B\rangle \\
2M_{Br_{18}} &= \langle B|\bar{b}iD_\rho iD_\mu(iv \cdot D)iD^\rho iD_\nu(-i\sigma^{\mu\nu})b|B\rangle.
\end{aligned} \tag{4.41}$$

Comparing this with the dimension eight matrix tensor decomposition, which is given in equation (4.26), we found

$$\begin{aligned}
r_8 &= 6\tilde{c}^{(8)} \\
r_9 &= -6 \left[\tilde{b}_{14}^{(8)} + \tilde{b}_{15}^{(8)} - \tilde{b}_{34}^{(8)} - \tilde{b}_{35}^{(8)} - 3\tilde{b}_{45}^{(8)} \right], \quad r_{10} = 6 \left[3\tilde{b}_{13}^{(8)} + \tilde{b}_{14}^{(8)} - \tilde{b}_{15}^{(8)} + \tilde{b}_{34}^{(8)} - \tilde{b}_{35}^{(8)} \right], \\
r_{11} &= 6 \left[\tilde{b}_{13}^{(8)} + 3\tilde{b}_{14}^{(8)} + \tilde{b}_{15}^{(8)} + \tilde{b}_{34}^{(8)} - \tilde{b}_{45}^{(8)} \right], \quad r_{12} = 6 \left[-\tilde{b}_{13}^{(8)} + \tilde{b}_{15}^{(8)} + \tilde{b}_{34}^{(8)} + 3\tilde{b}_{35}^{(8)} + \tilde{b}_{45}^{(8)} \right], \\
r_{13} &= -6 \left[\tilde{b}_{13}^{(8)} - \tilde{b}_{14}^{(8)} - 3\tilde{b}_{15}^{(8)} - \tilde{b}_{35}^{(8)} + \tilde{b}_{45}^{(8)} \right], \quad r_{14} = 6 \left[\tilde{b}_{13}^{(8)} + \tilde{b}_{14}^{(8)} + 3\tilde{b}_{34}^{(8)} + \tilde{b}_{35}^{(8)} + \tilde{b}_{45}^{(8)} \right], \\
r_{15} &= 6 \left[3\tilde{a}_{12}^{(8)} - \tilde{a}_{15}^{(8)} + 3\tilde{a}_{24}^{(8)} \right], \quad r_{16} = 6 \left[-2\tilde{a}_{12}^{(8)} + 2\tilde{a}_{14}^{(8)} + 3\tilde{a}_{15}^{(8)} \right], \\
r_{17} &= 6 \left[2\tilde{a}_{12}^{(8)} + 2\tilde{a}_{14}^{(8)} + 3\tilde{a}_{24}^{(8)} \right], \quad r_{18} = 6 \left[3\tilde{a}_{14}^{(8)} + \tilde{a}_{15}^{(8)} + \tilde{a}_{24}^{(8)} \right],
\end{aligned} \tag{4.42}$$

4.5 NRQED and NRQCD operators

In the following section we will relate the NRQED and NRQCD operators to tensor decomposition provided in sections 4.2 and 4.3. The NRQCD Lagrangian upto and including the order $1/M^3$ is provided in [55].

$$\begin{aligned}
\mathcal{L}_{\text{NRQCD}}^{\text{dim} \leq 7} = & \psi^\dagger \left\{ iD_t + c_2 \frac{\mathbf{D}^2}{2M} + c_{Fg} g \frac{\boldsymbol{\sigma} \cdot \mathbf{B}}{2M} + c_{Dg} g \frac{\mathbf{D} \cdot \mathbf{E} - \mathbf{E} \cdot \mathbf{D}}{8M^2} + ic_{Sg} g \frac{\boldsymbol{\sigma} \cdot (\mathbf{D} \times \mathbf{E} - \mathbf{E} \times \mathbf{D})}{8M^2} + \right. \\
& + c_4 \frac{\mathbf{D}^4}{8M^3} + ic_{Mg} g \frac{\{\mathbf{D}^i, (\mathbf{D} \times \mathbf{B} - \mathbf{B} \times \mathbf{D})^i\}}{8M^3} + c_{W1g} g \frac{\{\mathbf{D}^2, \boldsymbol{\sigma} \cdot \mathbf{B}\}}{8M^3} - c_{W2g} g \frac{\mathbf{D}^i \boldsymbol{\sigma} \cdot \mathbf{B} \mathbf{D}^i}{4M^3} + \\
& + c_{p'pg} g \frac{\boldsymbol{\sigma} \cdot \mathbf{D} \mathbf{B} \cdot \mathbf{D} + \mathbf{D} \cdot \mathbf{B} \boldsymbol{\sigma} \cdot \mathbf{D}}{8M^3} + c_{A1g^2} g^2 \frac{(\mathbf{B}_a^i \mathbf{B}_b^i - \mathbf{E}_a^i \mathbf{E}_b^i) T^a T^b}{8M^3} - c_{A2g^2} g^2 \frac{\mathbf{E}_a^i \mathbf{E}_b^i T^a T^b}{16M^3} + \\
& + c_{A3g^2} g^2 \frac{(\mathbf{B}_a^i \mathbf{B}_b^i - \mathbf{E}_a^i \mathbf{E}_b^i) \delta^{ab}}{8M^3} - c_{A4g^2} g^2 \frac{\mathbf{E}_a^i \mathbf{E}_b^i \delta^{ab}}{16M^3} \\
& \left. - c_{B1g^2} g^2 \frac{\boldsymbol{\sigma} \cdot (\mathbf{B}_a \times \mathbf{B}_b - \mathbf{E}_a \times \mathbf{E}_b) f^{abc} T^c}{16M^3} + c_{B2g^2} g^2 \frac{\boldsymbol{\sigma} \cdot (\mathbf{E}_a \times \mathbf{E}_b) f^{abc} T^c}{16M^3} \right\} \psi. \quad (4.43)
\end{aligned}$$

The operators in the last line are specific to NRQCD they do not appear in the NRQED. Also, in NRQED the operators corresponding to coefficients c_{A1} and c_{A3} (c_{A2} and c_{A4}) are identical.

The NRQED Lagrangian at order $1/M^4$ (dimension eight) is given by

$$\begin{aligned}
\mathcal{L}_{\text{NRQED}}^{\text{dim}=8} = & \psi^\dagger \left\{ c_{X1g} g \frac{[\mathbf{D}^2, \mathbf{D} \cdot \mathbf{E} + \mathbf{E} \cdot \mathbf{D}]}{M^4} + c_{X2g} g \frac{\{\mathbf{D}^2, [\boldsymbol{\partial} \cdot \mathbf{E}]\}}{M^4} + c_{X3g} g \frac{[\boldsymbol{\partial}^2 \boldsymbol{\partial} \cdot \mathbf{E}]}{M^4} \right. \\
& + ic_{X4g^2} g^2 \frac{\{\mathbf{D}^i, [\mathbf{E} \times \mathbf{B}]^i\}}{M^4} + ic_{X5g} g \frac{\mathbf{D}^i \boldsymbol{\sigma} \cdot (\mathbf{D} \times \mathbf{E} - \mathbf{E} \times \mathbf{D}) \mathbf{D}^i}{M^4} + ic_{X6g} g \frac{\epsilon^{ijk} \sigma^i \mathbf{D}^j [\boldsymbol{\partial} \cdot \mathbf{E}] \mathbf{D}^k}{M^4} \\
& + c_{X7g^2} g^2 \frac{\boldsymbol{\sigma} \cdot \mathbf{B} [\boldsymbol{\partial} \cdot \mathbf{E}]}{M^4} + c_{X8g^2} g^2 \frac{[\mathbf{E} \cdot \boldsymbol{\partial} \boldsymbol{\sigma} \cdot \mathbf{B}]}{M^4} + c_{X9g^2} g^2 \frac{[\mathbf{B} \cdot \boldsymbol{\partial} \boldsymbol{\sigma} \cdot \mathbf{E}]}{M^4} \\
& \left. + c_{X10g^2} g^2 \frac{[\mathbf{E}^i \boldsymbol{\sigma} \cdot \boldsymbol{\partial} \mathbf{B}^i]}{M^4} + c_{X11g^2} g^2 \frac{[\mathbf{B}^i \boldsymbol{\sigma} \cdot \boldsymbol{\partial} \mathbf{E}^i]}{M^4} + c_{X12g^2} g^2 \frac{\boldsymbol{\sigma} \cdot \mathbf{E} \times [\partial_t \mathbf{E} - \boldsymbol{\partial} \times \mathbf{B}]}{M^4} \right\} \psi. \quad (4.44)
\end{aligned}$$

Some of these operators need to be rewritten in a form appropriate for NRQCD operators, e.g. not assuming that \mathbf{E} and \mathbf{B} commute. We will do that below.

The general procedure we will follow is to take a general NRQCD (NRQED) operator of the form $\psi^\dagger O \psi$ where O is written in terms of \mathbf{D} , \mathbf{E} , \mathbf{B} . We change $\psi \rightarrow h$ and $\psi^\dagger \rightarrow \bar{h}$ and write O in terms of covariant derivatives iD^μ contracted with Π and v . The matrix element

of the resulting operator can be written in terms of the parameters of section 4.1. The utility of this method is that given two NRQCD operators we can immediately determine if they are linearly independent, based on the linear combination of parameters that corresponds to each operator. Possible multiple color factors for operators with the same Lorentz structure are considered separately. We will illustrate this procedure in detail below.

4.5.1 Spin independent operators

4.5.1.1 Dimension four

In equation (4.43) there is one operator with time-like covariant derivative ($\psi^\dagger iD_t \psi$) at dimension four. The corresponding HQET operator is $\bar{h} i v \cdot D h$. Therefore, the matrix element vanishes at dimension four.

4.5.1.2 Dimension five

At dimension five, there is only one spin independent operator in equation (4.43), which is $\psi^\dagger \mathbf{D}^2 \psi$. This operator can be written as $iD^{\mu_1} iD^{\mu_2} \Pi_{\mu_1 \mu_2}$. Using this operator and changing $\psi^\dagger \rightarrow \bar{h}$ and $\psi \rightarrow h$ we found

$$\psi^\dagger D^2 \psi \rightarrow \frac{1}{2M_H} \langle H | \bar{h} i D^{\mu_1} i D^{\mu_2} \Pi_{\mu_1 \mu_2} h | H \rangle = 3a^{(5)} \quad (4.45)$$

4.5.1.3 Dimension six

At dimension six, there is only one spin independent operator in equation (4.43), which is $g\psi^\dagger (\mathbf{D} \cdot \mathbf{E} - \mathbf{E} \cdot \mathbf{D}) \psi$. By re-writing this equation as $-v_{\mu_2} \Pi_{\mu_1 \mu_3} [iD^{\mu_1}, [iD^{\mu_2}, iD^{\mu_3}]]$ and changing $\psi^\dagger \rightarrow \bar{h}$ and $\psi \rightarrow h$ we found

$$-v_{\mu_2} \Pi_{\mu_1 \mu_3} [iD^{\mu_1}, [iD^{\mu_2}, iD^{\mu_3}]] \psi \rightarrow -\frac{1}{2M_H} \langle H | \bar{h} v_{\mu_2} \Pi_{\mu_1 \mu_3} [iD^{\mu_1}, [iD^{\mu_2}, iD^{\mu_3}]] h | H \rangle = -6a^{(6)} \quad (4.46)$$

4.5.1.4 Dimension seven

In equation (4.43) there are six spin independent operators at dimension seven. They are $\psi^\dagger \mathbf{D}^4 \psi$, $g\psi^\dagger \{D^i (\mathbf{D} \times \mathbf{B} - \mathbf{B} \times \mathbf{D})^i\} \psi$, $g^2 \psi^\dagger (\mathbf{B}_a^i \mathbf{B}_b^i - \mathbf{E}_a^i \mathbf{E}_b^i) T^a T^b \psi$, $-g^2 \psi^\dagger \mathbf{E}_a^i \mathbf{E}_b^i T^a T^b \psi$,

$g^2\psi^\dagger (\mathbf{B}_a^i \mathbf{B}_b^i - \mathbf{E}_a^i \mathbf{E}_b^i) \delta^{ab}\psi$. Changing the $\psi^\dagger \rightarrow \bar{h}$ and $\psi \rightarrow h$ we found

$$\begin{aligned}
\psi^\dagger \mathbf{D}^4 \psi &\rightarrow \frac{1}{2M_H} \langle H | \bar{h} iD^{\mu_1} iD^{\mu_2} iD^{\mu_3} iD^{\mu_4} h | H \rangle \Pi_{\mu_1\mu_2} \Pi_{\mu_3\mu_4} = 3 \left(3a_{12}^{(7)} + a_{13}^{(7)} + a_{14}^{(7)} \right), \\
\psi^\dagger g \{ \mathbf{D}^i, (\mathbf{D} \times \mathbf{B} - \mathbf{B} \times \mathbf{D})^i \} \psi &\rightarrow \frac{1}{2M_H} \langle H | \bar{h} \{ iD^{\mu_1}, [iD^{\mu_2}, [iD^{\mu_3}, iD^{\mu_4}]] \} h | H \rangle \Pi_{\mu_1\mu_4} \Pi_{\mu_2\mu_3} \\
&= 12 \left(a_{12}^{(7)} - 2a_{13}^{(7)} + a_{14}^{(7)} \right), \\
g^2\psi^\dagger (\mathbf{B}_a^i \mathbf{B}_b^i - \mathbf{E}_a^i \mathbf{E}_b^i) T^a T^b \psi, g^2\psi^\dagger (\mathbf{B}_a^i \mathbf{B}_b^i - \mathbf{E}_a^i \mathbf{E}_b^i) \delta^{ab}\psi &\rightarrow \\
-\frac{1}{2} \frac{1}{2M_H} \langle H | \bar{h} [iD^{\mu_1}, iD^{\mu_2}] [iD^{\mu_3}, iD^{\mu_4}] h | H \rangle g_{\mu_1\mu_3} g_{\mu_2\mu_4} &= 3 \left(-2a_{13}^{(7)} + 2a_{14}^{(7)} + b^{(7)} \right), \\
-g^2\psi^\dagger \mathbf{E}_a^i \mathbf{E}_b^i T^a T^b \psi, -g^2\psi^\dagger \mathbf{E}_a^i \mathbf{E}_b^i \delta^{ab}\psi &\rightarrow -\frac{1}{2M_H} \langle H | \bar{h} [iD^{\mu_1}, iD^{\mu_2}] [iD^{\mu_3}, iD^{\mu_4}] h | H \rangle g_{\mu_1\mu_3} v_{\mu_2} v_{\mu_4} \\
&= -3b^{(7)}.
\end{aligned} \tag{4.47}$$

All these linear combinations of $a_{12}^{(7)}$, $a_{13}^{(7)}$, $a_{14}^{(7)}$, and $b^{(7)}$ are independent of each other. As shown in the section 4.19, there are two operators with different color structures that has same Lorentz structure. The linear combinations for those two operators are $a_{12}^{(7)}$, $a_{13}^{(7)}$, and $a_{14}^{(7)}$.

4.5.1.5 Dimension eight

The NRQED Lagrangian in equation (4.44) provide four spin independent operators at dimension eight. These operators can be generalized to the NRQCD by using $g\psi^\dagger \{ \mathbf{D}^2, [\boldsymbol{\partial} \cdot \mathbf{E}] \} \psi \rightarrow g\psi^\dagger \{ \mathbf{D}^2, [\mathbf{D}^i, \mathbf{E}^i] \} \psi$ and $g\psi^\dagger [\boldsymbol{\partial}^2 \boldsymbol{\partial} \cdot \mathbf{E}] \psi \rightarrow g\psi^\dagger [\mathbf{D}^i, [D^i, [\mathbf{D}^j, \mathbf{E}^j]]] \psi$. The operator $g^2\psi^\dagger \{ i\mathbf{D}^i, [\mathbf{E} \times \mathbf{B}]^i \} \psi$ provides color octet and singlet structures, and they are $\frac{1}{2}g^2\psi^\dagger \{ i\mathbf{D}^i, \epsilon^{ijk} \mathbf{E}_a^j \mathbf{B}_b^k \{ T^a, T^b \} \} \psi$ and $g^2\psi^\dagger \{ i\mathbf{D}^i, \epsilon^{ijk} \mathbf{E}_a^j \mathbf{B}_b^k \delta^{ab} \} \psi$. By replacing the $\psi^\dagger \rightarrow \bar{h}$ and $\psi \rightarrow h$ we obtain:

$$\begin{aligned}
g\psi^\dagger [\mathbf{D}^2, \{ \mathbf{D}^i, \mathbf{E}^i \}] \psi &\rightarrow -\frac{1}{2M_H} \langle H | \bar{h} [iD^{\mu_1} iD^{\mu_2}, \{ iD^{\mu_3}, [iD^{\mu_4}, iD^{\mu_5}] \}] h | H \rangle v_{\mu_4} \Pi_{\mu_1\mu_2} \Pi_{\mu_3\mu_5} \\
&= -6 \left(3b_{12}^{(8)} + b_{14}^{(8)} + b_{15}^{(8)} \right),
\end{aligned}$$

$$\begin{aligned}
& g\psi^\dagger \{ \mathbf{D}^2, [\mathbf{D}^i, \mathbf{E}^i] \} \psi \rightarrow -\frac{1}{2M_H} \langle H | \bar{h} \{ iD^{\mu_1} iD^{\mu_2}, [iD^{\mu_3}, [iD^{\mu_4}, iD^{\mu_5}]] \} h | H \rangle v_{\mu_4} \Pi_{\mu_1 \mu_2} \Pi_{\mu_3 \mu_5} \\
& = -6 \left(6a_{12}^{(8)} + 2a_{13}^{(8)} + 2a_{15}^{(8)} - 3b_{12}^{(8)} - b_{14}^{(8)} - b_{15}^{(8)} \right), \\
& \psi^\dagger g[\mathbf{D}^i, [\mathbf{D}^i, [\mathbf{D}^j, \mathbf{E}^j]]] \psi \rightarrow \\
& \rightarrow -\frac{1}{2M_H} \langle H | \bar{h} [iD^{\mu_1}, [iD^{\mu_2}, [iD^{\mu_3}, [iD^{\mu_4}, iD^{\mu_5}]]]] h | B \rangle v_{\mu_4} \Pi_{\mu_1 \mu_2} \Pi_{\mu_3 \mu_5} \\
& = -6 \left(8a_{12}^{(8)} + 4a_{13}^{(8)} + 8a_{15}^{(8)} - 5b_{12}^{(8)} - 3b_{14}^{(8)} - 7b_{15}^{(8)} \right), \\
& \frac{g^2}{2} \psi^\dagger \{ i\mathbf{D}^i, \epsilon^{ijk} \mathbf{E}_a^j \mathbf{B}_b^k \{ T^a, T^b \} \} \psi, g^2 \psi^\dagger \{ i\mathbf{D}^i, \epsilon^{ijk} \mathbf{E}_a^j \mathbf{B}_b^k \delta^{ab} \} \psi \rightarrow \\
& \rightarrow \frac{1}{2} \frac{1}{2M_H} \langle H | \bar{h} \{ iD^{\mu_1}, \{ [iD^{\mu_2}, iD^{\mu_3}], [iD^{\mu_4}, iD^{\mu_5}] \} \} h | B \rangle v_{\mu_2} \Pi_{\mu_1 \mu_4} \Pi_{\mu_3 \mu_5} \\
& = 6 \left(a_{12}^{(8)} - a_{15}^{(8)} - b_{14}^{(8)} + b_{15}^{(8)} \right). \tag{4.48}
\end{aligned}$$

The NRQCD contains three other operators that are absent in NRQED. We will list these operators in section 4.6.2.

4.5.2 Spin dependent operators

For the Levi-Civita tensor we used the sign convention $\epsilon^{0123} = -1$ and $\epsilon_{0123} = +1$. Therefore, the three dimension operators such as $\epsilon_{ijk} A^i B^j C^k$ are generalized to the four dimension as $-\epsilon_{0\mu\nu\alpha} A^\mu B^\nu C^\alpha$. The overall minus sign arises due to three space-like contractions. For example, the covariant derivative $D^\mu = (D^0, -\mathbf{D})$ provides a overall minus sign when considering a triple product of space-like derivatives.

4.5.2.1 Dimension five

At dimension five we find the first non vanishing spin dependent operator in equation (4.43), and it is given by $g\psi^\dagger \boldsymbol{\sigma} \cdot \mathbf{B} \psi$. This operator can be rewritten as $-\frac{i}{2} \psi^\dagger \epsilon^{ijk} \boldsymbol{\sigma}^i [i\mathbf{D}^j, i\mathbf{D}^k] \psi$. The generalization of the three dimensional tripple product to four dimension provides an additional minus sign. As a result, the dimension five spin dependent matrix element is written as $\epsilon^{ijk} \boldsymbol{\sigma}^i [i\mathbf{D}^j, i\mathbf{D}^k] \rightarrow -\epsilon_{\rho\lambda\mu_1\mu_2} v^\rho s^\lambda [iD^{\mu_1}, iD^{\mu_2}]$. Changing the $\psi^\dagger \rightarrow \bar{h}$ and $\psi \rightarrow h$ provides:

$$g\psi^\dagger \boldsymbol{\sigma} \cdot \mathbf{B} \psi \rightarrow \frac{1}{2M_H} \frac{1}{2} i\epsilon_{\rho\lambda\mu_1\mu_2} v^\rho s^\lambda \langle H | \bar{h} s^\lambda [iD^{\mu_1}, iD^{\mu_2}] h | H \rangle = 6\tilde{a}^{(5)} \tag{4.49}$$

4.5.2.2 Dimension six

In equation (4.43), there is only one dimension six spin dependent operator, which is $ig\psi^\dagger\boldsymbol{\sigma}\cdot(\mathbf{D}\times\mathbf{E}-\mathbf{E}\times\mathbf{D})\psi$. As shown in the above, we construct the corresponding HQET matrix element as follows:

$$\begin{aligned} ig\psi^\dagger\boldsymbol{\sigma}\cdot(\mathbf{D}\times\mathbf{E}-\mathbf{E}\times\mathbf{D})\psi &\rightarrow -\frac{1}{2M_H}i\epsilon_{\rho\lambda\mu_1\mu_3}v^\rho v_{\mu_2}\langle H|\bar{h}s^\lambda\{iD^{\mu_1},[iD^{\mu_2},iD^{\mu_3}]\}h|H\rangle = \\ &= -12\tilde{a}^{(6)} \end{aligned} \quad (4.50)$$

4.5.2.3 Dimension seven

In equation (4.43), there are five spin dependent operators at dimension five. They are $g\psi^\dagger\{\mathbf{D}^2,\boldsymbol{\sigma}\cdot\mathbf{B}\}\psi$, $g\psi^\dagger\mathbf{D}^i\boldsymbol{\sigma}\cdot\mathbf{B}\mathbf{D}^i\psi$, $g\psi^\dagger\boldsymbol{\sigma}\cdot\mathbf{D}\mathbf{B}\cdot\mathbf{D}+\mathbf{D}\cdot\mathbf{B}\boldsymbol{\sigma}\cdot\mathbf{D}\psi$, $g^2\psi^\dagger\boldsymbol{\sigma}\cdot(\mathbf{B}_a\times\mathbf{B}_b)f^{abc}T^c\psi$, and $g^2\psi^\dagger\boldsymbol{\sigma}\cdot(\mathbf{E}_a\times\mathbf{E}_b)f^{abc}T^c\psi$. At dimension seven there are no operators with multiple color structures. Changing the $\psi^\dagger\rightarrow\bar{h}$ and $\psi\rightarrow h$ provides:

$$\begin{aligned} g\psi^\dagger\{\mathbf{D}^2,\boldsymbol{\sigma}\cdot\mathbf{B}\}\psi &\rightarrow \frac{1}{2M_H}\frac{1}{2}i\epsilon_{\rho\mu_3\mu_4\lambda}v^\rho\Pi_{\mu_1\mu_2}\langle H|\bar{h}s^\lambda\{iD^{\mu_1}iD^{\mu_2},[iD^{\mu_3},iD^{\mu_4}]\}h|H\rangle = \\ &= 12\left(3\tilde{a}_{12}^{(7)}-\tilde{a}_{14}^{(7)}+\tilde{a}_{23}^{(7)}\right), \\ g\psi^\dagger\mathbf{D}^i\boldsymbol{\sigma}\cdot\mathbf{B}\mathbf{D}^i\psi &\rightarrow \frac{1}{2M_H}\frac{1}{2}i\epsilon_{\rho\mu_2\mu_3\lambda}v^\rho\Pi_{\mu_1\mu_4}\langle H|\bar{h}s^\lambda iD^{\mu_1}[iD^{\mu_2},iD^{\mu_3}]iD^{\mu_4}h|H\rangle = \\ &= 6\left(-2\tilde{a}_{12}^{(7)}+2\tilde{a}_{13}^{(7)}+3\tilde{a}_{14}^{(7)}\right), \\ g\psi^\dagger\boldsymbol{\sigma}\cdot\mathbf{D}\mathbf{B}\cdot\mathbf{D}+\mathbf{D}\cdot\mathbf{B}\boldsymbol{\sigma}\cdot\mathbf{D}\psi &\rightarrow -\frac{1}{2M_H}\frac{1}{2}i\epsilon_{\rho\mu_1\mu_2\mu_3}v^\rho\Pi_{\lambda\mu_4}\langle H|\bar{h}s^\lambda iD^{\mu_1}[iD^{\mu_2},iD^{\mu_3}]iD^{\mu_4}h|H\rangle \\ &\quad -\frac{1}{2M_H}\frac{1}{2}i\epsilon_{\rho\mu_4\mu_2\mu_3}v^\rho\Pi_{\lambda\mu_1}\langle H|\bar{h}s^\lambda iD^{\mu_1}[iD^{\mu_2},iD^{\mu_3}]iD^{\mu_4}h|H\rangle = -12\left(\tilde{a}_{12}^{(7)}-\tilde{a}_{13}^{(7)}+\tilde{a}_{14}^{(7)}\right), \\ g^2\psi^\dagger\boldsymbol{\sigma}\cdot(\mathbf{B}_a\times\mathbf{B}_b)f^{abc}T^c\psi &\rightarrow \frac{1}{2M_H}\frac{1}{2}i\epsilon_{\rho\mu_1\mu_2\mu_4}v^\rho\Pi_{\lambda\mu_3}\langle H|\bar{h}s^\lambda[iD^{\mu_1},iD^{\mu_2}][iD^{\mu_3},iD^{\mu_4}]h|H\rangle = \\ &= 6\left(2\tilde{a}_{13}^{(7)}-\tilde{a}_{14}^{(7)}-\tilde{a}_{23}^{(7)}\right), \\ g^2\psi^\dagger\boldsymbol{\sigma}\cdot(\mathbf{E}_a\times\mathbf{E}_b)f^{abc}T^c\psi &\rightarrow \frac{1}{2M_H}i\epsilon_{\rho\mu_2\mu_4\lambda}v^\rho v_{\mu_1}v_{\mu_3}\langle H|\bar{h}s^\lambda[iD^{\mu_1},iD^{\mu_2}][iD^{\mu_3},iD^{\mu_4}]h|H\rangle = \\ &= -6\tilde{b}^{(7)}. \end{aligned} \quad (4.51)$$

4.5.2.4 Dimension eight

There are eight spin-dependent dimension-eight operators in the $1/M^4$ NRQED Lagrangian in equation (4.44). For the NRQCD operators we rewrite $\psi^\dagger \epsilon^{ijk} \sigma^i \mathbf{D}^j [\partial \cdot \mathbf{E}] \mathbf{D}^k \psi$ as $\psi^\dagger \epsilon^{ijk} \sigma^i \mathbf{D}^j [D^l, \mathbf{E}^l] \mathbf{D}^k \psi$. The operator $g^2 \psi^\dagger \sigma \cdot \mathbf{B} [\partial \cdot \mathbf{E}] \psi$ corresponds to two possible NRQCD operators $\frac{1}{2} g^2 \psi^\dagger \{ \sigma \cdot \mathbf{B}_a T^a, [D^i, \mathbf{E}^i]_b T^b \} \psi$ and $g^2 \psi^\dagger \sigma \cdot \mathbf{B}_a [D^i, \mathbf{E}^i]_a \psi$. The notation is such that $[D^i, \mathbf{E}^i]_a = \nabla \cdot \mathbf{E}_a + g f^{abc} \mathbf{A}_b \cdot \mathbf{E}_c$ [101]. Similarly $g^2 \psi^\dagger [\mathbf{E} \cdot \partial \sigma \cdot \mathbf{B}] \psi$ corresponds to $\frac{1}{2} g^2 \psi^\dagger \{ \mathbf{E}_a^i T^a, [D^i, \sigma \cdot \mathbf{B}]_b T^b \} \psi$ and $g^2 \psi^\dagger \mathbf{E}_a^i [D^i, \sigma \cdot \mathbf{B}]_a \psi$, $g^2 \psi^\dagger [\mathbf{B} \cdot \partial \sigma \cdot \mathbf{E}] \psi$ corresponds to $\frac{1}{2} g^2 \psi^\dagger \{ \mathbf{B}_a^i T^a, [D^i, \sigma \cdot \mathbf{E}]_b T^b \} \psi$ and $g^2 \psi^\dagger \mathbf{B}_a^i [D^i, \sigma \cdot \mathbf{E}]_a \psi$, $g^2 \psi^\dagger [\mathbf{E}^i \sigma \cdot \partial \mathbf{B}^i] \psi$ corresponds to $\frac{1}{2} g^2 \psi^\dagger \{ \mathbf{E}_a^i T^a, [\sigma \cdot \mathbf{D}, \mathbf{B}^i]_b T^b \} \psi$ and $g^2 \psi^\dagger \mathbf{E}_a^i [\sigma \cdot \mathbf{D}, \mathbf{B}^i]_a \psi$, and $g^2 \psi^\dagger [\mathbf{B}^i \sigma \cdot \partial \mathbf{E}^i] \psi$ corresponds to $\frac{1}{2} g^2 \psi^\dagger \{ \mathbf{B}_a^i T^a, [\sigma \cdot \mathbf{D}, \mathbf{E}^i]_b T^b \} \psi$ and $g^2 \psi^\dagger \mathbf{B}_a^i [\sigma \cdot \mathbf{D}, \mathbf{E}^i]_a \psi$. The last operator in equation (4.44) contains two parts: $\sigma \cdot \mathbf{E} \times [\partial_t \mathbf{E}]$ and $-\sigma \cdot \mathbf{E} \times [\partial \times \mathbf{B}]$. The second part can be expressed in terms of other operators in equation (4.44), so we will not consider it below. The first part corresponds to two possible NRQCD operators $\frac{1}{2} g^2 \psi^\dagger \epsilon^{ijk} \sigma^i \mathbf{E}_a^j [D_t, \mathbf{E}^k]_b \{ T^a, T^b \} \psi$ and $g^2 \psi^\dagger \epsilon^{ijk} \sigma^i \mathbf{E}_a^j [D_t, \mathbf{E}^k]_a \psi$. Changing $\psi \rightarrow h$, $\psi^\dagger \rightarrow \bar{h}$ we get

$$\begin{aligned}
& ig \psi^\dagger \mathbf{D}^i \sigma \cdot (\mathbf{D} \times \mathbf{E} - \mathbf{E} \times \mathbf{D}) \mathbf{D}^i \psi \rightarrow \\
& \rightarrow \frac{1}{2M_H} (-i) \epsilon_{\rho\lambda\mu_2\mu_4} v^\rho \Pi_{\mu_1\mu_5} v_{\mu_3} \langle H | \bar{h} s^\lambda i D^{\mu_1} \{ i D^{\mu_2}, [i D^{\mu_3}, i D^{\mu_4}] \} i D^{\mu_5} h | H \rangle = \\
& = 12 \left(2\tilde{a}_{12}^{(8)} - 2\tilde{a}_{14}^{(8)} - 3\tilde{a}_{15}^{(8)} - \tilde{b}_{13}^{(8)} + \tilde{b}_{14}^{(8)} + 3\tilde{b}_{15}^{(8)} + \tilde{b}_{35}^{(8)} - \tilde{b}_{45}^{(8)} \right), \\
& ig \psi^\dagger \epsilon^{ijk} \sigma^i \mathbf{D}^j [D^l, \mathbf{E}^l] \mathbf{D}^k \psi \rightarrow \\
& \rightarrow \frac{1}{2M_H} i \epsilon_{\rho\lambda\mu_1\mu_5} v^\rho \Pi_{\mu_2\mu_4} v_{\mu_3} \langle H | \bar{h} s^\lambda i D^{\mu_1} [i D^{\mu_2}, [i D^{\mu_3}, i D^{\mu_4}]] i D^{\mu_5} h | H \rangle = \\
& = 12 \left(2\tilde{a}_{12}^{(8)} + 2\tilde{a}_{14}^{(8)} + 3\tilde{a}_{24}^{(8)} - \tilde{b}_{13}^{(8)} - \tilde{b}_{14}^{(8)} - 3\tilde{b}_{34}^{(8)} - \tilde{b}_{35}^{(8)} - \tilde{b}_{45}^{(8)} \right), \\
& \frac{1}{2} g^2 \psi^\dagger \{ \sigma \cdot \mathbf{B}_a T^a, [D^i, \mathbf{E}^i]_b T^b \} \psi, g^2 \psi^\dagger \sigma \cdot \mathbf{B}_a [D^i, \mathbf{E}^i]_a \psi \rightarrow \\
& \rightarrow -\frac{1}{2M_H} \frac{i}{4} \epsilon_{\rho\lambda\mu_1\mu_2} v^\rho \Pi_{\mu_3\mu_5} v_{\mu_4} \langle H | \bar{h} s^\lambda \{ [i D^{\mu_1}, i D^{\mu_2}], [i D^{\mu_3}, [i D^{\mu_4}, i D^{\mu_5}]] \} h | H \rangle = \\
& = 6 \left(3\tilde{a}_{12}^{(8)} - \tilde{a}_{15}^{(8)} + \tilde{a}_{24}^{(8)} - 6\tilde{b}_{13}^{(8)} - 2\tilde{b}_{14}^{(8)} + 2\tilde{b}_{15}^{(8)} - 2\tilde{b}_{34}^{(8)} + 2\tilde{b}_{35}^{(8)} \right),
\end{aligned}$$

$$\begin{aligned}
& \frac{1}{2}g^2\psi^\dagger\{\mathbf{E}_a^iT^a, [\mathbf{D}^i, \boldsymbol{\sigma} \cdot \mathbf{B}]_bT^b\}\psi, g^2\psi^\dagger\mathbf{E}_a^i[\mathbf{D}^i, \boldsymbol{\sigma} \cdot \mathbf{B}]_a\psi \rightarrow \\
& \rightarrow -\frac{1}{2M_H}\frac{i}{4}\epsilon_{\rho\lambda\mu_4\mu_5}v^\rho\Pi_{\mu_2\mu_3}v_{\mu_1}\langle H|\bar{h}s^\lambda\{[iD^{\mu_1}, iD^{\mu_2}], [iD^{\mu_3}, [iD^{\mu_4}, iD^{\mu_5}]]\}h|H\rangle = \\
& = 6\left(4\tilde{b}_{13}^{(8)} - 4\tilde{b}_{15}^{(8)} + \tilde{b}_{34}^{(8)} - 2\tilde{b}_{35} + \tilde{b}_{45}\right), \\
& \frac{1}{2}g^2\psi^\dagger\{\mathbf{B}_a^iT^a, [\mathbf{D}^i, \boldsymbol{\sigma} \cdot \mathbf{E}]_bT^b\}\psi, g^2\psi^\dagger\mathbf{B}_a^i[\mathbf{D}^i, \boldsymbol{\sigma} \cdot \mathbf{E}]_a\psi \rightarrow \\
& \rightarrow \frac{1}{2M_H}\frac{i}{4}\epsilon_{\rho\mu_1\mu_2\mu_3}v^\rho\Pi_{\lambda\mu_5}v_{\mu_4}\langle H|\bar{h}s^\lambda\{[iD^{\mu_1}, iD^{\mu_2}], [iD^{\mu_3}, [iD^{\mu_4}, iD^{\mu_5}]]\}h|H\rangle = \\
& = -6\left(\tilde{a}_{12}^{(8)} + \tilde{a}_{14}^{(8)} - \tilde{a}_{24}^{(8)} - 2\tilde{b}_{13}^{(8)} + \tilde{b}_{14}^{(8)} - \tilde{b}_{15}^{(8)} + \tilde{b}_{34}^{(8)} - \tilde{b}_{35}^{(8)}\right), \\
& \frac{1}{2}g^2\psi^\dagger\{\mathbf{E}_a^iT^a, [\boldsymbol{\sigma} \cdot \mathbf{D}, \mathbf{B}^i]_bT^b\}\psi, g^2\psi^\dagger\mathbf{E}_a^i[\boldsymbol{\sigma} \cdot \mathbf{D}, \mathbf{B}^i]_a\psi \rightarrow \\
& \rightarrow \frac{1}{2M_H}\frac{i}{4}\epsilon_{\rho\mu_2\mu_4\mu_5}v^\rho\Pi_{\lambda\mu_3}v_{\mu_1}\langle H|\bar{h}s^\lambda\{[iD^{\mu_1}, iD^{\mu_2}], [iD^{\mu_3}, [iD^{\mu_4}, iD^{\mu_5}]]\}h|H\rangle = \\
& = -6\left(\tilde{b}_{13}^{(8)} - \tilde{b}_{15}^{(8)} - \tilde{b}_{34}^{(8)} + 2\tilde{b}_{35}^{(8)} - \tilde{b}_{45}^{(8)}\right), \\
& \frac{1}{2}g^2\psi^\dagger\{\mathbf{B}_a^iT^a, [\boldsymbol{\sigma} \cdot \mathbf{D}, \mathbf{E}^i]_bT^b\}\psi, g^2\psi^\dagger\mathbf{B}_a^i[\boldsymbol{\sigma} \cdot \mathbf{D}, \mathbf{E}^i]_a\psi \rightarrow \\
& \rightarrow \frac{1}{2M_H}\frac{i}{4}\epsilon_{\rho\mu_1\mu_2\mu_5}v^\rho\Pi_{\lambda\mu_3}v_{\mu_4}\langle H|\bar{h}s^\lambda\{[iD^{\mu_1}, iD^{\mu_2}], [iD^{\mu_3}, [iD^{\mu_4}, iD^{\mu_5}]]\}h|H\rangle = \\
& = -6\left(\tilde{a}_{12}^{(8)} - \tilde{a}_{14}^{(8)} + \tilde{a}_{15}^{(8)} - 2\tilde{b}_{13}^{(8)} + \tilde{b}_{14}^{(8)} - \tilde{b}_{15}^{(8)} + \tilde{b}_{34}^{(8)} - \tilde{b}_{35}^{(8)}\right), \\
& \frac{1}{2}g^2\psi^\dagger\epsilon^{ijk}\boldsymbol{\sigma}^i\mathbf{E}_a^j[D_t, \mathbf{E}^k]_b\{T^a, T^b\}\psi, g^2\psi^\dagger\epsilon^{ijk}\boldsymbol{\sigma}^i\mathbf{E}_a^j[D_t, \mathbf{E}^k]_a\psi \rightarrow \\
& \rightarrow -\frac{1}{2M_H}\frac{i}{2}\epsilon_{\rho\lambda\mu_2\mu_5}v^\rho v_{\mu_1}v_{\mu_3}v_{\mu_4}\langle H|\bar{h}s^\lambda\{[iD^{\mu_1}, iD^{\mu_2}], [iD^{\mu_3}, [iD^{\mu_4}, iD^{\mu_5}]]\}h|H\rangle = \\
& = 6\tilde{c}^{(8)}. \tag{4.52}
\end{aligned}$$

The NRQCD contains extra operators that are not presented in NRQED. We list these extra operators in section 4.6.2

4.6 Applications

4.6.1 Tensor decomposition of Dimension nine spin independent HQET matrix element

We extended the general tensor decomposition of HQET matrix elements discussed in section 4.2 to dimension nine. At dimension nine the matrix elements contain six covariant derivatives. The matrix element is decomposed into tensors that contains zero v 's, two v 's or four v 's. Thus we obtain 24 tensors for the spin independent matrix element, which are

given by

$$\begin{aligned}
\frac{1}{2M_H} \langle H | \bar{h} i D^{\mu_1} i D^{\mu_2} i D^{\mu_3} i D^{\mu_4} i D^{\mu_5} i D^{\mu_6} h | H \rangle = & a_{12,34}^{(9)} \Pi^{\mu_1 \mu_2} \Pi^{\mu_3 \mu_4} \Pi^{\mu_5 \mu_6} + \\
& + a_{12,35}^{(9)} (\Pi^{\mu_1 \mu_2} \Pi^{\mu_3 \mu_5} \Pi^{\mu_4 \mu_6} + \Pi^{\mu_1 \mu_3} \Pi^{\mu_2 \mu_4} \Pi^{\mu_5 \mu_6}) + a_{12,36}^{(9)} (\Pi^{\mu_1 \mu_2} \Pi^{\mu_3 \mu_6} \Pi^{\mu_4 \mu_5} + \Pi^{\mu_1 \mu_4} \Pi^{\mu_2 \mu_3} \Pi^{\mu_5 \mu_6}) + \\
& + a_{13,25}^{(9)} \Pi^{\mu_1 \mu_3} \Pi^{\mu_2 \mu_5} \Pi^{\mu_4 \mu_6} + a_{13,26}^{(9)} (\Pi^{\mu_1 \mu_3} \Pi^{\mu_2 \mu_6} \Pi^{\mu_4 \mu_5} + \Pi^{\mu_1 \mu_5} \Pi^{\mu_2 \mu_3} \Pi^{\mu_4 \mu_6}) + \\
& + a_{14,25}^{(9)} \Pi^{\mu_1 \mu_4} \Pi^{\mu_2 \mu_5} \Pi^{\mu_3 \mu_6} + a_{14,26}^{(9)} (\Pi^{\mu_1 \mu_4} \Pi^{\mu_2 \mu_6} \Pi^{\mu_3 \mu_5} + \Pi^{\mu_1 \mu_5} \Pi^{\mu_2 \mu_4} \Pi^{\mu_3 \mu_6}) + \\
& + a_{15,26}^{(9)} \Pi^{\mu_1 \mu_5} \Pi^{\mu_2 \mu_6} \Pi^{\mu_3 \mu_4} + a_{16,23}^{(9)} \Pi^{\mu_1 \mu_6} \Pi^{\mu_2 \mu_3} \Pi^{\mu_4 \mu_5} + a_{16,24}^{(9)} \Pi^{\mu_1 \mu_6} \Pi^{\mu_2 \mu_4} \Pi^{\mu_3 \mu_5} + \\
& + a_{16,25}^{(9)} \Pi^{\mu_1 \mu_6} \Pi^{\mu_2 \mu_5} \Pi^{\mu_3 \mu_4} + b_{12,36}^{(9)} (\Pi^{\mu_1 \mu_2} \Pi^{\mu_3 \mu_6} \nu^{\mu_4} \nu^{\mu_5} + \Pi^{\mu_1 \mu_4} \Pi^{\mu_5 \mu_6} \nu^{\mu_2} \nu^{\mu_3}) + \\
& + b_{12,46}^{(9)} (\Pi^{\mu_1 \mu_2} \Pi^{\mu_4 \mu_6} \nu^{\mu_3} \nu^{\mu_5} + \Pi^{\mu_1 \mu_3} \Pi^{\mu_5 \mu_6} \nu^{\mu_2} \nu^{\mu_4}) + b_{12,56}^{(9)} \Pi^{\mu_1 \mu_2} \Pi^{\mu_5 \mu_6} \nu^{\mu_3} \nu^{\mu_4} + \\
& + b_{13,26}^{(9)} (\Pi^{\mu_1 \mu_3} \Pi^{\mu_2 \mu_6} \nu^{\mu_4} \nu^{\mu_5} + \Pi^{\mu_1 \mu_5} \Pi^{\mu_4 \mu_6} \nu^{\mu_2} \nu^{\mu_3}) + \\
& + b_{13,46}^{(9)} \Pi^{\mu_1 \mu_3} \Pi^{\mu_4 \mu_6} \nu^{\mu_2} \nu^{\mu_5} + b_{14,26}^{(9)} (\Pi^{\mu_1 \mu_4} \Pi^{\mu_2 \mu_6} \nu^{\mu_3} \nu^{\mu_5} + \Pi^{\mu_1 \mu_5} \Pi^{\mu_3 \mu_6} \nu^{\mu_2} \nu^{\mu_4}) + \\
& + b_{14,36}^{(9)} \Pi^{\mu_1 \mu_4} \Pi^{\mu_3 \mu_6} \nu^{\mu_2} \nu^{\mu_5} + b_{15,26}^{(9)} \Pi^{\mu_1 \mu_5} \Pi^{\mu_2 \mu_6} \nu^{\mu_3} \nu^{\mu_4} + \\
& + b_{16,23}^{(9)} (\Pi^{\mu_1 \mu_6} \Pi^{\mu_2 \mu_3} \nu^{\mu_4} \nu^{\mu_5} + \Pi^{\mu_1 \mu_6} \Pi^{\mu_4 \mu_5} \nu^{\mu_2} \nu^{\mu_3}) + \\
& + b_{16,24}^{(9)} (\Pi^{\mu_1 \mu_6} \Pi^{\mu_2 \mu_4} \nu^{\mu_3} \nu^{\mu_5} + \Pi^{\mu_1 \mu_6} \Pi^{\mu_3 \mu_5} \nu^{\mu_2} \nu^{\mu_4}) + b_{16,25}^{(9)} \Pi^{\mu_1 \mu_6} \Pi^{\mu_2 \mu_5} \nu^{\mu_3} \nu^{\mu_4} + \\
& + b_{16,34}^{(9)} \Pi^{\mu_1 \mu_6} \Pi^{\mu_3 \mu_4} \nu^{\mu_2} \nu^{\mu_5} + c^{(9)} \Pi^{\mu_1 \mu_6} \nu^{\mu_2} \nu^{\mu_3} \nu^{\mu_4} \nu^{\mu_5}
\end{aligned} \tag{4.53}$$

The multiple color structures arise from the structures: $[iD^{\mu_i}, iD^{\mu_j}]$, $[iD^{\mu_i}, [iD^{\mu_j}, iD^{\mu_k}]]$ and $[iD^{\mu_i}, [iD^{\mu_j}, [iD^{\mu_k}, iD^{\mu_l}]]]$. However, we did not consider the possible operators arise from these structures in this discussion.

4.6.2 NRQCD Lagrangian at order $1/M^4$

As shown in the sections 4.5.1.5 and 4.5.2.4, there are three spin independent and three spin dependent operators that cannot be obtained from the generalization of NRQED operators to NRQCD. The NRQCD operators contains commutators of chromoelectric and chromomagnetic fields. These NRQCD operators do not arise in the NRQED. As a result, we list the set of new spin independent operators that are obtained from the commutator

relationships of the chromoelectric and chromomagnetic fields as follows:

$$\begin{aligned}
& g^2 \psi^\dagger [\mathbf{E}^i, [iD_t, \mathbf{E}^i]]_a T^a \psi \rightarrow \\
& \rightarrow \frac{1}{2M_H} \langle H | \bar{h} [[iD^{\mu_1}, iD^{\mu_2}], [iD^{\mu_3}, [iD^{\mu_4}, iD^{\mu_5}]]] h | H \rangle v_{\mu_1} v_{\mu_3} v_{\mu_4} \Pi_{\mu_2 \mu_5} = -6c^{(8)} \\
& ig^2 \psi^\dagger [\mathbf{B}^i, (\mathbf{D} \times \mathbf{E} + \mathbf{E} \times \mathbf{D})^i]_a T^a \psi \rightarrow \\
& \rightarrow \frac{1}{2M_H} \langle H | \bar{h} [[iD^{\mu_1}, iD^{\mu_2}], [iD^{\mu_3}, [iD^{\mu_4}, iD^{\mu_5}]]] h | H \rangle v_{\mu_4} \Pi_{\mu_1 \mu_3} \Pi_{\mu_2 \mu_5} = 12 (b_{14}^{(8)} - b_{15}^{(8)}) \\
& ig^2 \psi^\dagger [\mathbf{E}^i, (\mathbf{D} \times \mathbf{B} + \mathbf{B} \times \mathbf{D})^i]_a T^a \psi \rightarrow \\
& \rightarrow -\frac{1}{2M_H} \langle H | \bar{h} [[iD^{\mu_1}, iD^{\mu_2}], [iD^{\mu_3}, [iD^{\mu_4}, iD^{\mu_5}]]] h | H \rangle v_{\mu_1} \Pi_{\mu_3 \mu_4} \Pi_{\mu_2 \mu_5} = \\
& = 12 (a_{12}^{(8)} - 2a_{13}^{(8)} + a_{15}^{(8)}) \tag{4.54}
\end{aligned}$$

These operators are linearly independent to the operators found in equation (4.48).

In section 4.5.2.4 we considered the set of dimension eight NRQCD spin dependent operators that are obtained by generalizing the NRQED operators. They are: $O_{X7} \equiv \frac{1}{2} g^2 \psi^\dagger \{ \boldsymbol{\sigma} \cdot \mathbf{B}, [\mathbf{D}^i, \mathbf{E}^i] \} \psi$, $O_{X8} \equiv \frac{1}{2} g^2 \psi^\dagger \{ \mathbf{E}^i, [\mathbf{D}^i, \boldsymbol{\sigma} \cdot \mathbf{B}] \} \psi$, $O_{X9} \equiv \frac{1}{2} g^2 \psi^\dagger \{ B^i, [D^i, \boldsymbol{\sigma} \cdot \mathbf{E}] \} \psi$, $O_{X10} \equiv \frac{1}{2} g^2 \psi^\dagger \{ \mathbf{E}^i, [\boldsymbol{\sigma} \cdot \mathbf{D}, B^i] \} \psi$, and $Q_{Y11} = \frac{1}{2} a^2 \psi^\dagger \{ B^i, [\boldsymbol{\sigma} \cdot \mathbf{D}, \mathbf{E}^i] \} \psi$, where the notion follows from equation (4.44). The corresponding NRQCD operators can be obtained by replacing the commutators by anti-commutators in these operators and vice versa. Out of O_{X7}, O_{X9}, O_{X10} or O_{X7}, O_{X9}, O_{X11} or O_{X8}, O_{X9}, O_{X11} we can choose any set of operators to modify. In the following we modified the operators O_{X7}, O_{X9}, O_{X10} to obtain their NRQCD counterpart. We have:

$$\begin{aligned}
& g^2 \psi^\dagger [\boldsymbol{\sigma} \cdot \mathbf{B}, \{ \mathbf{D}^i, \mathbf{E}^i \}]_a T^a \psi \rightarrow \\
& \rightarrow -\frac{1}{2M_H} \frac{i}{2} \epsilon_{\rho\lambda\mu_1\mu_2} v^\rho \Pi_{\mu_3\mu_5} v_{\mu_4} \langle H | \bar{h} s^\lambda [[iD^{\mu_1}, iD^{\mu_2}], \{iD^{\mu_3}, [iD^{\mu_4}, iD^{\mu_5}]\}] h | H \rangle = \\
& = -12 (3\tilde{a}_{12}^{(8)} - \tilde{a}_{15} + \tilde{a}_{24}), \\
& g^2 \psi^\dagger [B^i, \{ \mathbf{D}^i, \boldsymbol{\sigma} \cdot \mathbf{E} \}]_a T^a \psi \rightarrow \\
& \rightarrow \frac{1}{2M_H} \frac{i}{2} \epsilon_{\rho\mu_1\mu_2\mu_3} v^\rho \Pi_{\lambda\mu_5} v_{\mu_4} \langle H | \bar{h} s^\lambda [[iD^{\mu_1}, iD^{\mu_2}], \{iD^{\mu_3}, [iD^{\mu_4}, iD^{\mu_5}]\}] h | H \rangle = \\
& = 12 (\tilde{a}_{12}^{(8)} + \tilde{a}_{14}^{(8)} - \tilde{a}_{24} - \tilde{b}_{14} + \tilde{b}_{15} + \tilde{b}_{34} - \tilde{b}_{35}),
\end{aligned}$$

$$\begin{aligned}
& g^2 \psi^\dagger [\mathbf{E}^i, \{\boldsymbol{\sigma} \cdot \mathbf{D}, \mathbf{B}^i\}]_a T^a \psi \rightarrow \\
& \rightarrow \frac{1}{2M_H} \frac{i}{2} \epsilon^{\rho\mu_2\mu_4\mu_5} v^\rho \Pi_{\lambda\mu_3\nu\mu_1} \langle H | \bar{h} s^\lambda [iD^{\mu_1}, iD^{\mu_2}], \{iD^{\mu_3}, [iD^{\mu_4}, iD^{\mu_5}]\} | h | H \rangle = \\
& = -12 \left(\tilde{b}_{13} + \tilde{b}_{15} - \tilde{b}_{34} + \tilde{b}_{45} \right). \tag{4.55}
\end{aligned}$$

All these operators are linearly independent to the operators found in equation (4.52).

4.6.2.1 Constructing the NRQCD Lagrangian at order $1/M^4$

Since we found the exclusive set of NRQCD operators, we list the dimension 8 Lagrangian.

$$\begin{aligned}
\mathcal{L}_{\text{NRQCD}}^{\text{dim}=8} = & \psi^\dagger \left\{ c_{X1} g \frac{[\mathbf{D}^2, \{\mathbf{D}^i, \mathbf{E}^i\}]}{M^4} + c_{X2} g \frac{\{\mathbf{D}^2, [\mathbf{D}^i, \mathbf{E}^i]\}}{M^4} + c_{X3} g \frac{[\mathbf{D}^i, [\mathbf{D}^i, [\mathbf{D}^j, \mathbf{E}^j]]]}{M^4} \right. \\
& + i c_{X4a} g^2 \frac{\{\mathbf{D}^i, \epsilon^{ijk} \mathbf{E}_a^j \mathbf{B}_b^k \{T^a, T^b\}\}}{2M^4} + i c_{X4b} g^2 \frac{\{\mathbf{D}^i, \epsilon^{ijk} \mathbf{E}_a^j \mathbf{B}_b^k \delta^{ab}\}}{M^4} \\
& + i c_{X5} g \frac{\mathbf{D}^i \boldsymbol{\sigma} \cdot (\mathbf{D} \times \mathbf{E} - \mathbf{E} \times \mathbf{D}) \mathbf{D}^i}{M^4} + i c_{X6} g \frac{\epsilon^{ijk} \boldsymbol{\sigma}^i \mathbf{D}^j [\mathbf{D}^l, \mathbf{E}^l] \mathbf{D}^k}{M^4} \\
& + c_{X7a} g^2 \frac{\{\boldsymbol{\sigma} \cdot \mathbf{B}_a T^a, [\mathbf{D}^i, \mathbf{E}^i]_b T^b\}}{2M^4} + c_{X7b} g^2 \frac{\boldsymbol{\sigma} \cdot \mathbf{B}_a [\mathbf{D}^i, \mathbf{E}^i]_a}{M^4} \\
& + c_{X8a} g^2 \frac{\{\mathbf{E}_a^i T^a, [\mathbf{D}^i, \boldsymbol{\sigma} \cdot \mathbf{B}]_b T^b\}}{2M^4} + c_{X8b} g^2 \frac{\mathbf{E}_a^i [\mathbf{D}^i, \boldsymbol{\sigma} \cdot \mathbf{B}]_a}{M^4} \\
& + c_{X11a} g^2 \frac{\{\mathbf{B}_a^i T^a, [\boldsymbol{\sigma} \cdot \mathbf{D}, \mathbf{E}^i]_b T^b\}}{2M^4} + c_{X11b} g^2 \frac{B_a^i [\boldsymbol{\sigma} \cdot \mathbf{D}, \mathbf{E}^i]_a}{M^4} \\
& + \tilde{c}_{X12a} g^2 \frac{\epsilon^{ijk} \boldsymbol{\sigma}^i \mathbf{E}_a^j [D_t, \mathbf{E}^k]_b \{T^a, T^b\}}{2M^4} + \tilde{c}_{X12b} g^2 \frac{\epsilon^{ijk} \boldsymbol{\sigma}^i \mathbf{E}_a^j [D_t, \mathbf{E}^k]_a}{M^4} \\
& + i c_{X13} g^2 \frac{[\mathbf{E}^i, [D_t, \mathbf{E}^i]]}{M^4} + i c_{X14} g^2 \frac{[\mathbf{B}^i, (\mathbf{D} \times \mathbf{E} + \mathbf{E} \times \mathbf{D})^i]}{M^4} + i c_{X15} g^2 \frac{[\mathbf{E}^i, (\mathbf{D} \times \mathbf{B} + \mathbf{B} \times \mathbf{D})^i]}{M^4} \\
& \left. + c_{X16} g^2 \frac{[\boldsymbol{\sigma} \cdot \mathbf{B}, \{\mathbf{D}^i, \mathbf{E}^i\}]}{M^4} + c_{X17} g^2 \frac{[\mathbf{B}^i, \{\mathbf{D}^i, \boldsymbol{\sigma} \cdot \mathbf{E}\}]}{M^4} + c_{X18} g^2 \frac{[\mathbf{E}^i, \{\boldsymbol{\sigma} \cdot \mathbf{D}, \mathbf{B}^i\}]}{M^4} \right\} \psi \tag{4.56}
\end{aligned}$$

CHAPTER 5 NEW RESULTS : REEVALUATING THE UNCERTAINTIES

IN $\bar{B} \rightarrow X_S \gamma$

As shown in section 3.1.5.1, the moments of the subleading shape function (g_{17}) are used to construct phenomenological models for non-local function h_{17} . These models were then used in estimating the $Q_1^q - Q_{7\gamma}$ contribution to the uncertainty on total rate ($\mathcal{F}_E|_{17}$). The moments of the h_{17} are related to the higher dimensional HQET matrix elements. In sections 4.2 and 4.3 we constructed a general tensor decomposition of these matrix elements up to and including dimension eight. In the following, we will use this general decomposition to relate the higher order moments of h_{17} to nonperturbative HQET parameters. The updated estimates for these HQET parameters are found in [64]. These estimates were obtained using moments of the semileptonic B decay spectra and information based on lowest lying state saturation approximation. Then a global fit was performed to these HQET parameters to estimate them. In our work, we use the information on HQET parameters to estimate the higher order moments of the h_{17} function. Based on these estimates we construct a new model, and use it to better constrain $\mathcal{F}_E|_{17}$ and the SM estimate of the CP asymmetry in $\bar{B} \rightarrow X_S \gamma$ decay.

5.1 Moments of the sub-leading shape function g_{17}

Equation (3.38) relates the nonlocal function h_{17} to subleading shape function g_{17} . Since g_{17} is a function of both ω and ω_1 , we consider three types of moments. They are moments of g_{17} over ω_1 alone, moments over ω alone and moments over both ω and ω_1 . In the previous sections we derive the general expression for these moments.

5.1.1 Moments in ω_1 alone

Using equation (3.23), we obtain the moments of g_{17} over ω_1 as follows [92]:

$$\begin{aligned} \langle \omega^0 \omega_1^k g_{17} \rangle &\equiv \int_{-\infty}^{\bar{\Lambda}} d\omega \int_{-\infty}^{\infty} d\omega_1 \omega_1^k g_{17}(\omega, \omega_1, \mu) = \\ &= (-1)^k \frac{1}{2M_B} \langle \bar{B} | (\bar{h} S_{\bar{n}})(0) \not{n} (1 + \gamma_5) i \gamma_{\alpha}^{\perp} \bar{n}_{\beta} (i \bar{n} \cdot \partial)^k (S_{\bar{n}}^{\dagger} g G_s^{\alpha\beta} S_{\bar{n}})(r \bar{n}) (S_{\bar{n}}^{\dagger} h)(0) | \bar{B} \rangle \Big|_{r=0}, \end{aligned} \quad (5.1)$$

where γ^\perp represents only the γ^1 and γ^2 , $n = (1, 0, 0, 1)$ and $\bar{n} = (1, 0, 0, -1)$. The integrals over ω and ω_1 , generates the delta functions of r, t . These delta functions restricts the evaluation of the matrix element at $r = 0, t = 0$. Using the identity $i\bar{n} \cdot \partial \left(S_{\bar{n}}^\dagger(x) O(x) S_{\bar{n}}(x) \right) = S_{\bar{n}}^\dagger(x) [i\bar{n} \cdot D, O(x)] S_{\bar{n}}(x)$, which is proved in appendix 7.2, we obtain

$$\begin{aligned}
\langle \omega^0 \omega_1^k g_{17} \rangle &\equiv \int_{-\infty}^{\bar{\Lambda}} d\omega \int_{-\infty}^{\infty} d\omega_1 \omega_1^k g_{17}(\omega, \omega_1, \mu) = \\
&= (-1)^k \frac{1}{2M_B} \langle \bar{B} | \bar{h} \not{n} (1 + \gamma_5) i\gamma_\alpha^\perp \bar{n}_\beta \underbrace{[i\bar{n} \cdot D, [i\bar{n} \cdot D, \dots [i\bar{n} \cdot D, g_s^{\alpha\beta}] \dots]]}_{k \text{ times}} h | \bar{B} \rangle = \\
&= (-1)^k \frac{1}{2M_B} \langle \bar{B} | \bar{h} \not{n} (1 + \gamma_5) \gamma_\alpha^\perp \underbrace{[i\bar{n} \cdot D, [i\bar{n} \cdot D, \dots [i\bar{n} \cdot D, [iD^\alpha, i\bar{n} \cdot D] \dots]]}_{k \text{ times}} h | \bar{B} \rangle.
\end{aligned} \tag{5.2}$$

The identity $[iD^\mu, iD^\nu] = igG^{\mu\nu}$ was used in the last line.

The Dirac structures in the matrix elements are simplified using the projection operators P_+ , which are defined in section 4.1.1. As shown in equation (4.5), the action of projection operators on $\gamma^\lambda \gamma^5$ provides s^λ . Using this we simplify the Dirac structure. For example, consider the term $\not{n} \gamma_\alpha^\perp$. The orthogonality between α and \bar{n} provides that $\not{n} \gamma_\alpha^\perp = -i\sigma_{\mu\alpha\perp} \bar{n}^\mu$. Equation (4.6) provides the relationship between $\sigma_{\mu\alpha}$ and s^λ . Note that we used the convention $\epsilon_{0123} = -1$. As a result, we obtain $\not{n} \gamma_\alpha^\perp \rightarrow iv^\rho \epsilon_{\rho\mu\alpha\perp\lambda} s^\lambda \bar{n}^\mu$. The Dirac structure $\not{n} \gamma^5 \gamma_\alpha^\perp$ is then simplified using equation (4.7), which provides $P_+ \not{n} \gamma^5 \gamma_\alpha^\perp P_+ \rightarrow -s^{\alpha\perp}$. Using this we obtain

$$\begin{aligned}
\langle \omega^0 \omega_1^k g_{17} \rangle &\equiv \int_{-\infty}^{\bar{\Lambda}} d\omega \int_{-\infty}^{\infty} d\omega_1 \omega_1^k g_{17}(\omega, \omega_1, \mu) = \\
&= (iv^\rho \epsilon_{\rho\mu\alpha\perp\lambda} \bar{n}^\mu - g_{\alpha\perp\lambda}) (-1)^k \frac{1}{2M_B} \langle \bar{B} | \bar{h} \underbrace{[i\bar{n} \cdot D, [i\bar{n} \cdot D, \dots [i\bar{n} \cdot D, [iD^\alpha, i\bar{n} \cdot D] \dots]]}_{k \text{ times}} s^\lambda h | \bar{B} \rangle,
\end{aligned} \tag{5.3}$$

where the parameters $g_\perp^{\mu\nu}$ and $\epsilon_\perp^{\mu\nu}$ are defined in equation (3.6). The nested commutators in equation (5.3) implies that the odd moments of g_{17} over ω_1 vanishes. This is due to

the odd number of commutators of Hermitian operators is a Hermitian operator. Thus the corresponding HQET matrix element becomes real. As shown in the chapter 4, the spin dependent matrix elements are imaginary [56]. As a result, the real matrix elements obtained from the odd moments in ω_1 must vanish.

We use the general decomposition constructed in the sections 4.2 and 4.3 to obtain the moments in ω_1 up to third moment. The moments of g_{17} over ω_1 are listed :

$$\begin{aligned}
\langle \omega^0 \omega_1^0 g_{17} \rangle &\equiv \int_{-\infty}^{\bar{\Lambda}} d\omega \int_{-\infty}^{\infty} d\omega_1 g_{17}(\omega, \omega_1, \mu) = 4\tilde{a}^{(5)} = 2\lambda_2 = 2\mu_G^2/3 \\
\langle \omega^0 \omega_1^1 g_{17} \rangle &\equiv \int_{-\infty}^{\bar{\Lambda}} d\omega \int_{-\infty}^{\infty} d\omega_1 \omega_1 g_{17}(\omega, \omega_1, \mu) = 0 \\
\langle \omega^0 \omega_1^2 g_{17} \rangle &\equiv \int_{-\infty}^{\bar{\Lambda}} d\omega \int_{-\infty}^{\infty} d\omega_1 \omega_1^2 g_{17}(\omega, \omega_1, \mu) = 4 \left(-4\tilde{a}_{12}^{(7)} + 2\tilde{a}_{13}^{(7)} + 3\tilde{a}_{14}^{(7)} - \tilde{a}_{23}^{(7)} + \tilde{b}^{(7)} \right) = \\
&= \frac{2}{15} (5m_5 + 3m_6 - 2m_9) \\
\langle \omega^0 \omega_1^3 g_{17} \rangle &\equiv \int_{-\infty}^{\bar{\Lambda}} d\omega \int_{-\infty}^{\infty} d\omega_1 \omega_1^3 g_{17}(\omega, \omega_1, \mu) = 0.
\end{aligned} \tag{5.4}$$

The zeroth moment is a known result, and the second moment was first obtained in [92].

5.1.2 Moments in ω alone

The moments of g_{17} over ω are obtained by evaluating

$$\begin{aligned}
\langle \omega^k \omega_1^0 g_{17} \rangle &\equiv \int_{-\infty}^{\bar{\Lambda}} d\omega \omega^k \int_{-\infty}^{\infty} d\omega_1 g_{17}(\omega, \omega_1, \mu) = \\
&= \int_{-\infty}^{\bar{\Lambda}} d\omega \omega^k \int \frac{dt}{2\pi} e^{-i\omega t} \frac{1}{2M_B} \langle \bar{B} | (\bar{h}S_n)(tn) \not{n} (1 + \gamma_5) S_n^\dagger(0) i\gamma_\alpha^\perp \bar{n}_\beta gG_s^{\alpha\beta}(0) h(0) | \bar{B} \rangle = \\
&= \int_{-\infty}^{\bar{\Lambda}} d\omega \omega^k \int \frac{dt}{2\pi} e^{i\omega t} \frac{1}{2M_B} \langle \bar{B} | (\bar{h}S_n)(0) \not{n} (1 + \gamma_5) S_n^\dagger(tn) i\gamma_\alpha^\perp \bar{n}_\beta gG_s^{\alpha\beta}(tn) h(tn) | \bar{B} \rangle = \\
&= \int dt \delta(t) \frac{1}{2M_B} \langle \bar{B} | \bar{h}(0) S_n(0) (in \cdot \partial)^k S_n^\dagger(tn) \not{n} (1 + \gamma_5) i\gamma_\alpha^\perp \bar{n}_\beta gG_s^{\alpha\beta}(tn) h(tn) | \bar{B} \rangle.
\end{aligned} \tag{5.5}$$

In the above expression we used the translational invariance of nonlocal matrix elements along n . Using the identity $S_n^\dagger(tn) in \cdot D = in \cdot \partial S_n^\dagger(tn)$ we obtain a general expression for the moments over ω :

$$\begin{aligned}
\langle \omega^k \omega_1^0 g_{17} \rangle &\equiv \int_{-\infty}^{\bar{\Lambda}} d\omega \omega^k \int_{-\infty}^{\infty} d\omega_1 g_{17}(\omega, \omega_1, \mu) = \\
&= (i\nu^\rho \epsilon_{\rho\mu\alpha\lambda} \bar{n}^\mu - g_{\alpha\perp\lambda}) \frac{1}{2M_B} \langle \bar{B} | \bar{h} (in \cdot D)^k [iD^\alpha, i\bar{n} \cdot D] s^\lambda h | \bar{B} \rangle.
\end{aligned} \tag{5.6}$$

We used the general decomposition defined in sections 4.2 and 4.3 to obtain the moments up to and including $\langle \omega^3 \omega_1^0 g_{17} \rangle$.

$$\begin{aligned}
\langle \omega^0 \omega_1^0 g_{17} \rangle &\equiv \int_{-\infty}^{\bar{\Lambda}} d\omega \int_{-\infty}^{\infty} d\omega_1 g_{17}(\omega, \omega_1, \mu) = 4\tilde{a}^{(5)} = 2\lambda_2 = 2\mu_G^2/3 \\
\langle \omega^1 \omega_1^0 g_{17} \rangle &\equiv \int_{-\infty}^{\bar{\Lambda}} d\omega \omega \int_{-\infty}^{\infty} d\omega_1 g_{17}(\omega, \omega_1, \mu) = -2\tilde{a}^{(6)} = -\rho_2 = -\rho_{LS}^3/3 \\
\langle \omega^2 \omega_1^0 g_{17} \rangle &\equiv \int_{-\infty}^{\bar{\Lambda}} d\omega \omega^2 \int_{-\infty}^{\infty} d\omega_1 g_{17}(\omega, \omega_1, \mu) = -2 \left(2\tilde{a}_{12}^{(7)} - \tilde{a}_{14}^{(7)} + \tilde{a}_{23}^{(7)} + \tilde{b}^{(7)} \right) = \\
&= -\frac{1}{60} (20m_5 + 2m_7 + m_8) \\
\langle \omega^3 \omega_1^0 g_{17} \rangle &\equiv \int_{-\infty}^{\bar{\Lambda}} d\omega \omega^3 \int_{-\infty}^{\infty} d\omega_1 g_{17}(\omega, \omega_1, \mu) = \\
&= -2 \left(2\tilde{a}_{12}^{(8)} - \tilde{a}_{15}^{(8)} + \tilde{a}_{24}^{(8)} + 2\tilde{b}_{13}^{(8)} + \tilde{b}_{14}^{(8)} - \tilde{b}_{15}^{(8)} - 2\tilde{b}_{35}^{(8)} - \tilde{b}_{45}^{(8)} + \tilde{c}^{(8)} \right) = \\
&= -\frac{1}{15} (5r_8 - r_9 + 2r_{10} + r_{11} - 2r_{12} - r_{13} + 2r_{15} - r_{16} + r_{17})
\end{aligned} \tag{5.7}$$

The first moment was derived in [78], and the third and fourth moments were first derived in [92].

5.1.3 Moments in both ω_1 and ω

General expression for mixed moments of g_{17} over ω and ω_1 can be obtained as follows:

$$\begin{aligned}
\langle \omega^l \omega_1^k g_{17} \rangle &\equiv \int_{-\infty}^{\bar{\Lambda}} d\omega \omega^l \int_{-\infty}^{\infty} d\omega_1 \omega^k g_{17}(\omega, \omega_1, \mu) = (iv^\rho \epsilon_{\rho\mu\alpha\lambda} \bar{n}^\mu - g_{\alpha\perp\lambda}) (-1)^k \times \\
&\times \frac{1}{2M_B} \langle \bar{B} | \bar{h} (in \cdot D)^l \underbrace{[i\bar{n} \cdot D, [i\bar{n} \cdot D, \dots [i\bar{n} \cdot D, [iD^\alpha, i\bar{n} \cdot D] \dots]]]}_{k \text{ times}} s^\lambda h | \bar{B} \rangle. \quad (5.8)
\end{aligned}$$

Using the tensor decomposition of HQET matrix elements we found the mixed moments of ω and ω_1 up to dimension eight matrix elements. They are :

$$\begin{aligned}
\langle \omega^1 \omega_1^1 g_{17} \rangle &\equiv \int_{-\infty}^{\bar{\Lambda}} d\omega \omega \int_{-\infty}^{\infty} d\omega_1 \omega_1 g_{17}(\omega, \omega_1, \mu) = 2 \left(-4\tilde{a}_{12}^{(7)} + 2\tilde{a}_{13}^{(7)} + 3\tilde{a}_{14}^{(7)} - \tilde{a}_{23}^{(7)} + \tilde{b}^{(7)} \right) = \\
&= \frac{1}{15} (5m_5 + 3m_6 - 2m_9) \\
\langle \omega^2 \omega_1^1 g_{17} \rangle &\equiv \int_{-\infty}^{\bar{\Lambda}} d\omega \omega^2 \int_{-\infty}^{\infty} d\omega_1 \omega_1 g_{17}(\omega, \omega_1, \mu) = \\
&= 2 \left(3\tilde{a}_{12}^{(8)} - \tilde{a}_{14}^{(8)} - 2\tilde{a}_{15}^{(8)} + \tilde{a}_{24}^{(8)} - 3\tilde{b}_{13}^{(8)} + \tilde{b}_{14}^{(8)} + 4\tilde{b}_{15}^{(8)} + 3\tilde{b}_{35}^{(8)} - \tilde{b}_{45}^{(8)} + \tilde{c}^{(8)} \right) = \\
&= \frac{1}{15} (5r_8 - r_9 - 3r_{10} + r_{11} + 3r_{12} + 4r_{13} + 3r_{15} - 2r_{16} + r_{17} - r_{18}) \\
\langle \omega^1 \omega_1^2 g_{17} \rangle &\equiv \int_{-\infty}^{\bar{\Lambda}} d\omega \omega^1 \int_{-\infty}^{\infty} d\omega_1 \omega_1^2 g_{17}(\omega, \omega_1, \mu) = \\
&= 2 \left(3\tilde{a}_{12}^{(8)} - \tilde{a}_{14}^{(8)} - 2\tilde{a}_{15}^{(8)} + \tilde{a}_{24}^{(8)} + 3\tilde{b}_{13}^{(8)} + \tilde{b}_{14}^{(8)} - 2\tilde{b}_{15}^{(8)} + 2\tilde{b}_{34}^{(8)} - \tilde{b}_{35}^{(8)} + \tilde{b}_{45}^{(8)} - \tilde{c}^{(8)} \right) = \\
&= \frac{1}{15} (-5r_8 + r_9 + 3r_{10} + r_{11} - r_{12} - 2r_{13} + 2r_{14} + 3r_{15} - 2r_{16} + r_{17} - r_{18}) \quad (5.9)
\end{aligned}$$

These moments were all first obtained in [92].

5.2 Applications

5.2.1 Estimating the moments of subleading shape function

As shown in the section 5.1, the moments of the subleading shape function are related to nonperturbative HQET parameters. In [64] the numerical estimates for these HQET parameters were provided up to and including dimension eight. For this, the moments of the semileptonic B decay spectra and lowest lying saturation approximation (LLSA) were used [62, 102]. Using the LLSA the higher dimensional matrix elements were related to the

lower dimensional matrix elements and to the excitation energy ϵ [64]. This approximation provides 50 – 100% accuracy [102]. Based on the central values and the standard deviation provided in the table 2 of [64] we obtain the moments of the g_{17} as follows:

$$\begin{aligned}
\langle \omega^0 \omega_1^0 g_{17} \rangle &= 0.237 \pm 0.040 \text{ GeV}^2 \\
\langle \omega^0 \omega_1^2 g_{17} \rangle &= 0.15 \pm 0.12 \text{ GeV}^4 \\
\langle \omega^1 \omega_1^0 g_{17} \rangle &= 0.056 \pm 0.032 \text{ GeV}^3 \\
\langle \omega^2 \omega_1^0 g_{17} \rangle &= 0.015 \pm 0.021 \text{ GeV}^4 \\
\langle \omega^3 \omega_1^0 g_{17} \rangle &= 0.008 \pm 0.011 \text{ GeV}^5 \\
\langle \omega^1 \omega_1^1 g_{17} \rangle &= 0.073 \pm 0.059 \text{ GeV}^4 \\
\langle \omega^2 \omega_1^1 g_{17} \rangle &= -0.034 \pm 0.016 \text{ GeV}^5 \\
\langle \omega^1 \omega_1^2 g_{17} \rangle &= 0.027 \pm 0.014 \text{ GeV}^5,
\end{aligned} \tag{5.10}$$

The errors of the HQET parameters were added in the quadrature. In [64] the errors of the HQET parameters were reported without the correlated error. Therefore, in our work we did not consider the correlated error as well.

Even though the relative errors of these nonperturbative parameters are large, they still provide useful information regarding the moments of the subleading shape function. For example, using the model provided in [78] for h_{17} we found that $\langle \omega^0 \omega_1^2 g_{17} \rangle \in [-0.31, 0.49] \text{ GeV}^4$. This should be compared to the $\langle \omega^0 \omega_1^2 g_{17} \rangle = 0.15 \pm 0.12 \text{ GeV}^4$ in equation (5.10). The range of $\langle \omega^0 \omega_1^2 g_{17} \rangle$ found in [78] is roughly three times bigger compared to the new one.

The nonperturbative HQET parameters that are defined in [62] and listed in [64] used the full QCD b fields. Whereas, the HQET matrix elements are defined in heavy quark limit. As a result, there is a $1/m_b$ difference between the parameters defined in these two basis. For instance, the relation between λ_2 and μ_G^2 contains a $1/m_b$ correction term. However, this difference is not numerically important. This is due to the relatively large error bars in our

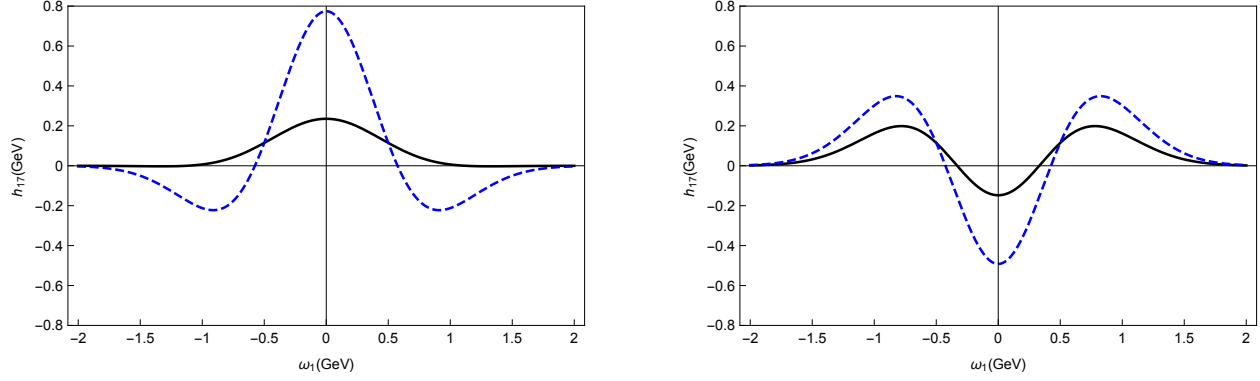


Figure 5.1: A comparison of the extremal models for h_{17} as a sum of two lowest even Hermite polynomials times a Gaussian of width 0.5 GeV used in [78] (dashed blue) to the same models allowed by current (2019) data (solid black). Left hand side: The model with 2010 smallest possible second moment of -0.31 GeV^4 compared to 2019 smallest possible second moment of 0.03 GeV^4 . Right hand side: The model with 2010 largest possible second moment of 0.49 GeV^4 compared to 2019 largest possible second moment of 0.27 GeV^4 .

moment estimates. To illustrate this further, consider the value of $\mu_G^2/3$ obtained in [64]. We compare this estimate of $\mu_G^2/3$ to the λ_2 , which is extracted from the B and D meson spectroscopy. Note that the value of λ_2 is defined in the heavy quark limit.

We define the mass split as $\Delta m_H = m_H^* - m_H$, where m_H is a pseudo-scalar and m_H^* is vector heavy meson containing a heavy quark of mass m_Q . At order $1/m_b$ the $\lambda_2 = \Delta m_H m_H/2$. We extracted the value of λ_2 using the isospin-averaged meson mass data [18]. Following from this, we obtain $\lambda_2 = 0.119 \pm 0.001 \text{ GeV}^2$ for B meson data. For the D meson data we obtain $\lambda_2 = 0.13193 \pm 0.00002 \text{ GeV}^2$ [92].

At order $\mathcal{O}(1/m_b^2)$ the expression for λ_2 is [103]

$$\lambda_2(m_b) = \frac{\Delta m_B m_B^2 - \Delta m_D m_D^2}{2(m_B - \kappa(m_c) m_D)} \quad (5.11)$$

Equation (5.11) provides $\lambda_2 = 0.112 \pm 0.001 \text{ GeV}^2$. In comparison, $\mu_G^2/3 = 0.118 \pm 0.020 \text{ GeV}^2$ [64] is equal to all these values of λ_2 within the error. As a result, it is currently not possible to distinguish between λ_2 and $\mu_G^2/3$. Hence, in the following work we use $\mu_G^2/3$ from [64], and we assume a similar behavior for all other HQET parameters. This

situation can be improved with the availability of the future Belle II data and Lattice QCD. These new data can improve the estimates of HQET parameters and the moments.

5.2.2 Resolved photon contributions for $Q_1^q - Q_{7\gamma}$

In the following work, we will use the moments of subleading shape function to better constrain the resolved photon contributions from the $Q_1^q - Q_{7\gamma}$. As shown in [78] the contribution from $Q_1^u - Q_{7\gamma}$ vanishes. The contribution from $Q_1^c - Q_{7\gamma}$ is given by

$$\mathcal{F}_E^{17} = \frac{C_1(\mu)}{C_{7\gamma}(\mu)} \frac{\Lambda_{17}(m_c^2/m_b, \mu)}{m_b}, \quad (5.12)$$

where the nonperturbative quantity Λ_{17} is defined in equation (3.37), and it depends on non-local forward scattering matrix element h_{17} . Since the h_{17} cannot be obtained from first principles, we use its moments to construct a phenomenological model to describe h_{17} . Using the general decomposition provided in sections 4.2, 4.3 and the numerical estimates of HQET parameters found in [64] we construct new model to better constraint \mathcal{F}_E^{17} .

The $Q_1^q - Q_{7\gamma}$ part of the resolved photon contribution to the estimate of CP asymmetry is given in equation (3.62). This contribution is defined by the nonperturbative parameters $\tilde{\Lambda}_{17}^u$ and $\tilde{\Lambda}_{17}^c$. With the new information on the moments of subleading shape function h_{17} we would like to revisit the evaluation of these nonperturbative parameters. In addition, we consider the uncertainty generated in evaluation of charm and bottom quark masses.

5.2.2.1 Uncertainty due to the running quark masses

For the evaluation of CP averaged rate we use the $m_c = m_c(\mu)$ defined in the $\overline{\text{MS}}$ scheme with $\mu = 1.5$ GeV. Whereas, the evaluation of CP asymmetry is carried out by using $m_c = m_c(\mu)$ defined in the $\overline{\text{MS}}$ scheme with $\mu = 2.0$ GeV.

The running of the quark masses is given as [15]

$$m(\mu) = m(\mu_0) \left[\frac{\alpha_s(\mu)}{\alpha_s(\mu_0)} \right]^{\frac{\gamma_m^{(0)}}{2\beta_0}} \left[1 + \left(\frac{\gamma_m^{(1)}}{2\beta_0} - \frac{\beta_1 \gamma_m^{(0)}}{2\beta_0^2} \right) \frac{\alpha_s(\mu) - \alpha_s(\mu_0)}{4\pi} \right], \quad (5.13)$$

where $\alpha_s, v(\mu), \gamma_m^{0,1}$, and $\beta_{0,1}$ are given by

$$\alpha_s(\mu) = \frac{\alpha_s(M_Z)}{v(\mu)} \left[1 - \frac{\beta_1 \alpha_s(M_Z) \ln v(\mu)}{\beta_0 4\pi v(\mu)} \right], \quad (5.14)$$

and

$$\begin{aligned} v(\mu) &= 1 - \beta_0 \frac{\alpha_s(M_Z)}{2\pi} \ln \left(\frac{M_Z}{\mu} \right) \\ \gamma_m(\alpha_s) &= \gamma_m^{(0)} \frac{\alpha_s}{4\pi} + \gamma_m^{(1)} \left(\frac{\alpha_s}{4\pi} \right)^2 \\ \beta_{0,1}(\alpha_s) &= a_1 \frac{\alpha_s}{4\pi} + a_2 \left(\frac{\alpha_s}{4\pi} \right)^2 \\ \gamma_m^{(0)} &= 6C_F \quad \gamma_m^{(1)} = C_F \left(3C_F + \frac{97}{3}N - \frac{10}{3}f \right) \end{aligned} \quad (5.15)$$

$C_F = \frac{N^2-1}{2N}$, where N is the number of color charges, and f is the number of effective flavors. In the 2019 update of the 2018 PDG listing we found $m_c(m_c) = 1.27 \pm 0.02$ GeV [18]. The coupling constant is given by $\alpha_s(\mu = m_c) = 0.38 \pm 0.03$ [18]. Using these values and equation (5.13) we obtain $m_c(1.5 \text{ GeV}) = 1.20 \pm 0.03$ GeV and $m_c(2.0 \text{ GeV}) = 1.10 \pm 0.03$ GeV.

In [78] the estimate of Λ_{17} was obtained by using the $m_c = 1.131$ GeV. This charm quark mass is based on smaller value of $m_c(m_c)$ [104], and it was used in [90, 105] as well. This change in the charm mass tends to slightly affect the estimates of $\Lambda_{17}, \tilde{\Lambda}_{17}^c$.

The mass of the bottom quark is obtained by using the shape function scheme [78, 83]. The updated HFLAG [106] value of m_b is 4.58 ± 0.03 GeV. This value should be compared to the $m_b = 4.65$ GeV used in [78].

5.2.2.2 Λ_{17} estimates based on expanded penguin function

As shown in the equation (3.37), the soft function h_{17} , which appears in the expression of Λ_{17} , is convoluted with the penguin function ($F(x)$), where F is defined in equation (3.21). The expansion of the $1 - F(x)$ is given in equation (3.22), which is obtained for $x > 1/4$.

In the region $\omega_1 \ll 4m_c^2/m_b \approx 1.2 - 1.3$ GeV we can expand the $F(x)$ and obtain the

Λ_{17} in terms of moments of the subleading shape function. Starting from the expression of Λ_{17} [78]

$$\Lambda_{17}\left(\frac{m_c^2}{m_b}, \mu\right) = e_c \operatorname{Re} \int_{-\infty}^{\bar{\Lambda}} d\omega \int_{-\infty}^{\infty} \frac{d\omega_1}{\omega_1} \times \left\{ \left(\frac{m_b + \omega}{m_b}\right)^3 \left[1 - F\left(\frac{m_c^2 - i\varepsilon}{(m_b + \omega)\omega_1}\right)\right] + \frac{m_b \omega_1}{12m_c^2} \right\} g_{17}(\omega, \omega_1, \mu) \quad (5.16)$$

Using the definition of h_{17} we have $\langle \omega^0 \omega_1^k g_{17} \rangle = \langle \omega_1^k h_{17} \rangle$. Then the expansion of the penguin function provides [92]:

$$\Lambda_{17}^{\text{expanded}} = -\frac{e_c m_b^3}{560 m_c^6} \langle \omega^0 \omega_1^2 g_{17} \rangle + \dots = -6 \pm 5 \text{ MeV} + \dots, \quad (5.17)$$

where \dots denotes the contributions from the higher order moments over ω_1 . Traditionally, the contribution from the zeroth moment in ω_1 is subtracted in equations (3.37) and (5.16), and its magnitude is $-e_c m_b 2\lambda_2 / (12m_c^2) = -42 \pm 7 \text{ MeV}$. The contributors to the uncertainty in the equation (5.17) are $\langle \omega^0 \omega_1^2 g_{17} \rangle$, m_b , and m_c . These uncertainties were added in quadrature.

In the past, the size of the contribution from higher operators was a concern for the authors in [107–110]. They have noticed the numerical suppression arising from the expansion of the penguin function [92]. They have noticed the numerical suppression arising from the expansion of the penguin function, but the lack of knowledge of the matrix elements prevented them from making conclusive statements.

The first term in the equation (3.22) is suppressed by a factor ~ 50 compared to the third term. However, when the third term is combined with the second moment, we obtain -6 MeV . This is only suppressed by a factor of 7 compared to the zeroth moment. This smaller suppression is consistent with the power counting of $m_c^2 \sim m_b \Lambda_{\text{QCD}}$, which disfavors the expansion of the penguin function [92].

Consider the $1/m_b^n$ corrections to $\Lambda_{17}^{\text{expanded}}$, which are obtained by expansion of $F(x)$ in

ω/m_b . By definition, $\Lambda_{17}^{\text{expanded}} = \delta\Lambda_{17}^{(0)}$. For $\delta\Lambda_{17}^{(1)}$ we have [92]:

$$\begin{aligned}\delta\Lambda_{17}^{(1)} &= -\frac{e_c}{3m_c^2}\langle\omega^1\omega_1^0g_{17}\rangle - \frac{e_cm_b}{18m_c^4}\langle\omega^1\omega_1^1g_{17}\rangle - \frac{3e_cm_b^2}{280m_c^6}\langle\omega^1\omega_1^2g_{17}\rangle + \dots \\ &= (-9 \pm 5 \text{ MeV}) + (-6 \pm 5 \text{ MeV}) + (-1 \pm 1 \text{ MeV}) + \dots = -16 \pm 7 \text{ MeV} + \dots\end{aligned}\quad (5.18)$$

Again in the equation (5.18), we observe a slow convergence. Only in the third term we see a suppression compared to the first two terms. Although $\delta\Lambda_{17}^{(1)}$ is a Λ_{QCD}/m_b correction, equation (5.18) indicates that the $\delta\Lambda_{17}^{(1)}$ is comparable in size to $\Lambda_{17}^{\text{expanded}}$. Even if we add the contribution of $\langle\omega^0\omega_1^0g_{17}\rangle$ to $\Lambda_{17}^{\text{expanded}}$, $\delta\Lambda_{17}^{(1)}$ is only suppressed by a factor of three [92].

The $\Lambda_{\text{QCD}}^2/m_b^2$ correction to the $\Lambda_{17}^{\text{expanded}}$ is given by

$$\begin{aligned}\delta\Lambda_{17}^{(2)} &= -\frac{e_c}{2m_b m_c^2}\langle\omega^2\omega_1^0g_{17}\rangle - \frac{e_c}{9m_c^4}\langle\omega^2\omega_1^1g_{17}\rangle + \dots \\ &= (-0.8 \pm 1.1 \text{ MeV}) + (1.2 \pm 0.6 \text{ GeV}) + \dots = 0.4 \pm 1.3 \text{ MeV} + \dots\end{aligned}\quad (5.19)$$

The convergence generated by the expansion of $F(x)$ is again provide a slow convergence in the series. Finally, the $\Lambda_{\text{QCD}}^3/m_b^3$ correction for $\Lambda_{17}^{\text{expanded}}$ is given by

$$\delta\Lambda_{17}^{(3)} = -\frac{e_c}{3m_b^2 m_c^2}\langle\omega^3\omega_1^0g_{17}\rangle = -0.06 \pm 0.08 \text{ MeV} + \dots\quad (5.20)$$

As we expected, the $\delta\Lambda_{17}^{(3)}$ is order of magnitude smaller than the $\delta\Lambda_{17}^{(2)}$ correction.

The Λ_{QCD}/m_b expansion for $\delta\Lambda_{17}$ works well with the exception of the first term. We speculate that this is due to the vanishing of $\langle\omega^0\omega_1^1g_{17}\rangle$, which makes the zeroth term in the expansion Λ_{17} given in equation (5.16) smaller than it “should” be. Since in general for $l > 0$ the moments $\langle\omega^l\omega_1^kg_{17}\rangle$ do not vanish, there is no such suppression beyond the zeroth term [92]. Altogether we find $\Lambda_{17}^{\text{expanded}} + \delta\Lambda_{17}^{(1)} + \delta\Lambda_{17}^{(2)} + \delta\Lambda_{17}^{(3)} = -22 \pm 9 \text{ MeV}$, where the uncertainties were added in quadrature.

Since the assumptions on the support of h_{17} and resulting expansion of the penguin function are too restrictive [78, 92], we will turn to a different approach to analyze the Λ_{17} .

5.3 Modeling of h_{17}

The h_{17} is an even function, and it has a dimension of mass and in the heavy quark limit. As shown in the section 3.1.3.1, the ω_1 is defined in the domain of $-\infty \leq \omega_1 \leq \infty$. For the modeling of h_{17} it is beneficial to have a systematic expansion of h_{17} , e.g. in terms of a complete orthonormal set of basis functions [92]. In [111] such an expansion was suggested to describe the leading order shape function. In our work we use an expansion in terms of Hermite polynomials multiplied by a Gaussian of width σ [92]:

$$h_{17}(\omega_1, \mu) = \sum_n a_{2n} H_{2n} \left(\frac{\omega_1}{\sqrt{2}\sigma} \right) e^{-\frac{\omega_1^2}{2\sigma^2}}, \quad (5.21)$$

where H_{2n} are even Hermite polynomials, and the coefficients a_{2n} are related to the moments of the h_{17} . In the following we refer to these models by the numbers of Hermite polynomials they contain. It is important to note that the $2k$ -th moment of h_{17} only depends on the coefficients a_{2n} with $n \leq k$, for a given value of σ . This is due to the orthogonality between Hermite polynomials. For instance, the zeroth moment of h_{17} only depends on a_0 and the second moment of h_{17} only depends on a_0 and a_2 . As a result, we use the first $2k$ -th moments to determine a_{2n} with $n \leq k$. Using $\langle \omega^0 \omega_1^k g_{17} \rangle = \langle \omega_1^k h_{17} \rangle$ we obtain a_0 and a_2 [92]:

$$a_0 = \frac{\langle \omega_1^0 h_{17} \rangle}{\sqrt{2\pi}|\sigma|}, \quad a_2 = \frac{\langle \omega_1^2 h_{17} \rangle - \sigma^2 \langle \omega_1^0 h_{17} \rangle}{4\sqrt{2\pi}|\sigma|^3}. \quad (5.22)$$

Since the h_{17} is a soft function, it can be further constrained by using $|h_{17}(\omega_1, \mu)| \leq 1$ GeV. as in [78], that it should not have any significant structures, such as peaks or zeros, outside the range $|\omega_1| \leq 1$ GeV. This allows us to restrict the range of σ . For example, assuming a model of a sum of two Hermite polynomials, for given values of $\langle \omega_1^0 h_{17} \rangle$ and $\langle \omega_1^2 h_{17} \rangle$, the requirement on significant structures only for $|\omega_1| \leq 1$ GeV gives an upper bound on σ and the condition $|h_{17}(\omega_1, \mu)| \leq 1$ GeV gives a lower bound on σ . For example, assuming the central

values for $\langle \omega_1^0 h_{17} \rangle = 0.237 \text{ GeV}^2$ and $\langle \omega_1^2 h_{17} \rangle = 0.15 \text{ GeV}^4$ gives $0.27 \text{ GeV} < \sigma < 0.62 \text{ GeV}$. For other values of $\langle \omega_1^0 h_{17} \rangle$ and $\langle \omega_1^2 h_{17} \rangle$ within their one standard deviation range, the range of σ can be larger, but we restrict σ to be less than 1 GeV. As we will see below, this does not affect our estimates in practice since the extremal values we obtain are for $\sigma < 1 \text{ GeV}$ anyway [92].

In the following, we consider models up to and including four Hermite polynomials. The models with one and two hermite polynomials are defined using known moments. However, models with three and four Hermite polynomials are defined with unknown moments.

5.3.1 One Hermite polynomial model

The σ is not defined by the moments of h_{17} . As a result, we use both zero and second moments to fix the value of σ in one Hermite polynomial model. Following from this, we define the one Hermite polynomial model

$$h_{17}^{\text{model-1}}(\omega_1) = \frac{\langle \omega_1^0 h_{17} \rangle}{\sqrt{2\pi}|\sigma|} e^{-\frac{\omega_1^2}{2\sigma^2}}. \quad (5.23)$$

The second moment of $h_{17}^{\text{model-1}}$ implies $\sigma = \sqrt{\langle \omega_1^2 h_{17} \rangle / \langle \omega_1^0 h_{17} \rangle}$. This is also the condition for $a_2 = 0$ in (5.22) [92].

When we fix the value of the second moment to $\langle \omega_1^2 h_{17} \rangle = 0.27 \text{ GeV}^4$, the σ exceeds 1 GeV for almost all the values of $\langle \omega_1^0 h_{17} \rangle$ within its one standard deviation range. Based on the above constrains we reject such models. Even if we include these models we obtain Λ_{17} , $\tilde{\Lambda}_{17}^u$, and $\tilde{\Lambda}_{17}^c$ that are included in the ranges for the two Hermite polynomials model below. The one Hermite polynomial model provides $\Lambda_{17} \in [-8, -1] \text{ MeV}$, $\tilde{\Lambda}_{17}^c \in [0, 7.5] \text{ MeV}$, and $\tilde{\Lambda}_{17}^u \in [45, 220] \text{ MeV}$ [92].

5.3.2 Sum of two Hermite polynomial model

Including the zeroth and second moments of h_{17} we construct the two Hermite polynomial model. The corresponding coefficients a_0 and a_2 for a given σ are provided in equation (5.22).

Numerically scanning over the one standard deviation range of the moments and the possible values of σ in increments of $\delta\sigma = 0.01 \text{ GeV}$, and based on the restrictions above

on h_{17} gives $\Lambda_{17} \in [-21, -1]$ MeV. The lower value is obtained for $\langle \omega_1^0 h_{17} \rangle = 0.197$ GeV², $\langle \omega_1^2 h_{17} \rangle = 0.27$ GeV⁴, $\sigma = 0.44$ GeV, $m_c = 1.17$ GeV, and $m_b = 4.61$ GeV. The upper value is obtained for $\langle \omega_1^0 h_{17} \rangle = 0.277$ GeV², $\langle \omega_1^2 h_{17} \rangle = 0.03$ GeV⁴, $\sigma = 0.14$ GeV, $m_c = 1.23$ GeV, and $m_b = 4.55$ GeV. Thus the extremal values are obtained for extremal values of the two moments, anti-correlated, and the extremal values of m_c and m_b , anti-correlated [92].

The dependence on m_b and m_c can be illustrated as follows: consider the set $\langle \omega_1^0 h_{17} \rangle = 0.197$ GeV², $\langle \omega_1^2 h_{17} \rangle = 0.27$ GeV⁴, $\sigma = 0.44$ GeV that leads to $\Lambda_{17} = -21$ MeV. Changing $m_b = 4.61$ to $m_b = 4.55$ GeV while keeping $m_c = 1.17$ GeV changes Λ_{17} by +1 MeV. Thus the dependance on the value of m_b is rather mild. Changing $m_c = 1.17$ GeV to $m_c = 1.23$ GeV while keeping $m_b = 4.61$ GeV changes Λ_{17} by +6 MeV. Thus the dependance on the value of m_c is more pronounced [92].

Similarly, we find the values of $\tilde{\Lambda}_{17}^c$. We have $\tilde{\Lambda}_{17}^c \in [0, 10]$ MeV. The lower value is obtained for $\langle \omega_1^0 h_{17} \rangle = 0.277$ GeV², $\langle \omega_1^2 h_{17} \rangle = 0.03$ GeV⁴, $\sigma = 0.14$ GeV, $m_c = 1.13$ GeV, and $m_b = 4.55$ GeV. The upper value is obtained for $\langle \omega_1^0 h_{17} \rangle = 0.197$ GeV², $\langle \omega_1^2 h_{17} \rangle = 0.27$ GeV⁴, $\sigma = 0.58$ GeV, $m_c = 1.07$ GeV, and $m_b = 4.61$ GeV. Again the extremal values are obtained for extremal values of the two moments, anti-correlated, and the extremal values of m_c and m_b , anti-correlated [92].

Finally, we consider the $\tilde{\Lambda}_{17}^u$. Using the parameterization above we have the expression

$$\tilde{\Lambda}_{17}^u = \frac{2}{3} h_{17}(0) = \frac{3\sigma^2 \langle \omega_1^0 h_{17} \rangle - \langle \omega_1^2 h_{17} \rangle}{3\sqrt{2\pi}|\sigma|^3}. \quad (5.24)$$

Since both moments are positive within their one standard deviation range, we can easily make $h_{17}(0)$ negative by choosing a small value of σ . Thus the smallest value of $h_{17}(0)$ based on $|h_{17}(\omega_1, \mu)| \leq 1$ GeV is -1 GeV. For example, for the central values of $\langle \omega_1^0 h_{17} \rangle$ and $\langle \omega_1^2 h_{17} \rangle$, the value of $\sigma = 0.27$ GeV gives $h_{17}(0) = -1$ GeV. To make $h_{17}(0)$ reach its highest possible value, we can choose the smallest value of $\langle \omega_1^2 h_{17} \rangle$, 0.03 GeV⁴ and the largest value of $\langle \omega_1^0 h_{17} \rangle$, 0.277 GeV². The extremal value of $h_{17}(0) = 0.33$ GeV is obtained

for $\sigma = \sqrt{\langle \omega_1^2 h_{17} \rangle / \langle \omega_1^0 h_{17} \rangle} = 0.33$ GeV. Based on this we find that $\tilde{\Lambda}_{17}^u \in [-660, 220]$ MeV [92].

5.3.3 Sum of three Hermite polynomial model

The sum of three Hermite polynomial model is obtained by using the fourth moment of h_{17} . For a given value of σ we find the coefficient a_4 as [92]

$$a_4 = \frac{\langle \omega_1^4 h_{17} \rangle - 6\sigma^2 \langle \omega_1^2 h_{17} \rangle + 3\sigma^4 \langle \omega_1^0 h_{17} \rangle}{96\sqrt{2\pi}|\sigma|^5}. \quad (5.25)$$

The fourth moment is currently unknown since it relates to dimension 9 HQET matrix elements. The impact of this moment can be assessed, however, by considering the conservative bound $\langle \omega_1^4 h_{17} \rangle \in [-0.3, 0.3]$ GeV⁶. Note that this range covers all the numerical values obtained in equation (5.10). The bounds on Λ_{17} , $\tilde{\Lambda}_{17}^c$ and $\tilde{\Lambda}_{17}^u$ were obtained by restrictions of the values, zeros, and extremal points of h_{17} to be below 1 GeV [92].

Numerically scanning over the one standard deviation range of the known zero and second moments, the range $[-0.3, 0.3]$ GeV⁶ for the unknown fourth moment in increments of 0.05 GeV and the possible values of σ based on the restrictions above gives $\Lambda_{17} \in [-24, 3]$ MeV. The lower value is obtained for $\langle \omega_1^0 h_{17} \rangle = 0.277$ GeV², $\langle \omega_1^2 h_{17} \rangle = 0.27$ GeV⁴, $\langle \omega_1^4 h_{17} \rangle = 0.3$ GeV⁶, $\sigma = 0.32$ GeV, $m_c = 1.17$ GeV, and $m_b = 4.61$ GeV. The upper value is obtained for $\langle \omega_1^0 h_{17} \rangle = 0.237$ GeV², $\langle \omega_1^2 h_{17} \rangle = 0.03$ GeV⁴, $\langle \omega_1^4 h_{17} \rangle = -0.1$ GeV⁶, $\sigma = 0.34$ GeV, $m_c = 1.17$ GeV, and $m_b = 4.61$ GeV. The obtained range is only slightly different from the two Hermite polynomial model and reflects our generous range for the unknown fourth moment.

Similarly we find the range for $\tilde{\Lambda}_{17}^c$. The positive values are included in the range obtained for a sum of two Hermite polynomials. We also get negative values in the range $[-5.6, 0]$ MeV. The smallest value is obtained for $\langle \omega_1^0 h_{17} \rangle = 0.277$ GeV², $\langle \omega_1^2 h_{17} \rangle = 0.03$ GeV⁴, $\langle \omega_1^4 h_{17} \rangle = -0.11$ GeV⁶, $\sigma = 0.34$ GeV, $m_c = 1.07$ GeV, and $m_b = 4.61$ GeV.

Unlike the two Hermite polynomial model we can make $h_{17}(0)$ reach a value of 1 GeV. For example, taking the central values of the zeroth and second moment $\langle \omega_1^0 h_{17} \rangle = 0.237$ GeV²,

$\langle \omega_1^2 h_{17} \rangle = 0.15 \text{ GeV}^4$ we find that for $\langle \omega_1^4 h_{17} \rangle = 0.1 \text{ GeV}^6$ and $\sigma = 0.25 \text{ GeV}$ $h_{17}(0) = 1 \text{ GeV}$. This result is not surprising. The moments are global properties of the function and it is hard to restrict using them values of the function at a single point. We conclude that for this model $\tilde{\Lambda}_{17}^u$ can be as large as 660 MeV, which is the largest value possible under the condition $|h_{17}(\omega_1, \mu)| \leq 1 \text{ GeV}$ [92].

5.3.4 Sum of four Hermite polynomials model

The four Hermite polynomial model is constructed by considering the conservative estimate of $[-0.3, 0.3] \text{ GeV}^8$ for the sixth moment $\langle \omega_1^6 h_{17} \rangle$. This moment is related to the coefficient of the sixth Hermite polynomial (H_6).

Scanning over the values of the fourth and sixth moment we find that the smallest value of Λ_{17} is -22 MeV , i.e. in the range we obtained for three Hermite polynomials. The highest value we obtain is 5 MeV for $\langle \omega_1^0 h_{17} \rangle = 0.277 \text{ GeV}^2$, $\langle \omega_1^2 h_{17} \rangle = 0.03 \text{ GeV}^4$, $\langle \omega_1^4 h_{17} \rangle = -0.1 \text{ GeV}^6$, $\langle \omega_1^6 h_{17} \rangle = -0.2 \text{ GeV}^8$, $\sigma = 0.29 \text{ GeV}$, $m_c = 1.17 \text{ GeV}$, and $m_b = 4.61 \text{ GeV}$. This should be compared to the maximum value of -1 MeV and 3 MeV for the two and three Hermite polynomial models, respectively.

For $\tilde{\Lambda}_{17}^c$ we find positive values that are already included in the ranges of the two and three Hermite polynomial models above. The smallest negative value we find for $\tilde{\Lambda}_{17}^c$ is -7 MeV for $\langle \omega_1^0 h_{17} \rangle = 0.277 \text{ GeV}^2$, $\langle \omega_1^2 h_{17} \rangle = 0.03 \text{ GeV}^4$, $\langle \omega_1^4 h_{17} \rangle = -0.1 \text{ GeV}^6$, $\langle \omega_1^6 h_{17} \rangle = -0.2 \text{ GeV}^8$, $\sigma = 0.29 \text{ GeV}$, $m_c = 1.07 \text{ GeV}$, and $m_b = 4.61 \text{ GeV}$.

Since $\tilde{\Lambda}_{17}^u$ obtains its smallest and largest possible values for the two and three Hermite polynomial models, there is no need to check the effect of the four Hermite polynomials model [92].

5.3.5 Sum of five and six Hermite polynomials model

Similarly, we can continue with five and six Hermite polynomial models. For this we assume k -th moment is in the range $[-0.3, 0.3] \text{ GeV}^{k+2}$. Scanning over the ranges in increments of 0.1 GeV^{k+2} we find that there are no solutions that satisfy our requirements on $h_{17}(0)$. One reason is the fast growth of the value of $H_n(0)$. Thus the coefficient of $H_n(0)$

needs to be smaller to maintain $|h_{17}(0)| \leq 1$ GeV.

5.3.5.1 Summary

Using a two Hermite polynomial model we find $\Lambda_{17} \in [-21, -1]$ MeV, $\tilde{\Lambda}_{17}^c \in [0, 10]$ MeV, and $\tilde{\Lambda}_{17}^u \in [-660, 220]$ MeV. Using a three Hermite polynomial model we find $\Lambda_{17} \in [-24, 3]$ MeV, where $\langle \omega_1^4 h_{17} \rangle$ is assumed to be in the range $[-0.3, 0.3]$ GeV⁶. The range for $\tilde{\Lambda}_{17}^c$ is found as $\tilde{\Lambda}_{17}^c \in [-5.6, 0]$ MeV. Also, the largest value of $\tilde{\Lambda}_{17}^u$ is 660 MeV, which is based on our assumptions for h_{17} . Using the four Hermite polynomial model with similar assumptions on the fourth and sixth moments changes the highest value of Λ_{17} to 5 MeV and the lowest value of $\tilde{\Lambda}_{17}^c$ to -7 MeV.

Altogether, we find $\Lambda_{17} \in [-24, 5]$ MeV, $\tilde{\Lambda}_{17}^c \in [-7, 10]$ MeV, and $\tilde{\Lambda}_{17}^u \in [-660, 660]$ MeV after rounding to the closest integer.

5.3.6 Phenomenological estimates

The 2010 phenomenological estimates of $\mathcal{F}_E|_{17}$ were given in section 3.1.5. Based on the new estimates of Λ_{17} , $\tilde{\Lambda}_{17}^u$ and $\tilde{\Lambda}_{17}^c$ we update the results found in [78] and [95].

The $Q_1^q - Q_{7\gamma}$ contribution to the total uncertainty was evaluated by using $C_1(\mu) = 1.257$, $C_7(\mu) = -0.407$ (calculated at $\mu = 1.5$ GeV) and $m_b = 4.58$ GeV. This gives [92, 112]:

$$\mathcal{F}_E|_{17} \in [-0.3, +1.6]\% \quad (5.26)$$

This should be compared to the range given in equation (3.48) [78]. The total uncertainty of the rate can be obtained by using $\mathcal{F}_E|_{88} \in [-0.3, +1.9]\%$ [78] along with either $\mathcal{F}_E|_{78}^{\text{VIA}} \in [-2.8, -0.3]\%$ or the new experimental value from PDG, $\mathcal{F}_E|_{78}^{\text{exp}} \in [-1.4, +2]\%$, which was obtained in section 3.1.5.3. Scanning over various contributions give [92, 112]

$$-3.4\% < \mathcal{F}_E(\Delta) < +3.2\% \quad (\text{ using VIA}) \quad (5.27)$$

This new range should be compared with the 2010 range given in equation (3.50), and it

implies a reduction to the total error by a third. In contrast, by using the experimental estimate the new range becomes

$$-2.0\% < \mathcal{F}_E(\Delta) < +5.5\% \quad \text{using exp.} \quad (5.28)$$

Compared to the 2010 range given in equation (3.51), the new estimate reduces the total error by a half [92, 112].

Plugging in our new estimates for $\tilde{\Lambda}_{17}^u$ and $\tilde{\Lambda}_{17}^c$ found in the section 3.2.1 to the following expression

$$\mathcal{A}_{X_s\gamma}^{\text{SM}} = \left(1.15 \times \frac{\tilde{\Lambda}_{17}^u - \tilde{\Lambda}_{17}^c}{300\text{MeV}} + 0.71 \right) \% \quad (5.29)$$

gives us $-1.9\% < \mathcal{A}_{X_s\gamma}^{\text{SM}} < 3.3\%$. This should be compared to the 2010 range $-0.6\% < \mathcal{A}_{X_s\gamma}^{\text{SM}} < 2.8\%$ in [95]

CHAPTER 6 NEW RESULTS : SEMILEPTONIC DECAYS OF HEAVY MESONS WITH ARTIFICIAL NEURAL NETWORKS

The study of semileptonic decays is an important new physics probe. For example, the recent analysis of semileptonic B decays provides an anomaly in measurement related by lepton universality requirements. The advent of higher precision data provides new opportunities to explore whether similar anomalies exist in semileptonic decays of charmed particles [113–116].

Accurate theoretical description on charmed semileptonic decays provides useful information to extract the CKM matrix elements. Specifically, the decays of charmed D^0 , D^+ , or D_s mesons provide one of the simplest way to determine the magnitudes of quark mixing parameters [117]. To extract these CKM matrix elements we use the knowledge of matrix elements of quark currents that describe strong interaction effects. Following from this, we find accurate description of semileptonic transitions, which is also needed for improvement of our understanding of quark hadronization mechanisms in QCD [117]. The exclusive semileptonic transition between two meson states makes it a suitable system to theoretically analyze matrix elements of flavor changing currents. These flavor changing currents are parameterized by momentum dependent form factors. These form factors describes the hadronic part of the decay amplitude given by [117]

$$\langle K(\pi)(p_{K(\pi)})|\bar{q}\gamma_\mu c|D(p_D)\rangle = F_+(q^2) \left(P_\mu - \frac{m_D^2 - m_{K(\pi)}^2}{q^2} q_\mu \right) + F_0(q^2) \frac{m_D^2 - m_{K(\pi)}^2}{q^2} q_\mu, \quad (6.1)$$

where $P = p_D + p_{K(\pi)}$ and $q = p_D - p_{K(\pi)}$. The differential decay rates ($d\Gamma/dq^2$) provide the means to study these form factors. By neglecting the final state fermion mass we write the differential decay rate for the semileptonic decay $D \rightarrow K(\pi)\ell\nu_\ell$ as [117]:

$$\frac{d\Gamma(D \rightarrow K(\pi)\ell\nu_\ell)}{dq^2} = \frac{G_F^2 |V_{cq}|^2}{24\pi^3} |\mathbf{p}_{K(\pi)}|^3 |F_+(q^2)|^2, \quad (6.2)$$

where $|\mathbf{p}_{K(\pi)}|$ is the magnitude of the $K(\pi)$ 3-momentum vector in the D -meson rest frame. Equation (6.2) implies that only the $F_+(q^2)$ contributes for the analysis.

Accurate calculations of the non-perturbative form factors $F_{+/\prime 0}(q^2)$ in the whole momentum range are very challenging [117]. Currently, we do not have a complete description of these form factors. Only Lattice QCD (LQCD) [118] and QCD sum rules (QCDSR) [119] provide a model independent description in a limited q^2 range. However, these calculations are still improving.

We use rather general arguments based on analyticity of $F_+(q^2)$ to put constraints on shape of the form factors. The z expansion is one of the popular approaches that uses the analyticity requirement to derive constraints on form factors. Here we series expand the form factor at some point $t = q^2$. This series can be improved by employing a conformal transformation to the parameter z

$$z(q^2) = \frac{\sqrt{t_+ - t_0} - \sqrt{t_+ - q^2}}{\sqrt{t_+ - t_0} + \sqrt{t_+ - q^2}}, \quad (6.3)$$

where the transformation $z(q^2)$ maps the interval $-\infty < q^2 < t_+$ onto the line segment $-1 < z < 1$. t_0 is a free parameter that corresponds to the values of q^2 that maps onto $z = 0$, and $t_{\pm} = (m_D \pm m_{\pi})^2$ [117]. Then the form factor is expanded as

$$F_+(q^2) = \frac{1}{\Phi(q^2, t_0)} \sum_{k=0}^{\infty} a_k(t_0) z^k(q^2, t_0), \quad (6.4)$$

where $\Phi(q^2, t_0)$ is an arbitrary function that is analytic anywhere but the unitarity cut [117,120,121]. If there are poles present in between $q^2 = 0$ and the beginning of the unitarity cut, then the function $\Phi(q^2, t_0)$ can be written as $\Phi(q^2, t_0) = P(q^2)\phi(q^2, t_0)$, where $P(q^2) = z(q^2, m_V^2)$. For example, in $B \rightarrow \pi$ transitions such a pole present at $m_V = m_{B^*}$ [122,123]. For the $B \rightarrow \pi$ transitions the expansion in equation (6.4) is converging rapidly, so only a few terms in the expansion are really needed. Thus the results from LQCD and QCDSR can be used to constrain the coefficients a_k to provide a model-independent parameterization of

the form factor [117].

Since the form factors cannot be obtained from the first principles, phenomenological parameterizations are used to describe them. The “simple pole” model is the common parameterization, where “pole” refers to the lowest mass vector resonance formed in the t-channel with quantum numbers of the quark current [117]. For instance, the D^* vector state with quantum numbers 1^- is the dominant pole in the $D \rightarrow \pi e \bar{\nu}_e$ decay. The simple pole model is given as follows [117]:

$$F_+^{\text{pole}}(q^2) = \frac{F_+(0)}{1 - \hat{q}^2}, \quad (6.5)$$

where $F_+(0)$ is the value of the form factor at zero momentum recoil that has to be fixed either from the lattice QCD or from other arguments, and $\hat{q}^2 = q^2/m_{D^*}^2$. The m_{D^*} is often taken as a fit parameter. However, physical masses of the states $D^*(2010)$ (for $D \rightarrow \pi$ transition) or $D_s^*(2112)$ (for $D \rightarrow K$ transition) could be used as well. Using more effective poles we construct more complicated models [117]

$$F_+(q^2) = \frac{F_+(0)}{(1 - \alpha)} \frac{1}{1 - q^2/m_V^2} + \sum_{k=1}^N \frac{\rho_k}{1 - \frac{1}{\gamma_k} \frac{q^2}{m_V^2}}, \quad (6.6)$$

where α provides the strength of the dominant pole, ρ_k is the strength of the k th term in the expansion, and $\gamma_k = m_{V_k}^2/m_V^2$, with m_{V_k} are masses of the higher mass states with vector quantum numbers. We can improve the accuracy of a given model by considering more effective poles. For example, a popular model that is due to Becirevic and Kaidalov (BK) [124] is given as

$$F_+^{BK}(q^2) = \frac{F_+(0)}{(1 - \hat{q}^2)(1 - a_{BK}\hat{q}^2)}, \quad (6.7)$$

where a_{BK} is a fit parameter. Note that this model is obtained for the $N = 1$ truncation of the expansion in equation (6.6). As shown in the simple pole model, a good fit to experimental distribution is obtained by considering m_V as a fit parameter. Further extension to the BK

model is obtained by Ball and Zwicky [125],

$$F_+^{BZ}(q^2) = \frac{F_+(0)}{1 - \hat{q}^2} \left(1 + \frac{r_{BZ}\hat{q}^2}{1 - a_{BZ}\hat{q}^2} \right), \quad (6.8)$$

where r_{BZ} and a_{BZ} are the shape parameters.

In this work we are interested in learning whether choosing a specific functional form for the form factor induces a bias in the interpretation of an experimental analysis. This is analyzed in the machine learning (ML) approach. In particular, we are using the artificial neural networks (ANN) for this analysis. As shown in [126, 127], ANN can be used as an unbiased estimator of data. This fact has been used by the NNPDF collaboration to parameterize nucleon's parton distribution functions (PDF) [128–130], and in form factor analysis of nucleon data [131, 132].

In the following we build a statistical interpolating model based on ANNs, which contains information on experimental uncertainties and correlations. Nevertheless, ANN does not introduce theoretical bias. Following from [128, 129], we employ an approach based on multilayer feed-forward neural networks trained using the back-propagation learning algorithm [117].

6.1 Artificial Neural Networks

6.1.1 Basic facts

Recently, artificial neural networks are gaining traction in both academia and industry. As a result, ANN are widely used in experimental particle physics analysis. Specifically, the ANNs are extensively used in the jet finding algorithms [133]. A neural network can be thought of as a nonlinear function that connects the input and output data. In [117], we explored another feature of ANNs, which is their ability to provide unbiased universal approximants to incomplete data [126, 127]

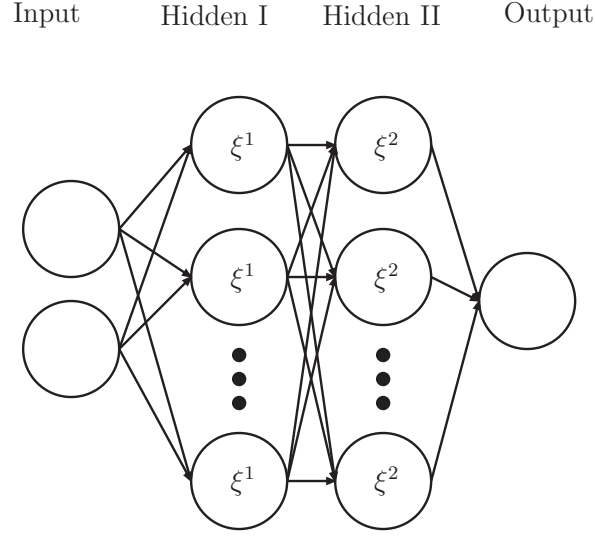


Figure 6.1: Structure of an artificial neural network with two hidden layers [117].

ANN mimic the structure of human neurons and consists of a set of interconnected units (see Figure. 6.1) called *neurons* or *nodes* [117]. The activation state of a neuron is determined by the activation function ($g(x)$), which is determined by the activation status of the i neurons connected to it. Each pair of these neurons is connected by a synapsis, which is characterized by a weight ω_i . Also, we add a threshold θ_i to control the activation state (“fire”) of neurons. In ANNs we categorize groups of neurons into layers. The first layer is called as input layer, which is associated with the input information. In the following work we used the value of q^2 for each bin in q^2 distribution of the CKM matrix element times the semileptonic form factor ($V_{cd}F_+(q^2)$) [117]. Furthermore, We used two nodes in the input layer, which improved the stability and the efficiency of the ANN. In section 6.2.2, we provide further information on the input nodes. The final layer of the ANN is the output layer. The output layer provides fit for the $V_{cd}F_+(q^2)$ data along with its uncertainty. Conventionally, the layers between input and output layers are known as *hidden layers*. Our ANN employs two hidden layers. Each of these hidden layers contain hundred nodes as well.

6.1.2 Forward propagation

In the ANN training process we incrementally update the weights and thresholds so that they obtain optimal set of ω_i and θ_i . This is achieved by minimizing the error function,

$$E[\omega, \theta] \equiv \frac{1}{2} \sum_{A=1}^{n_p} (o(q_A^2) - y_A)^2, \quad (6.9)$$

where n_p is the number of pseudo-data used to train an ANN, $o(q_A^2)$ is the output, which is given by the ANN's fit for a given input data q_A^2 . Here the target data point y_A , is obtained from the magnitude of the CKM matrix element times the semileptonic form factor, $|V_{cd}F_+(q^2)|$. Note that the differential distribution of Eq. (6.2) is proportional to $|V_{cd}F_+(q^2)|^2$. The $o(q_A^2)$ is obtained using forward propagation. In order to achieve this we pass the input through a network of hidden nodes. The output from the first hidden layer with n_1 number of nodes is [117]

$$\xi^{[1]} = g \left(\sum_{i=1}^{n_1} \omega_i^{[1]} q^2 - \theta^{[1]} \right). \quad (6.10)$$

In this equation the response of each neuron is given by [117]

$$g(x) \equiv \frac{1}{1 + e^{-x}}, \quad (6.11)$$

which is the *sigmoid* activation function, and the summation over the q^2 data points is implied. The $\xi^{[1]}$ is then used as an input for the second hidden layer with n_2 number of hidden nodes, and so on. The process is continued until the output layer of ANN is reached. In general, we can construct the output from ℓ th hidden layer with n_ℓ number of nodes as [117]

$$\xi^{[\ell]} = g \left(\sum_{i=1}^{n_\ell} \omega_i^{[\ell]} \xi^{[\ell-1]} - \theta^{[\ell]} \right). \quad (6.12)$$

where $\xi^{[\ell-1]}$ is the output from the $(\ell - 1)$ th layer. The fit of the L layer ANN $o(q^2)$ is then defined as

$$o(q^2) = \xi^{[L]}. \quad (6.13)$$

As shown above, the error function needed to be minimized. The popular choice of minimization is the *gradient descent* (GC). Instead, we decided to use the non-linear conjugate gradient (NLCG) method [134, 135] to minimize equation (6.9). In each iteration the ω_i and the θ_i update as [117]

$$\begin{aligned} \delta\omega^{[\ell]} &= -\eta \frac{\partial E}{\partial \omega^{[\ell]}}, \\ \delta\theta^{[\ell]} &= -\eta \frac{\partial E}{\partial \theta_i^{[\ell]}}, \end{aligned} \quad (6.14)$$

where η is the learning rate at a given iteration. The NLCG method employed here does not require a pre-defined learning rate. The learning rate is initially determined by using line search algorithms [134], and then iteratively updated based on the gradients that are in a conjugate direction to original gradient used in the line search algorithm. As it turns out, the NLCG method converges much faster than steepest descent method for the fits employed in this in this work. For more details on the NLCG method, see Ref. [135].

6.1.3 Back propagation

The gradients of the error function are obtained by using the method of back propagation [136]. Back propagation can be thought of as a consecutive application of the chain rule. By applying the chain rule to the L th layer we find [117]

$$\Delta^{[L]} = g'(h^{[L]})[o(q^2) - y] \quad (6.15)$$

where $g'(h^{[L]})$ is the derivative of the activation function with respect to $h^{[L]}$ and

$$h^{[L]} = \sum_{i=1}^{n_{L-1}} \omega^{[L]} \xi_i^{[L-1]} - \theta^{[L]} \quad (6.16)$$

The derivatives with respect to ω_i and θ_i for layer L are given by [117]

$$\begin{aligned} \frac{\partial E}{\partial \omega_i^{[L]}} &= \Delta^{[L]} \xi_i^{[L-1]}, & i = 1, \dots, n_{L-1}, \\ \frac{\partial E}{\partial \theta_i^{[L]}} &= -\Delta^{[L]}. \end{aligned} \quad (6.17)$$

The output of equation (6.15) is used to obtain the derivatives of the $(L-1)$ th layer, $\Delta_j^{[L-1]}$,

$$\Delta_j^{[L-1]} = g'(h^{[L-1]}) \Delta_i^{[L]} \omega^{[L]}. \quad (6.18)$$

The procedure is repeated for the hidden layers to find derivatives of error function with respect to ω_i and θ_i in each layer [117],

$$\begin{aligned} \frac{\partial E}{\partial \omega_{ij}^{[\ell]}} &= \Delta_i^{[\ell]} \xi_j^{[\ell-1]}, & i = 1, \dots, n_\ell, \quad j = 1, \dots, n_{\ell-1}, \\ \frac{\partial E}{\partial \theta_i^{[\ell]}} &= -\Delta_i^{[\ell]}, & i = 1, \dots, n_\ell, \end{aligned} \quad (6.19)$$

Using these we can obtain the numerical gradient of the error function and find the corrections to the weights and thresholds.

6.2 Neural network training

6.2.1 Preparation of the data set

The neural network training is performed on the real and artificial (pseudo) data. The pseudo data is generated based on the information from experimental data. Here we used the uncorrelated data, correlated data, normalized data, or some combination of these data types. These pseudo data was generated by following the method provided in [130]. The ex-

perimental data set that is required to generate the pseudo data were provided in [137]. This experimental data set contains both uncorrelated and correlated statistical and systematic uncertainties. Also, the data set is provided with correlation matrices. The artificial data is generated as [117]

$$|V_{cd}F_+(q^2)|_i^{(\text{art}), (k)} = |V_{cd}F_+(q^2)|_i^{(\text{exp})} + r_{t,i}^{(k)} \sigma_{t,i} + \sum_{j=1}^{N_{\text{sys}}} r_{\text{sys},j}^{(k)} \sigma_{\text{sys},ji} + \sum_{m=1}^{N_{\text{stat}}} r_{\text{stat},m}^{(k)} \sigma_{\text{stat},mi} \quad (6.20)$$

where $i = 1, \dots, N_{\text{data}}$ is the number of experimental data entries, which is equal to the number of q^2 bins. The term $|V_{cd}F_+(q^2)|_i^{(\text{exp})}$ is the central value of the experimental data point for a given q^2 . The last three terms in the right hand side of the equation (6.20) provide the variation in the pseudo data sample. These terms represent total uncorrelated, correlated systematic, and correlated statistical uncertainties respectively. Following from the [130], we use all these information to generate the pseudo data samples. Here each ‘‘uncertainty term’’ is multiplied by a Gaussian random number $r_{t,i}^{(k)}$, $r_{\text{sys},j}^{(k)}$, or $r_{\text{stat},m}^{(k)}$ [117]. These random numbers have the mean of zero, and their standard deviation is equal to the bin uncertainty provided in [137]. The total uncorrelated uncertainty, $\sigma_{t,i}$, is defined as

$$\sigma_{t,i} = \sum_{j=1}^{N_{u,\text{sys}}} \tilde{\sigma}_{\text{sys},ji} + \sum_{m=1}^{N_{u,\text{sys}}} \tilde{\sigma}_{\text{stat},mi} \quad (6.21)$$

where the $\tilde{\sigma}_{\text{sys},ji}$ is uncorrelated systematic uncertainty and $\tilde{\sigma}_{\text{stat},mi}$ statistical uncertainty.

In [137] we find the correlation matrix elements, $\text{corr}(j, i)$ as

$$\sigma_{j,i} = \sqrt{\tilde{\sigma}_i \tilde{\sigma}_j \text{corr}(j, i)}, \quad (6.22)$$

where $\tilde{\sigma}_i$ is the uncorrelated uncertainty in the i -th bin of data. The q^2 values were randomly generated with a flat prior across the entire q^2 bin. Thus, every value of $d\Gamma^{(\text{art})}/dq^2$ has a different q^2 input.

6.2.2 Feature engineering

We divided the generated pseudo data into 100 batches (one batch per network). Each batch has an average q^2 and a standard deviation relating to the q^2 values, which are used to scale the each value of q^2 which we have generated. Using the scaled q^2 data as a secondary input is recommended to improve the stability and the performance of ANNs [138]. In particular, data standardization is a popular data scaling choice, and it is defined as $\tilde{q}_{i\rho}^2 = (q_{i\rho}^2 - \bar{q}_\rho^2) / \sigma_\rho$, where ρ is the batch number and i is a single q^2 value in the batch. With this transformed data, each of our ANNs has the structure (2, 100, 100, 1), as the two hidden layers, each with 100 nodes, provide the most efficient structure without compromising the performance or accuracy. With a higher number of nodes, the ANN's fit would be more accurate, but the training speed would also be reduced. This data transformation, along with the conjugate gradient method, provides the minimum of the error function at 100 iterations. In contrast, steepest descent method with a constant learning rate provides a comparable result only at 20000 iterations [117].

6.3 Form factor parameterization with neural networks

The 2×10^6 data points were generated for each of the 14 q^2 bins. As shown above, this data set was divided to hundred subsets, and each of these subsets contains with 280,000 unique pseudo-data points. After training all networks individually, we found the average ANN curve, with uncertainty, at every calculated q^2 value. The differential decay rate, $d\Gamma/dq^2$, and the $|V_{cd}F_+(q^2)|$ curves are shown in Fig. 6.2 and Figure 6.3 respectively. Further results of the ANN training and relevant graphs are available at the URL <https://s.wayne.edu/hepmachinelearning/>.

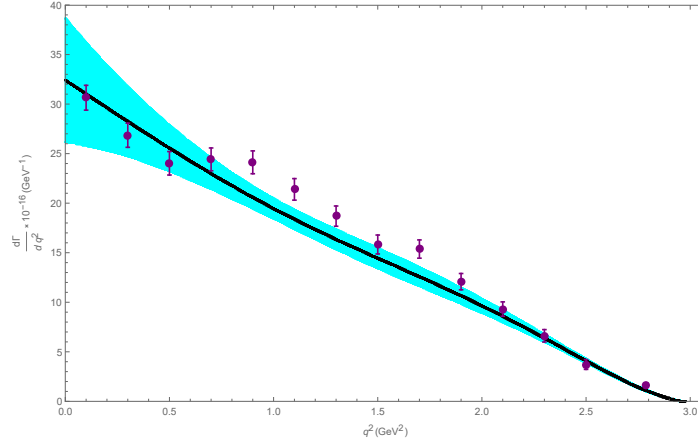


Figure 6.2: The averaged ANN result for the differential decay rate plotted against the experimental measurement [117]. The purple data points are the experimental data from [137]. The black and cyan curves are the average value and one standard deviation, respectively, from the output of our averaged ANN .

In figure 6.3 ANN fit is compared with some common form factor models: simple pole, the BK model (or modified pole), and the BZ model [124, 125] .

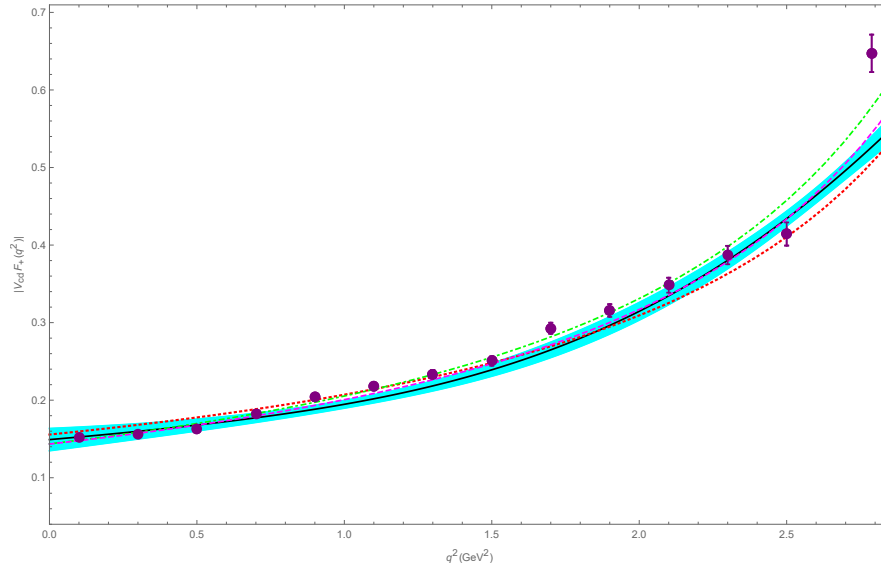


Figure 6.3: ANN fits for $|V_{cd}F_+(q^2)|$ plotted against the three models described in the text [117]. The black and cyan curves are the average value and one standard deviation, respectively, from the output of our neural network. The dotted red curve is the simple pole model. The dot-dashed green curve is the modified pole model. The dashed magenta curve is the BZ model. The purple data points are calculated from the experimental data in Ref [137].

The $|V_{cd}F_+(0)|$ obtained from the model fits are roughly consistent with the ANN fit of the semileptonic decay data.

CHAPTER 7 CONCLUSION AND FUTURE WORK

7.1 Conclusion

Flavor physics is the study of different species of elementary particles [139], and it provides tools to expand the boundaries of SM. For example, the radiative FCNC decay $\bar{B} \rightarrow X_s \gamma$ is considered as one of the standard candles of BSM [30]. As another example, semileptonic decays of heavy mesons provide the means to extract the CKM matrix elements. Due to the effects of QCD, these decays are plagued with nonperturbative uncertainties. Therefore, it is important to control these uncertainties to understand new physics in above processes.

In this work we discussed the controlling the nonperturbative uncertainties in $\bar{B} \rightarrow X_s \gamma$ and semileptonic $D \rightarrow \pi l \nu$. In chapter 4, we provided the construction of a new basis for the tensor decomposition of HQET and NRQCD matrix elements of any dimension. In chapter 5, we used the new basis for HQET/NRQCD to obtain the higher dimensional moments of subleading shape function. This function parameterizes the nonperturbative effects. We used these moments to model the subleading shape function and reevaluate the nonperturbative uncertainties. Finally, in chapter 6, we used artificial neural networks to parameterize the shape of the form factor $F_+(q^2)$, which describes the nonperturbative effects of $D \rightarrow \pi l \nu$.

7.1.1 On HQET and NRQCD operators of dimension eight and above

In chapter 4, we provided the method to construct operators for the HQET and NRQCD Lagrangians at any given dimension. Although these theories employ different power counting schemes, the Lagrangians are closely related [55]. We analyzed operators that contain two HQET fields or two NRQCD (NRQED) fields with an arbitrary number of covariant derivatives. These matrix elements can be written as nonperturbative HQET parameters multiplied by tensors constructed from the heavy quark velocity, the metric tensor, and the Levi-Civita tensor. We also use constraints coming from the time-reversal (T) and parity (P) symmetries, hermitian conjugation, and the fact that we work in $3 + 1$ dimension. At a given dimension, the number of allowed HQET operators are equivalent to the number of HQET parameters up to a possible color factor.

The new basis of HQET matrix elements allows us to easily determine the number of allowed HQET/NRQCD operators at a given dimension. This decomposition of matrix elements allows us to check whether given operators are linearly independent. The method also allows relating operators to one another easily. Following this, we constructed the HQET and NRQCD Lagrangian at mass dimension 8 for the first time.

As shown in [101], operators that contain symmetric product of two color matrices, such as $\psi^\dagger E_a^i T^a E_b^i T^b \psi$, can be decomposed in terms of a color octet and a color singlet operators, $\psi^\dagger E_a^i E_b^i d^{abc} T^c \psi$ and $\psi^\dagger E_a^i E_b^i \delta^{ab} \psi$. Since they only differ in their color structure, both will give the same linear combination of parameters. Alternatively we can use the basis of $\psi^\dagger E_a^i E_b^i \{T^a, T^b\} \psi$ and $\psi^\dagger E_a^i E_b^i \delta^{ab} \psi$. The operator $\psi^\dagger E_a^i E_b^i \{T^a, T^b\} \psi$ is generated by commutator and anti-commutators of covariant derivatives, and it is the only of the two that appears when calculating observables at tree level. The operator $\psi^\dagger E_a^i E_b^i \delta^{ab} \psi$ will be generated when considering radiative corrections [55]. For applications to inclusive B decays, this operator arises only at order α_s/m_b^4 , beyond the current level of precision [56]. Using the method presented above allows determining how many linearly independent operators there are for possible different color structures.

In section 4.4, we relate the HQET parameters of operators of dimension four, five, six, seven, and eight known from the literature to our basis. NRQCD operators up to dimension seven and NRQED operators up to dimension eight were previously known in the literature. We related these operators to the corresponding HQET matrix elements. The relation between the HQET/NRQCD operators and the matrix elements allows us to write the operators in terms of nonperturbative HQET parameters. [56].

In section 4.6, we analyzed dimension nine spin-independent HQET parameters. Here we found 24 possible parameters (not including multiple color structures). Most importantly, we constructed the dimension eight NRQCD operators that do not appear in the $1/M^4$ NRQED Lagrangian. These allow presenting for the full $1/M^4$ bilinear NRQCD Lagrangian.

7.1.2 Reevaluating the uncertainties in $\bar{B} \rightarrow X_s \gamma$

The section 5.1 provides the moments of subleading shape function using data given in [64] and the basis developed in chapter 4 [56]. This subleading shape function relates to the soft function h_{17} , which parameterize the nonperturbative uncertainty. The function h_{17} defined in equation (3.38), and it has the following properties: it is a real and even function over gluon momentum ω_1 , it's odd moments over ω_1 vanish and it has dimensions of mass. Based on these properties we developed a new model for soft function h_{17} based on a combination of *Hermite polynomials* multiplied *Gaussian*. The explicit form of the new model is given in section 5.3.

The h_{17} is is a soft function, so one expects it not to have significant structures beyond $\omega_1 \leq 1$ GeV. This provides other constraints such as $|h_{17}(\omega_1)| \leq 1$ GeV, and it limits the function from having structures beyond $|\omega_1| \leq 1$ GeV. Scanning through different values of moments, we found a new estimate for $Q_1^q - Q_{7\gamma}$. Our estimate reduced the 2010 estimate [78] by a third. Also, we combined the new estimate for $Q_{7\gamma} - Q_{8g}$ with our new result for $Q_1^q - Q_{7\gamma}$ to obtain a new range for the total rate. Following from this we found that the uncertainty of the total rate is reduced by half compared to the 2010 values [78].

The SM prediction for CP asymmetry is obtained by nonperturbative parameters $\tilde{\Lambda}_{17}^u$ and $\tilde{\Lambda}_{17}^c$. These parameters are also related to h_{17} . We reevaluated their ranges using our analysis. From this we found a new estimate for SM CP asymmetry as $-1.9\% < \mathcal{A}_{X_s \gamma}^{\text{SM}} < 3.3\%$, which is an increased range compared to the 2010 estimate [95]. This is because of the increased range of the $\tilde{\Lambda}_{17}^u$.

7.1.3 Semileptonic decays of heavy mesons with artificial neural networks

The CKM matrix element $|V_{cd}|$ can be extracted most easily from semileptonic $D \rightarrow \pi l \nu$ decays. This decay is parameterized by the form factor $F_+(q^2)$, which describes the hadronic part of the decay amplitude. Experimentally, this form factor is studied by analyzing the differential decay rate of $d\Gamma/dq^2$. The lack of precise information about these form factors from the first principles of QCD is one of the main sources of uncertainties when extracting

the CKM parameters. In spite of the recent progress from lattice QCD (LQCD), still, there is no ab-initio approach to describe the shape of the form factors in the whole physical region of momentum transfer q^2 .

In view of the lack of first principle calculation for decay rates, phenomenological parameterizations of form factors are used to model the shape. These models first estimate the hadronic form factor at one kinematic point and then extrapolate based on the assumed functional shape of the form factor. What systematic uncertainty does choosing a particular function brings to such extrapolation? To answer this question, we use machine learning (ML) framework. In section 6.1, we used artificial neural networks (ANN) as an unbiased estimator of data.

We used an average of 100 feed-forward ANN with two hidden layers to obtain the unbiased estimate for $|V_{cd}|F_+(q^2)$. Each hidden layer contains 100 nodes [117]. The ANN performance was improved by using NLCG optimization method. We observed that NLCG method is 200 times faster compared to the common optimization methods such as gradient descent. The python code for ANN, results of the ANN training and relevant graphs are available at <https://s.wayne.edu/hepmachinelearning/>. The comparison between our ANN extrapolation of $|V_{cd}|F_+(q^2)$ against the existing models is provided in figure 6.3. From this we observe ANN fit is consistent with all the phenomenological models at low q^2 region. This implies that the ANN successfully extrapolated the $|V_{cd}|F_+(q^2)$ data to $q^2 \rightarrow 0$. Most importantly, our ANN fit provides model independent parameterization of the $F_+(q^2)$ shape for the first time in literature. This was instrumental in developing the unitarity constraints on the form factor, which allowed for model-independent bounds on V_{cd} [117].

7.2 Future work

We conclude with a remark on future developments. In section 4.1, we provided a general method of writing down all the possible HQET operators of any given dimension. It would be interesting to automatize the procedure using a computer program to construct these higher dimensional operators and the NRQCD Lagrangian. Also, certain multiple color structures

were considered separately from the general method. It would be desirable to find a method that automatically generates these color structures.

We have not considered operators with more than two HQET or NRQCD (NRQED) fields. The one non-relativistic fermion sector can be combined with an additional non-relativistic field or an additional relativistic field. Results for each case were presented in the literature [99, 140–143], but not for an arbitrary operator dimension.

With the new information on the moments, we can better control the hadronic effects. However, the scale dependence on $1/m_b$ corrections is not fully controlled because, currently, we treat them at the leading order in α_s . Therefore, to improve the $Q_1^q - Q_{7\gamma}$ contributions further, we need to take account of the α_s corrections.

Our model relies on the numerical estimates of the matrix elements of dimension eight operators. Still, it could further be improved if we knew the numerical estimates of dimension nine matrix elements. With the Belle II data, we can hope to have improvements on this.

In section 5.1, we only considered the quantities that are integrated over photon energy. The above moment information can be used to model $Q_1^q - Q_{7\gamma}$ contributions for quantities that are not integrated over photon spectrum.

The large amount of data that will be obtained at the B factory Belle II will be ideal for deep learning. The extraction of CKM parameters using machine learning can be further improved with the new knowledge of optimization methods and deep learning. For example, our work provided in section 6.1 uses the nonlinear conjugate methods (NLCG) to minimize the error function in the training process. The NLCG is a local optimizer. Whereas stochastic methods such as simulated annealing could have been more successful in optimizing the error function, and they are more suitable for deep learning. This is because these stochastic methods provide global optimization. With a large data set, we expect to develop deep neural networks utilizing parallel computation and graphical processing units.

APPENDIX A : RUNNING OF WILSON COEFFICIENTS C_1, C_7 AND C_{8G}

The expressions for the running of Wilson coefficients C_1, C_7 and C_{8g} are found in [12,15].

$$\begin{aligned}
 C_j^{(0)}(\mu_b) &= \sum_{i=1}^8 k_{ji} \eta^{a_i} \quad (j = 1, \dots, 6) \\
 C_{7\gamma}^{(0)eff}(\mu_b) &= \eta^{\frac{16}{23}} C_{7\gamma}^{(0)}(\mu_W) + \frac{8}{3} \left(\eta^{\frac{14}{23}} - \eta^{\frac{16}{23}} \right) C_{8G}^{(0)}(\mu_W) + C_1^{(0)}(\mu_W) \sum_{i=1}^8 h_i \eta^{a_i} \\
 C_{8G}^{(0)eff}(\mu_b) &= \eta^{\frac{14}{23}} C_{8G}^{(0)}(\mu_W) + C_1^{(0)}(\mu_W) \sum_{i=1}^8 \bar{h}_i \eta^{a_i}
 \end{aligned} \tag{1}$$

where

$$\eta = \frac{\alpha_s(\mu_W)}{\alpha_s(\mu_b)} \tag{2}$$

To evaluate the Wilson coefficients at $\mu = 1.5$ GeV we use following boundary conditions [18,144].

$$\begin{aligned}
 m_Z &= (91.188 \pm 0.002) \text{ GeV} \\
 m_W &= (80.379 \pm 0.001) \text{ GeV} \\
 \alpha_s(M_Z) &= 0.1181(1) \\
 m_t^{\text{pole}} &= 172.9 \pm 0.4 \text{ GeV} \\
 m_b &= 4.18_{-0.02}^{0.03} \text{ GeV}
 \end{aligned} \tag{3}$$

Note that the quark masses are given in pole mass scheme. However, pole masses of quarks can be converted into $\overline{\text{MS}}$ scheme as follows [18]:

$$\bar{m}_q = m_q^{\text{pole}} \left(m_q^{\text{pole}} \right) \left(1 - \frac{4\alpha_s(m_q^{\text{pole}})}{3\pi} + \mathcal{O}(\alpha_s^2) \right) \tag{4}$$

The top quark mass obtained in equation (4) is scaled down to $\mu = M_W$. Therefore, this gives us $m_t^{\overline{\text{MS}}}(\mu = M_W) = 175.05$ GeV.

In addition, the $C_{7\gamma}^{(0)}$, $C_{8G}^{(0)}$ and $C_1^{(0)}$ are given by:

$$\begin{aligned}
 C_1^{(0)}(\mu_W) &= 1 \\
 C_{7\gamma}^{(0)}(\mu_W) &= \frac{3x_t^3 - 2x_t^2}{4(x_t - 1)^4} \ln x_t + \frac{-8x_t^3 - 5x_t^2 + 7x_t}{24(x_t - 1)^3} \equiv -\frac{1}{2}D'_0(x_t) \\
 C_{8G}^{(0)}(\mu_W) &= \frac{-3x_t^2}{4(x_t - 1)^4} \ln x_t + \frac{-x_t^3 + 5x_t^2 + 2x_t}{8(x_t - 1)^3} \equiv -\frac{1}{2}E'_0(x_t)
 \end{aligned} \tag{5}$$

where $x_t = \frac{m_t^2}{M_W^2}$. Also, running of the C_1 is given by

$$C_1^{(0)}(\mu) = \frac{1}{2}\eta^{-12/23} + \frac{1}{2}\eta^{6/23} \tag{6}$$

APPENDIX B : USEFUL IDENTITY

The Wilson line

$$S_{\bar{n}}(x) = \mathbf{P} \exp \left(ig \int_{-\infty}^0 du \bar{n} \cdot A_s(x + u\bar{n}) \right), \quad (7)$$

obeys the equation $i\bar{n} \cdot D S_{\bar{n}}(x) = 0$, where $iD^\mu = i\partial^\mu + gA^\mu$, see, e.g., [?] for a derivation. Thus $i\bar{n} \cdot \partial S_{\bar{n}}(x) = -g\bar{n} \cdot A(x)S_{\bar{n}}(x)$. Taking the Hermitian conjugate of this identity gives $i\bar{n} \cdot \partial S_{\bar{n}}^\dagger(x) = S_{\bar{n}}^\dagger(x)g\bar{n} \cdot A(x)$. Consider now $i\bar{n} \cdot \partial \left(S_{\bar{n}}^\dagger(x)O(x)S_{\bar{n}}(x) \right)$, where $O(x)$ is an operator. Using the identities above we have

$$\begin{aligned} & i\bar{n} \cdot \partial \left(S_{\bar{n}}^\dagger(x)O(x)S_{\bar{n}}(x) \right) = \\ &= (i\bar{n} \cdot \partial S_{\bar{n}}^\dagger(x))O(x)S_{\bar{n}}(x) + S_{\bar{n}}^\dagger(x)(i\bar{n} \cdot \partial O(x))S_{\bar{n}}(x) + S_{\bar{n}}^\dagger(x)O(x)(i\bar{n} \cdot \partial S_{\bar{n}}(x)) \\ &= S_{\bar{n}}^\dagger(x)g\bar{n} \cdot A(x)O(x)S_{\bar{n}}(x) + S_{\bar{n}}^\dagger(x)(i\bar{n} \cdot \partial O(x))S_{\bar{n}}(x) - S_{\bar{n}}^\dagger(x)O(x)g\bar{n} \cdot A(x)S_{\bar{n}}(x) = \\ &= S_{\bar{n}}^\dagger(x)[g\bar{n} \cdot A(x), O(x)]S_{\bar{n}}(x) + S_{\bar{n}}^\dagger(x)[i\bar{n} \cdot \partial, O(x)]S_{\bar{n}}(x) = S_{\bar{n}}^\dagger(x)[i\bar{n} \cdot D, O(x)]S_{\bar{n}}(x) \end{aligned} \quad (8)$$

In the last line we have used the identity $[i\bar{n} \cdot \partial, O(x)]f(x) = (i\bar{n} \cdot \partial O(x))f(x)$ for an arbitrary function $f(x)$. Thus we have the identity

$$i\bar{n} \cdot \partial \left(S_{\bar{n}}^\dagger(x)O(x)S_{\bar{n}}(x) \right) = S_{\bar{n}}^\dagger(x)[i\bar{n} \cdot D, O(x)]S_{\bar{n}}(x). \quad (9)$$

BIBLIOGRAPHY

- [1] V. D. Barger and R. J. N. Phillips, *Collider Physics*, ADDISON-WESLEY 1987
- [2] S. L. Glashow, Nucl. Phys. **22**, 579 (1961). doi:10.1016/0029-5582(61)90469-2
- [3] S. Weinberg, Phys. Rev. Lett. **19**, 1264 (1967). doi:10.1103/PhysRevLett.19.1264
- [4] Wikipedia, URL: <https://commons.wikimedia.org/w/index.php?curid=4286964>
- [5] E. Noether, Gott. Nachr. **1918**, 235 (1918) [Transp. Theory Statist. Phys. **1**, 186 (1971)] doi:10.1080/00411457108231446 [physics/0503066].
- [6] D. Griffiths, *Introduction to elementary particles*, Wiley-VCH 2008
- [7] T. D. Lee and C. N. Yang, Phys. Rev. **104**, 254 (1956). doi:10.1103/PhysRev.104.254
- [8] R. Peccei, Lect. Notes Phys. **521**, 1-50 (1999) doi:10.1007/BFb010552 [arXiv:hep-ph/9807516 [hep-ph]].
- [9] M. E. Peskin and D. V. Schroeder, *An Introduction to quantum field theory*, Westview Press 1995
- [10] C. N. Yang and R. L. Mills, Phys. Rev. **96**, 191 (1954). doi:10.1103/PhysRev.96.191
- [11] T. Lancaster and S. J. Blundell, *Quantum Field Theory for the Gifted Amateur*, Oxford University Press 2014
- [12] A. V. Manohar and M. B. Wise, Camb. Monogr. Part. Phys. Nucl. Phys. Cosmol. **10**, 1 (2000).
- [13] C. H. Llewellyn Smith, Phys. Lett. **46B**, 233 (1973). doi:10.1016/0370-2693(73)90692-8
- [14] G. Isidori, Y. Nir and G. Perez, Ann. Rev. Nucl. Part. Sci. **60**, 355 (2010) doi:10.1146/annurev.nucl.012809.104534 [arXiv:1002.0900 [hep-ph]].
- [15] A. J. Buras, hep-ph/9806471.
- [16] L. L. Chau and W. Y. Keung, Phys. Rev. Lett. **53**, 1802 (1984). doi:10.1103/PhysRevLett.53.1802

- [17] L. Wolfenstein, Phys. Rev. Lett. **51**, 1945 (1983). doi:10.1103/PhysRevLett.51.1945
- [18] M. Tanabashi *et al.* [Particle Data Group], Phys. Rev. D **98**, no. 3, 030001 (2018). doi:10.1103/PhysRevD.98.030001
- [19] A. J. Buras, M. E. Lautenbacher and G. Ostermaier, Phys. Rev. D **50**, 3433 (1994) doi:10.1103/PhysRevD.50.3433 [hep-ph/9403384].
- [20] C. Jarlskog and R. Stora, Phys. Lett. B **208**, 268 (1988). doi:10.1016/0370-2693(88)90428-5
- [21] S. L. Glashow, J. Iliopoulos and L. Maiani, Phys. Rev. D **2**, 1285 (1970). doi:10.1103/PhysRevD.2.1285
- [22] M. K. Gaillard and B. W. Lee, Phys. Rev. D **10**, 897 (1974). doi:10.1103/PhysRevD.10.897
- [23] I. Ahmed,
- [24] J. R. Ellis, M. K. Gaillard, D. V. Nanopoulos and S. Rudaz, Nucl. Phys. B **131**, 285 (1977) Erratum: [Nucl. Phys. B **132**, 541 (1978)]. doi:10.1016/0550-3213(77)90374-1
- [25] M. A. Shifman, A. I. Vainshtein and V. I. Zakharov, Nucl. Phys. B **120**, 316 (1977). doi:10.1016/0550-3213(77)90046-3
- [26] M. Bander, D. Silverman and A. Soni, Phys. Rev. Lett. **43**, 242 (1979). doi:10.1103/PhysRevLett.43.242
- [27] M. Misiak *et al.*, Phys. Rev. Lett. **114**, no. 22, 221801 (2015) doi:10.1103/PhysRevLett.114.221801 [arXiv:1503.01789 [hep-ph]].
- [28] K. Lingel, T. Skwarnicki and J. G. Smith, Ann. Rev. Nucl. Part. Sci. **48**, 253 (1998) doi:10.1146/annurev.nucl.48.1.253 [hep-ex/9804015].
- [29] B. Grinstein, [arXiv:1701.06916 [hep-ph]].
- [30] M. Neubert, doi:10.1142/9789812773579-0004 hep-ph/0512222.
- [31] A. A. Petrov and A. E. Blechman, *Effective Field Theories*, World Scientific 2016

- [32] A. J. Buras, Lect. Notes Phys. **558**, 65 (2000) [hep-ph/9901409].
- [33] K. G. Wilson, Phys. Rev. **179**, 1499 (1969). doi:10.1103/PhysRev.179.1499
- [34] K. G. Wilson and W. Zimmermann, Commun. Math. Phys. **24**, 87 (1972). doi:10.1007/BF01878448
- [35] W. Zimmermann, Annals Phys. **77**, 570 (1973) [Lect. Notes Phys. **558**, 278 (2000)]. doi:10.1016/0003-4916(73)90430-2
- [36] M. Neubert, Phys. Rev. D **49**, 3392 (1994) doi:10.1103/PhysRevD.49.3392 [hep-ph/9311325].
- [37] E. C. Poggio, H. R. Quinn and S. Weinberg, Phys. Rev. D **13**, 1958 (1976). doi:10.1103/PhysRevD.13.1958
- [38] M. A. Shifman, doi:10.1142/9789812810458-0032 hep-ph/0009131.
- [39] G. Buchalla, A. J. Buras and M. E. Lautenbacher, Rev. Mod. Phys. **68**, 1125 (1996) doi:10.1103/RevModPhys.68.1125 [hep-ph/9512380].
- [40] D. J. Gross and F. Wilczek, Phys. Rev. Lett. **30**, 1343 (1973). doi:10.1103/PhysRevLett.30.1343
- [41] M. Neubert, Adv. Ser. Direct. High Energy Phys. **15**, 239 (1998) [hep-ph/9702375].
- [42] E. Eichten and F. Feinberg, Phys. Rev. D **23**, 2724 (1981). doi:10.1103/PhysRevD.23.2724
- [43] N. Isgur and M. B. Wise, Phys. Lett. B **232**, 113 (1989). doi:10.1016/0370-2693(89)90566-2
- [44] C. Balzereit and T. Ohl, Phys. Lett. B **386**, 335 (1996) doi:10.1016/0370-2693(96)00947-1 [hep-ph/9604352].
- [45] B. Grinstein, Nucl. Phys. B **339**, 253 (1990). doi:10.1016/0550-3213(90)90349-I
- [46] W. Pauli, Rev. Mod. Phys. **13**, 203 (1941). doi:10.1103/RevModPhys.13.203

- [47] W. Dittrich and M. Reuter, Lect. Notes Phys. **220**, 1 (1985).
- [48] H. K. Lee and Y. Yoon, JHEP **0703**, 086 (2007) doi:10.1088/1126-6708/2007/03/086 [hep-th/0611134].
- [49] T. Mannel, W. Roberts and Z. Ryzak, Nucl. Phys. B **368**, 204 (1992). doi:10.1016/0550-3213(92)90204-O
- [50] B. E. Lautrup, Phys. Lett. **69B**, 109 (1977). doi:10.1016/0370-2693(77)90145-9
- [51] G. Parisi, Nucl. Phys. B **150**, 163 (1979). doi:10.1016/0550-3213(79)90298-0
- [52] F. David, Nucl. Phys. B **263**, 637 (1986). doi:10.1016/0550-3213(86)90279-8
- [53] J. Komijani, JHEP **1708**, 062 (2017) doi:10.1007/JHEP08(2017)062 [arXiv:1701.00347 [hep-ph]].
- [54] M. Beneke and V. M. Braun, Nucl. Phys. B **426**, 301 (1994) doi:10.1016/0550-3213(94)90314-X [hep-ph/9402364].
- [55] A. V. Manohar, Phys. Rev. D **56**, 230 (1997) doi:10.1103/PhysRevD.56.230 [hep-ph/9701294].
- [56] A. Gunawardana and G. Paz, JHEP **1707**, 137 (2017) doi:10.1007/JHEP07(2017)137 [arXiv:1702.08904 [hep-ph]].
- [57] J. G. Korner and G. Thompson, Phys. Lett. B **264**, 185 (1991). doi:10.1016/0370-2693(91)90725-6
- [58] G. P. Lepage, L. Magnea, C. Nakhleh, U. Magnea and K. Hornbostel, Phys. Rev. D **46**, 4052 (1992) doi:10.1103/PhysRevD.46.4052 [hep-lat/9205007].
- [59] A. F. Falk, Nucl. Phys. B **378**, 79 (1992). doi:10.1016/0550-3213(92)90004-U
- [60] N. Isgur and M. B. Wise, Phys. Rev. Lett. **66**, 1130 (1991). doi:10.1103/PhysRevLett.66.1130
- [61] T. Mannel, Phys. Rev. D **50**, 428 (1994) doi:10.1103/PhysRevD.50.428 [hep-ph/9403249].

- [62] T. Mannel, S. Turczyk and N. Uraltsev, JHEP **1011**, 109 (2010) doi:10.1007/JHEP11(2010)109 [arXiv:1009.4622 [hep-ph]].
- [63] P. Ball and V. M. Braun, Phys. Rev. D **49**, 2472 (1994) doi:10.1103/PhysRevD.49.2472 [hep-ph/9307291].
- [64] P. Gambino, K. J. Healey and S. Turczyk, Phys. Lett. B **763**, 60 (2016) doi:10.1016/j.physletb.2016.10.023 [arXiv:1606.06174 [hep-ph]].
- [65] A. F. Falk and M. Neubert, Phys. Rev. D **47**, 2965 (1993) doi:10.1103/PhysRevD.47.2965 [hep-ph/9209268].
- [66] J. L. Ritchie [BaBar Collaboration], arXiv:1301.0836 [hep-ex].
- [67] D. Benson, I. I. Bigi and N. Uraltsev, Nucl. Phys. B **710**, 371 (2005) doi:10.1016/j.nuclphysb.2004.12.035 [hep-ph/0410080].
- [68] M. Neubert, Phys. Rev. D **72**, 074025 (2005) doi:10.1103/PhysRevD.72.074025 [hep-ph/0506245].
- [69] M. Czakon, P. Fiedler, T. Huber, M. Misiak, T. Schutzmeier and M. Steinhauser, JHEP **1504**, 168 (2015) doi:10.1007/JHEP04(2015)168 [arXiv:1503.01791 [hep-ph]].
- [70] Y. S. Amhis *et al.* [HFLAV Collaboration], arXiv:1909.12524 [hep-ex].
- [71] B. Aubert *et al.* [BaBar Collaboration], Phys. Rev. D **77**, 051103 (2008) doi:10.1103/PhysRevD.77.051103 [arXiv:0711.4889 [hep-ex]].
- [72] S. Chen *et al.* [CLEO Collaboration], Phys. Rev. Lett. **87**, 251807 (2001) doi:10.1103/PhysRevLett.87.251807 [hep-ex/0108032].
- [73] J. P. Lees *et al.* [BaBar Collaboration], Phys. Rev. D **86**, 052012 (2012) doi:10.1103/PhysRevD.86.052012 [arXiv:1207.2520 [hep-ex]].
- [74] J. P. Lees *et al.* [BaBar Collaboration], Phys. Rev. Lett. **109**, 191801 (2012) doi:10.1103/PhysRevLett.109.191801 [arXiv:1207.2690 [hep-ex]].

- [75] T. Saito *et al.* [Belle Collaboration], Phys. Rev. D **91**, no. 5, 052004 (2015) doi:10.1103/PhysRevD.91.052004 [arXiv:1411.7198 [hep-ex]].
- [76] A. Abdesselam *et al.* [Belle Collaboration], arXiv:1608.02344 [hep-ex].
- [77] B. O. Lange, M. Neubert and G. Paz, Phys. Rev. D **72**, 073006 (2005) doi:10.1103/PhysRevD.72.073006 [hep-ph/0504071].
- [78] M. Benzke, S. J. Lee, M. Neubert and G. Paz, JHEP **1008**, 099 (2010) doi:10.1007/JHEP08(2010)099 [arXiv:1003.5012 [hep-ph]].
- [79] E. Kou *et al.* [Belle-II Collaboration], PTEP **2019**, no. 12, 123C01 (2019) doi:10.1093/ptep/ptz106 [arXiv:1808.10567 [hep-ex]].
- [80] G. Paz, JHEP **0906**, 083 (2009) doi:10.1088/1126-6708/2009/06/083 [arXiv:0903.3377 [hep-ph]].
- [81] G. P. Korchemsky and G. F. Sterman, Phys. Lett. B **340**, 96 (1994) doi:10.1016/0370-2693(94)91304-8 [hep-ph/9407344].
- [82] C. W. Bauer, D. Pirjol and I. W. Stewart, Phys. Rev. D **65**, 054022 (2002) doi:10.1103/PhysRevD.65.054022 [hep-ph/0109045].
- [83] S. W. Bosch, B. O. Lange, M. Neubert and G. Paz, Nucl. Phys. B **699**, 335 (2004) doi:10.1016/j.nuclphysb.2004.07.041 [hep-ph/0402094].
- [84] S. J. Lee, M. Neubert and G. Paz, Phys. Rev. D **75**, 114005 (2007) doi:10.1103/PhysRevD.75.114005 [hep-ph/0609224].
- [85] G. Paz, hep-ph/0607217.
- [86] K. Melnikov and A. Mitov, Phys. Lett. B **620**, 69 (2005) doi:10.1016/j.physletb.2005.06.015 [hep-ph/0505097].
- [87] T. Becher and M. Neubert, Phys. Lett. B **637**, 251 (2006) doi:10.1016/j.physletb.2006.04.046 [hep-ph/0603140].

- [88] M. Neubert, Phys. Rev. D **49**, 4623 (1994) doi:10.1103/PhysRevD.49.4623 [hep-ph/9312311].
- [89] S. W. Bosch, M. Neubert and G. Paz, JHEP **0411**, 073 (2004) doi:10.1088/1126-6708/2004/11/073 [hep-ph/0409115].
- [90] M. Misiak *et al.*, Phys. Rev. Lett. **98**, 022002 (2007) doi:10.1103/PhysRevLett.98.022002 [hep-ph/0609232].
- [91] B. Aubert *et al.* [BaBar Collaboration], Phys. Rev. D **72**, 052004 (2005) doi:10.1103/PhysRevD.72.052004 [hep-ex/0508004].
- [92] A. Gunawardana and G. Paz, JHEP **1911**, 141 (2019) doi:10.1007/JHEP11(2019)141 [arXiv:1908.02812 [hep-ph]].
- [93] S. Watanuki *et al.* [Belle Collaboration], Phys. Rev. D **99**, no. 3, 032012 (2019) doi:10.1103/PhysRevD.99.032012 [arXiv:1807.04236 [hep-ex]].
- [94] A. L. Kagan and M. Neubert, Phys. Rev. D **58**, 094012 (1998) doi:10.1103/PhysRevD.58.094012 [hep-ph/9803368].
- [95] M. Benzke, S. J. Lee, M. Neubert and G. Paz, Phys. Rev. Lett. **106**, 141801 (2011) doi:10.1103/PhysRevLett.106.141801 [arXiv:1012.3167 [hep-ph]].
- [96] A. G. Grozin and M. Neubert, Phys. Rev. D **55**, 272 (1997) doi:10.1103/PhysRevD.55.272 [hep-ph/9607366].
- [97] S. Balk, J. G. Korner and D. Pirjol, Nucl. Phys. B **428**, 499 (1994) doi:10.1016/0550-3213(94)90211-9 [hep-ph/9307230].
- [98] B. M. Dassinger, T. Mannel and S. Turczyk, JHEP **0703**, 087 (2007) doi:10.1088/1126-6708/2007/03/087 [hep-ph/0611168].
- [99] R. J. Hill, G. Lee, G. Paz and M. P. Solon, Phys. Rev. D **87**, 053017 (2013) doi:10.1103/PhysRevD.87.053017 [arXiv:1212.4508 [hep-ph]].
- [100] G. Paz, Mod. Phys. Lett. A **30**, no. 26, 1550128 (2015) [arXiv:1503.07216 [hep-ph]].

- [101] A. Kobach and S. Pal, Phys. Lett. B **772**, 225 (2017) doi:10.1016/j.physletb.2017.06.026 [arXiv:1704.00008 [hep-ph]].
- [102] J. Heinonen and T. Mannel, Nucl. Phys. B **889**, 46 (2014) doi:10.1016/j.nuclphysb.2014.09.017 [arXiv:1407.4384 [hep-ph]].
- [103] M. Gremm and A. Kapustin, Phys. Rev. D **55**, 6924 (1997) doi:10.1103/PhysRevD.55.6924 [hep-ph/9603448].
- [104] A. H. Hoang and A. V. Manohar, Phys. Lett. B **633**, 526 (2006) doi:10.1016/j.physletb.2005.12.020 [hep-ph/0509195].
- [105] M. Misiak and M. Steinhauser, Nucl. Phys. B **764**, 62 (2007) doi:10.1016/j.nuclphysb.2006.11.027 [hep-ph/0609241].
- [106] Y. Amhis *et al.* [HFLAV Collaboration], Eur. Phys. J. C **77**, no. 12, 895 (2017) doi:10.1140/epjc/s10052-017-5058-4 [arXiv:1612.07233 [hep-ex]].
- [107] M. B. Voloshin, Phys. Lett. B **397**, 275 (1997) doi:10.1016/S0370-2693(97)00173-1 [hep-ph/9612483].
- [108] Z. Ligeti, L. Randall and M. B. Wise, Phys. Lett. B **402**, 178 (1997) doi:10.1016/S0370-2693(97)00304-3 [hep-ph/9702322].
- [109] A. K. Grant, A. G. Morgan, S. Nussinov and R. D. Peccei, Phys. Rev. D **56**, 3151 (1997) doi:10.1103/PhysRevD.56.3151 [hep-ph/9702380].
- [110] G. Buchalla, G. Isidori and S. J. Rey, Nucl. Phys. B **511**, 594 (1998) doi:10.1016/S0550-3213(97)00674-3 [hep-ph/9705253].
- [111] Z. Ligeti, I. W. Stewart and F. J. Tackmann, Phys. Rev. D **78**, 114014 (2008) doi:10.1103/PhysRevD.78.114014 [arXiv:0807.1926 [hep-ph]].
- [112] A. Gunawardana, arXiv:1909.09081 [hep-ph].
- [113] M. Ablikim *et al.* [BESIII Collaboration], Phys. Rev. Lett. **122**, no. 1, 011804 (2019) doi:10.1103/PhysRevLett.122.011804 [arXiv:1810.03127 [hep-ex]].

- [114] M. Ablikim *et al.* [BESIII Collaboration], Phys. Rev. Lett. **121**, no. 17, 171803 (2018) doi:10.1103/PhysRevLett.121.171803 [arXiv:1802.05492 [hep-ex]].
- [115] C. Z. Yuan and S. L. Olsen, Nature Rev. Phys. **1**, no. 8, 480 (2019) doi:10.1038/s42254-019-0082-y [arXiv:2001.01164 [hep-ex]].
- [116] L. Riggio, G. Salerno and S. Simula, Eur. Phys. J. C **78**, no. 6, 501 (2018) doi:10.1140/epjc/s10052-018-5943-5 [arXiv:1706.03657 [hep-lat]].
- [117] C. M. Grant, A. Gunawardana and A. A. Petrov, arXiv:1912.09058 [hep-ph].
- [118] S. Aoki *et al.* [Flavour Lattice Averaging Group], Eur. Phys. J. C **80**, no. 2, 113 (2020) doi:10.1140/epjc/s10052-019-7354-7 [arXiv:1902.08191 [hep-lat]].
- [119] A. Khodjamirian, C. Klein, T. Mannel and N. Offen, Phys. Rev. D **80**, 114005 (2009) doi:10.1103/PhysRevD.80.114005 [arXiv:0907.2842 [hep-ph]].
- [120] C. G. Boyd, B. Grinstein and R. F. Lebed, Phys. Rev. Lett. **74**, 4603 (1995) doi:10.1103/PhysRevLett.74.4603 [hep-ph/9412324].
- [121] T. Becher and R. J. Hill, Phys. Lett. B **633**, 61 (2006) doi:10.1016/j.physletb.2005.11.063 [hep-ph/0509090].
- [122] B. Ananthanarayan, I. Caprini and I. Sentitemsu Imsong, Eur. Phys. J. A **47**, 147 (2011) doi:10.1140/epja/i2011-11147-7 [arXiv:1108.0284 [hep-ph]].
- [123] B. Grinstein and R. F. Lebed, Phys. Rev. D **92**, no. 11, 116001 (2015) doi:10.1103/PhysRevD.92.116001 [arXiv:1509.04847 [hep-ph]].
- [124] D. Becirevic and A. B. Kaidalov, Phys. Lett. B **478**, 417 (2000) doi:10.1016/S0370-2693(00)00290-2 [hep-ph/9904490].
- [125] P. Ball and R. Zwicky, Phys. Rev. D **71**, 014015 (2005) doi:10.1103/PhysRevD.71.014015 [hep-ph/0406232].
- [126] K. Hornik, M. Stinchcombe, and H. White, Neural Networks **2**, no. 5, 359-366 (1989)
- [127] G. Cybenko Math. Control Signals Systems (1989) **2** 303-314

- [128] S. Forte, L. Garrido, J. I. Latorre and A. Piccione, *JHEP* **0205**, 062 (2002) doi:10.1088/1126-6708/2002/05/062 [hep-ph/0204232].
- [129] R. D. Ball *et al.* [NNPDF Collaboration], *JHEP* **1504**, 040 (2015) doi:10.1007/JHEP04(2015)040 [arXiv:1410.8849 [hep-ph]].
- [130] J. C. Rojo, “The Neural network approach to parton distribution functions,” hep-ph/0607122.
- [131] K. M. Graczyk, P. Plonski and R. Sulej, *JHEP* **1009**, 053 (2010) doi:10.1007/JHEP09(2010)053 [arXiv:1006.0342 [hep-ph]].
- [132] L. Alvarez-Ruso, K. M. Graczyk and E. Saul-Sala, *Phys. Rev. C* **99**, no. 2, 025204 (2019) doi:10.1103/PhysRevC.99.025204 [arXiv:1805.00905 [hep-ph]].
- [133] G. Carleo, I. Cirac, K. Cranmer, L. Daudet, M. Schuld, N. Tishby, L. Vogt-Maranto and L. Zdeborová, *Rev. Mod. Phys.* **91**, no. 4, 045002 (2019) doi:10.1103/RevModPhys.91.045002 [arXiv:1903.10563 [physics.comp-ph]].
- [134] J. Nocedal and S. J. Wright, doi:10.1007/b98874
- [135] M. F. Moller, *Neural Networks* **6**, no. 4, 525-533 (1993)
- [136] Demuth, Howard B. and Beale, Mark H. and De Jess, Orlando and Hagan, Martin T., “Neural Network Design,” ISBN 0971732116, 9780971732117
- [137] M. Ablikim *et al.* [BESIII Collaboration], *Phys. Rev. D* **92**, no. 7, 072012 (2015)
- [138] S. G. Krishna and K. K. Sahu, arXiv:1503.06462 [cs.OH].
- [139] Wikipedia, URL: [https://en.wikipedia.org/wiki/Flavour_\(particle_physics\)](https://en.wikipedia.org/wiki/Flavour_(particle_physics))
- [140] G. T. Bodwin, E. Braaten and G. P. Lepage, *Phys. Rev. D* **51**, 1125 (1995) Erratum: [*Phys. Rev. D* **55**, 5853 (1997)] [hep-ph/9407339].
- [141] N. Brambilla, E. Mereghetti and A. Vairo, *JHEP* **0608**, 039 (2006) Erratum: [*JHEP* **1104**, 058 (2011)] [hep-ph/0604190].

- [142] N. Brambilla, E. Mereghetti and A. Vairo, Phys. Rev. D **79**, 074002 (2009) Erratum:
[Phys. Rev. D **83**, 079904 (2011)] [arXiv:0810.2259 [hep-ph]].
- [143] S. P. Dye, M. Gonderinger and G. Paz, Phys. Rev. D **94**, no. 1, 013006 (2016)
[arXiv:1602.07770 [hep-ph]].
- [144] P. J. Mohr, D. B. Newell and B. N. Taylor, Rev. Mod. Phys. **88**, no. 3, 035009 (2016)
doi:10.1103/RevModPhys.88.035009 [arXiv:1507.07956 [physics.atom-ph]].

ABSTRACT

EFFECTIVE FIELD THEORY AND MACHINE LEARNING APPROACHES
TO CONTROLLING NONPERTURBATIVE UNCERTAINTIES IN FLAVOR
PHYSICS

by

AYESH GUNAWARDANA

August 2020

Advisor: Dr. Gil Paz**Major:** Physics**Degree:** Doctor of Philosophy

The radiative decay $\bar{B} \rightarrow X_s \gamma$ and semileptonic heavy meson decay $D \rightarrow \pi l \nu$ are important flavor physics probes of new physics. However, these decays are plagued with non-perturbative uncertainties that are needed to be controlled to obtain a theoretically clean description. In this dissertation, we provide effective field theory and machine learning approaches to controlling these uncertainties

In $\bar{B} \rightarrow X_s \gamma$, the largest uncertainty on the total rate arises from $Q_1 - Q_{7\gamma}$ operator pair. This contribution is given by a soft function whose moments are related to nonperturbative heavy quark effective theory (HQET) operators' matrix elements. The extraction of higher-order moments requires the knowledge of higher dimensional HQET operators. We present a general method that allows for an easy construction of HQET and non-relativistic quantum-chromodynamics (NRQCD) operators containing *any* number of covariant derivatives. As an application, we list, for the first time, all operators in the dimension eight NRQCD Lagrangian. Then we use recently extracted HQET matrix elements to reevaluate the nonperturbative uncertainty of $\bar{B} \rightarrow X_s \gamma$ total decay rate and CP asymmetry.

The decay rate of semileptonic $D \rightarrow \pi l \nu$ is proportional to the hadronic form factors. Currently, these form factors cannot be determined analytically in the whole range of available momentum transfer q^2 , but can be parameterized with a varying degree of model dependency. We propose a machine learning approach with artificial neural networks trained

from experimental pseudo-data to predict the shape of these form factors with a prescribed uncertainty. This provides the first model-independent parameterization of $D \rightarrow \pi l \nu$ vector form factor shape in the literature.

AUTOBIOGRAPHICAL STATEMENT

Name: Ayesh Gunawardana

Education:

B.S. Physics, University of Kelaniya, Kelaniya, Sri Lanka, 2013

Professional Experience:

Rumble Fellow, Dept. of Physics and Astronomy, Wayne State University, 2018-2019

Graduate Research Assistant, Dept. of Physics and Astronomy, Wayne State University, 2017-2018

Graduate Teaching Assistant, Dept. of Physics and Astronomy, Wayne State University, 2014-2017

Teaching Assistant, Dept. of Physics, University of Kelaniya, Sri Lanka, 2013-2014

Publications:

- C. M. Grant, A. Gunawardana, and A. A. Petrov, *Semileptonic decays of heavy mesons with artificial neural networks*, [arXiv:1912.09058 [hep-ph]]
- A. Gunawardana, *Reevaluating uncertainties in $\bar{B} \rightarrow X_s \gamma$ decay* [arXiv:1909.09081] (DPF 2019 Conference proceedings)
- A. Gunawardana and G. Paz, *Reevaluating uncertainties in $\bar{B} \rightarrow X_s \gamma$ decay*, JHEP 11, 141 (2019) [arXiv:1908.02812]
- A. Gunawardana and G. Paz, *On HQET and NRQCD operators of dimension 8 and above*, JHEP 1707, 137 (2017), [arXiv:1702.08904]